MULTI-BAND LOW PROFILE ANTENNAS FOR WLAN AND WIMAX APPLICATIONS

by

Ernst Willem Coetzee

Submitted in partial fulfilment of the requirements for the degree
Master of Engineering (Electronic Engineering)

in the

Department of Electrical, Electronic and Computer Engineering
Faculty of Engineering, Built Environment and Information Technology

UNIVERSITY OF PRETORIA

October 2018

SUMMARY

MULTI-BAND LOW PROFILE ANTENNAS FOR WLAN AND WIMAX APPLICATIONS

by

Ernst Willem Coetzee

Supervisor: Prof. J.W. Odendaal

Co-supervisor: Prof. J. Joubert

Department: Electrical, Electronic and Computer Engineering

University: University of Pretoria

Degree: Master of Engineering (Electronic Engineering)

Keywords: WLAN, dual-band, triple-band, quad-band, directional, high-gain, low profile, slot antenna single-polarised, AMC reflector

The demand for modern wireless communication systems have grown at a remarkable rate and the Wireless Local Area Network (WLAN) and Worldwide Interoperability for Microwave Access (WiMAX) frequency bands have been recognized as a cost-effective and reliable solution for high-speed wireless communication. The WLAN frequency bands are from 2.4 – 2.483 GHz, 5.15 – 5.25 GHz and 5.725 – 5.825 GHz, while the WiMAX frequency band is from 3.4 – 3.6 GHz, which are for the IEEE802.11a, IEEE802.11b, IEEE802.16d and IEEE802.16e standards. The objective of this dissertation was to develop a new and improved high gain WLAN antenna with a low profile and directional radiation pattern.

The proposed antennas were based on an ultra-wideband slot radiating element, which consisted of a microstrip feedline with a strip-slot pair. The work also required the design of an artificial magnetic conductor (AMC) surface, to achieve a low profile antenna with high gain. The antenna combined with the AMC reflector, achieved a high gain and a directional radiation pattern. The design of the proposed antenna resulted in a triple-band WLAN antenna with an overall size of $80\times80\times10.01$ mm^3 with an average gain of 10.2 dBi across the WLAN bands. The antenna also achieved a directional radiation pattern with a front-to-back better than 24 dB in the WLAN bands.

The design of a quad-band WLAN and WiMAX antenna was also performed. The quad-band antenna operated in the 2.4 GHz, 5.2 GHz and 5.8 GHz WLAN bands as well as the 3.5 GHz WiMAX band. The antenna had an overall size of $80\times80\times10.01$ mm^3 with an average gain of 9.3 dBi across the WLAN and WiMAX frequency bands. The antenna also achieved a directional radiation pattern with a front-to-back better than 22 dB in the WLAN and WiMAX bands. The simulated and measured results for both antennas were compared and have a good agreement. The results achieved by the proposed triple- and quad-band antennas exceeded the performance of other high gain and directional WLAN antennas found in the literature. Comparing the results of the quad-band antenna with a strip-slot antenna found in literature, the overall volume and average gain has improved by 34.7% and 2.2%, respectively.

LIST OF ABBREVIATIONS

AMC	Artificial Magnetic Conductor
CEM	Computational Electromagnetic
EBG	Electromagnetic Bandgap
FEM	Finite Element Method
FDS	Frequency Domain Solver
FDTD	Finite Difference Time Domain
FIT	Finite Integration Technique
MoM	Method of Moments
PEC	Perfect Electric Conductor
PMC	Perfect Magnetic Conductor
TDS	Time Domain Solver
VNA	Vector Network Analyser
WiMAX	Worldwide Interoperability for Microwave Access
WLAN	Wireless Local Area Network

TABLE OF CONTENTS

CHAPTER 1 INTRODUCTION

1.1 PROBLEM STATEMENT

1.1.1 Context of the problem

The demand for modern wireless communication systems have grown at a remarkable rate and the Wireless Local Area Network (WLAN) has been acknowledged as a reliable and cost-effective solution for high-speed wireless communication [1]. WLAN applications are used in multiple electronic devices, e.g. mobile phones, computers, laptops and smart televisions. The IEEE802.11a/b WLAN band operates in the lower frequency band from 2.4 – 2.483 GHz and in the higher frequency band from 5.15 – 5.25 GHz and 5.725 – 5.825 GHz [1]. There is a demand for high-gain, directional WLAN antennas, which cover the WLAN frequency bands [1]. Modern wireless communication devices also operate in the Worldwide Interoperability for Microwave Access (WiMAX) frequency band, which operate at IEEE802.16d/e in the frequency band 3.4 – 3.6 GHz [2]. The application of WLAN as well as WiMAX antennas is investigated for wall mounting applications.

The literature study indicated that printed circuit board antennas received more coverage than machined antennas. The literature study illustrated that the printed antennas had omnidirectional radiation patterns with a low total efficiency and low gain. The omnidirectional dual-band WLAN antennas consisted of various topologies such as, T-, U-, L- and F-shaped, circular, slotted and branched monopoles, as well as wide slot antennas [3], [4], [13], [5]–[12]. These antennas achieved very low gain and with an omnidirectional radiation pattern, which was not suitable for wall mount applications. Directional WLAN antennas were then investigated for wall mounted applications.

Directional antennas usually include a reflector plane to enhance the gain and achieve a directional radiation pattern. The directional antennas included various microstrip topologies such as F-, H-, U-, T-shaped and triangular monopoles, slot array antennas, as well as circular slot antennas [14]–[21]. A reflector plane operates at a quarter-wavelength away from the antenna and can make the overall volume of the antenna large at lower frequencies.

The one method to achieve a low profile antenna was with the implementation of an artificial magnetic conductor (AMC) surface. In literature, it was found that the implementation of AMC surfaces have become more popular and gives the antenna a low profile as well as improved gain, radiation pattern and front-to-back ratio. The design of single-, dual- and triple-band AMC surfaces were found in the literature, which illustrated various geometries available for implementation.

The literature study indicated that the majority of the WLAN antennas with an AMC surface operated in the 2.4 GHz, 5.2 GHz and 5.8 GHz WLAN bands. The WLAN dual-band antennas, which operated in the lower (2.4 GHz) and upper (5.2 GHz and 5.8 GHz) WLAN bands, were combined with dual-band AMC surfaces to achieve a dual-band response. The design of a wideband circularly polarized antenna with an AMC reflector was presented in [22]. The antenna had an overall size of 80×80×20 mm^3 with an average gain of 6.6 and 7.4 dBi in the lower and upper WLAN bands, respectively. The combination of a dual-band C-slotted antenna with a dual-band AMC reflector was presented in [23]. The antenna had an overall size of 90×90×6.5 mm^3 with an average gain of 5.3 dBi and 10.7 dBi in the 2.4 GHz and 5.8 GHz WLAN bands, respectively. The design of a V-shaped slot etched out of a trapezoidal monopole with a dual-band AMC in [24] achieved the smallest overall size of 57×57×8 mm^3. The antenna operated in the 2.4 GHz, 5.2 GHz and 5.8 GHz WLAN bands and had an average gain of 6.6 dBi and 7.8 dBi at 2.4 GHz and 5.5 GHz, respectively. The implementation of WLAN antennas with AMC surfaces for a low profile and high-gain performance was achieved by the various antennas in literature, which can be used for wall mounted applications.

1.1.2 Research gap

The WLAN and WiMAX frequency bands are implemented widely in modern wireless communication systems such as mobile devices and laptops. It was found that the design of wall mounted antennas for WLAN and WiMAX antennas for access points was limited. Through the literature study, it was found that there are limited antenna designs on

directional, high gain, single-polarized WLAN and WiMAX antennas with a gain of more than 9 dBi. The best possible result was a directional, high gain, strip-slot antenna with an overall size of 96×73×14 mm^3. The average gain achieved by the antenna was 9.1 dBi and a front-to-back ratio better than 14 dB across the respective WLAN and WiMAX bands.

1.2 RESEARCH OBJECTIVE AND GOALS

The objective and goals of the research is to design a new and improved low profile and directional antenna for WLAN and WiMAX applications. The antenna should have better performance than the latest WLAN and WiMAX antennas with regards to quad-band frequency capability, gain, front-to-back ratio and overall size.

The antenna should cover the WLAN frequency bands 2.4 – 2.483 GHz, 5.15 – 5.25 GHz and 5.725 – 5.825 GHz also known as the IEEE802.11a/b standard. This requires the antenna to have a triple-band operation. In addition to the WLAN bands, the antenna should also operate in the WiMAX IEEE802.16d/e standards, with the frequency band 3.4 – 3.6 GHz.

The goal of the research is that it should achieve a high gain response of more than 9 dBi with a directional radiation pattern and a front-to-back ratio better than 20 dB. This was the gain and front-to-back ratio achieved by the high gain antenna for WLAN and WiMAX frequency bands in [21]. The antenna should have a low profile design, to make it more compact, and the overall size has to be smaller than the other antennas found in the literature.

1.3 HYPOTHESIS AND APPROACH

The high gain, strip-slot pair antenna in [21] was used as a starting point for the investigation of the antenna. The strip-slot antenna is combined with a perfect electric conductor (PEC) reflector to achieve a directional radiation pattern with high gain. It is hypothesized that the height of the antenna can be reduced by replacing the PEC reflector with an artificial magnetic conductor (AMC) surface. The impedance bandwidth achieved by the strip-slot

antenna can also be improved by including an additional slot element in the ground plane of the antenna.

The following approach will be followed in order to verify the hypothesis. A literature study will be performed on present WLAN and WiMAX directional antenna geometries. This will give an indication of what directional antennas have been proposed in the literature and also to understand the functionality of directional antennas. One of the objectives and goals is to achieve a low profile antenna and to achieve this goal, the antenna will be combined with an AMC surface. A literature study will also be performed on the combination of various WLAN antennas with AMC surfaces and determine how they operate.

The geometry of the strip-slot antenna will be combined with the AMC reflector and the antenna will then be optimized to operate in the respective WLAN and WiMAX bands. The design and simulation of the antenna will be made possible with the electromagnetic software package, CST Microwave Studio [25]. The final antenna will be manufactured and the measured results will be compared to the simulated results.

1.4 RESEARCH CONTRIBUTION

The combination of an antenna with an AMC reflector resulted in a low profile design with improved gain. The design of a triple- and quad-band antenna was realized with an overall size of $80\times80\times10.01$ mm^3. The triple-band antenna covered the 2.4 GHz, 5.2 GHz and 5.8 GHz WLAN bands and achieved an average gain of 10.2 dBi across the band of operation. The triple-band antenna achieved a directional radiation pattern with a front-to-back better than 24 dB across the three WLAN bands. The quad-band antenna also covered the 2.4 GHz, 5.2 GHz and 5.8 GHz WLAN bands, as well as the 3.5 GHz WiMAX band with an average gain of 9.3 dBi across the bands of operation. The quad-band antenna also achieved a directional pattern with a front-to-back ratio of better than 22 dB across the WLAN and WiMAX bands. A 3D-model of the proposed triple- and quad-band antennas are shown in Figure 1.1.

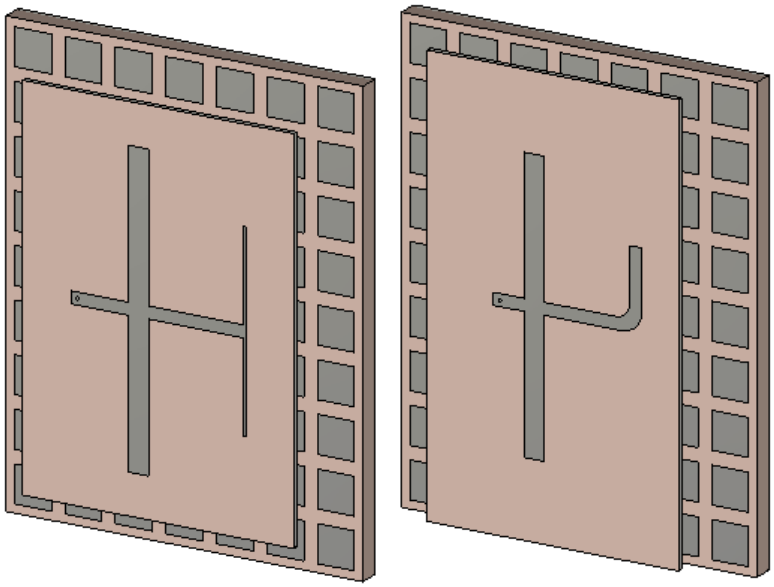

(a) (b)

Figure 1.1. 3D model of proposed antenna designs.

(a) triple-band antenna (b) quad-band antenna

The performance, with regards to gain and size, of the proposed quad-band antenna was compared to the strip-slot antenna in [21] that covered the 2.4 GHz, 5.2 GHz and 5.8 GHz WLAN bands, as well as the 3.5 GHz WiMAX band. The strip-slot antenna in [21] achieved directional and high gain response for WLAN and WiMAX applications. The antenna had an overall size of 96×73×14 mm^3 ($0.768\lambda_0 \times 0.584\lambda_0 \times 0.112\lambda_0$ at 2.4 GHz) with an average gain of 9.1 dBi across the WLAN and WiMAX bands. The antenna achieved a directional radiation pattern with a front-to-back ratio better than 14 dB. Comparing the results of the quad-band antenna with the strip-slot antenna, it can be seen that the overall size and the average gain has improved by 34.7% and 2.2%, respectively.

1.5 RESEARCH OUTPUTS

A conference paper focusing on a dual-band antenna with an AMC reflector for WLAN and WiMAX applications was proposed in the study. The paper has been accepted by the IEEE

Radio and Antenna Days of the Indian Ocean (RADIO) International Conference. The conference will be held from the 15th to the 18th of October 2018 in Mauritius.

A journal paper presenting a quad-band antenna for WLAN and WiMAX applications, has been accepted for publication in Applied Computational Electromagnetic Society (ACES). The antenna consisted of a strip-slot pair, with an additional slot element and a microstrip feedline that was terminated with an open circuit termination. The antenna was combined with a single-band AMC reflector to achieve a quad-band response.

1.6 DISSERTATION/THESIS OVERVIEW

Chapter 2 contains a literature study and focusses on WLAN and WiMAX antennas in general as well as AMC surfaces. The literature study focusses on omnidirectional and directional WLAN antennas, to determine what antennas are presented in the literature. Lastly, a literature study on directional antennas with AMC reflectors were discussed and the various geometries found in the literature were reviewed.

In Chapter 3, a background study is performed. The background study focuses on the various components that will be used to design the proposed antennas. The background study was performed on patch and slot antennas, as well as a strip-slot pair structure with secondary slot elements. The design and implementation of artificial magnetic conductor (AMC) surfaces are also performed. The different components are simulated and combined.

In Chapter 4 the design of the proposed antennas is performed. The antenna geometries are designed from the background study and the final design of the antennas are given. The antenna simulations results are also presented in this chapter. The assembly of the final prototype antennas are presented.

In Chapter 5, the measured results are compared to the simulated results of the manufactured triple- and quad-band antennas. A thorough discussion of the results is also included in the chapter.

In Chapter 6, the work done and the contribution made by the research are discussed. The chapter also explains how the objectives were achieved by the proposed antennas and how they compare to other antennas found in literature.

CHAPTER 2 LITERATURE STUDY

2.1 CHAPTER OVERVIEW

In this chapter a literature study will firstly be performed on WLAN and WiMAX antennas in general. Thereafter, the literature study will focus more in-depth on directional WLAN and WiMAX antennas, with regard to the overall size and performance. Lastly, a literature study will be performed on artificial magnetic conductor (AMC) surfaces, as well as the combination of WLAN and WiMAX antennas with AMC surfaces. The goal of the literature study is to determine which directional antenna designs are available with the most optimum size and gain for WLAN and WiMAX applications.

2.2 LITERATURE STUDY ON WLAN AND WIMAX ANTENNAS

A literature study on WLAN and WiMAX antennas was conducted. Only printed microstrip antennas were investigated as they are easy to implement for antenna fabrication. The printed WLAN and WiMAX antennas are divided into two sections, namely omnidirectional antennas and directional antennas. Examples of the different printed WLAN and WiMAX antennas are discussed in their respective sections.

2.2.1 Omnidirectional WLAN and WiMAX antennas

The application of omnidirectional antennas are widely used for mobile devices such as laptops, mobile phones, and Wi-Fi routers. These antennas are usually small in size with low gain and some also exhibited low efficiency. The applications of omnidirectional antennas are more suitable for mobile use and not necessarily for wall mounting applications.

Tailored monopole antennas were among the most common printed WLAN antennas found in the literature. The antennas included E-, F, L, T and Y-shaped, circular and slotted monopoles [4]–[13]. The majority of the monopole antennas consisted of a feedline with a shortened ground plane on the opposite side of the substrate.

The design of a double-T monopole antenna was constructed by placing two T-shaped monopoles on a microstrip feedline. The gain achieved by the monopole antenna ranged from 0.8 – 1.8 dBi [4], [13]. The double T-shaped monopole is symmetrical around the microstrip feedline. By removing the one side an F-shaped monopole antenna can be formed. An F-shaped monopole was proposed in [5] and achieved gain between 1.9 – 2.9 dBi. The radiation patterns between the T- and F-shaped monopoles were quite similar.

A branched monopole antenna consisted of an etched monopole with an added microstrip radiating branch on each side of the monopole substrate. The branches had an L-shaped design and produced more resonant modes for the antenna [6]. An E-shaped monopole antenna also incorporated a microstrip feedline with two L-shaped stubs mirrored to achieve a dual-band response in [7]. The radiation patterns achieved by the branched monopole antennas were omnidirectional in the lower WLAN band but squinted in the upper WLAN band. The E-shaped monopole achieved a gain that ranged from 2.8 – 4.6 dBi.

The combination of a patch and a monopole was presented in [8]. The antenna consists of a patch with two L-shaped slots as well as two small square patches on the one side of the substrate and a partial ground plane on the opposite side, which resulted in a monopole design. The gain achieved by the antenna ranged from 3 dBi in the lower 2.45 GHz band and 1.8 dBi in the upper 5.8 GHz band. The design of another patch monopole antenna, which consisted of a partial ground plane, a Y-shaped radiating patch and a modified circle monopole was presented in [9]. The printed antenna was small in size and had a truncated ground plane on the opposite side of the antenna. The gain achieved by the antenna ranged to 2.5 dBi in the lower 2.45 GHz band and 1 dBi in the upper 5.8 GHz band.

A dual-band circularly polarized annular-slot antenna was presented in [10]. The antenna consisted of a circular slot in the ground plane with a coupled microstrip feedline on the other side of the substrate. The radiation patterns by the antenna were directional in the lower 2.4 GHz WLAN band and omnidirectional in the upper 5.2 GHz WLAN band. The gain achieved by the antenna ranged from 1.8 – 3.1 dBi in the two frequency bands. The design of another annular-ring slot antenna with dual-band operation was proposed in [11]. The

antenna consisted of three concentric annular-ring slots etched on the substrate with a coupled microstrip feedline on the other side of the substrate. The radiation pattern achieved was omnidirectional in both the lower and upper WLAN bands. The gain achieved by the antenna ranged from 3.6 – 4.3 dBi.

The design of a convoluted monopole with a wide slot antenna was proposed in [12]. The antenna is a combination of a U-shaped radiating patch, with a T-shaped monopole patch connected to the patch fed with a microstrip line. A pentagonal-shaped wide slot is cut in the ground plane on the other side of the substrate. The antenna has an overall size of 28×28×1 mm^3 and covered the 2.4 GHz WLAN band. It was also matched from 3.1 – 10.6 GHz. The T-shaped monopole resonated at the lower frequency band, while the U-shape patch operated at the higher frequencies. The gain of the antenna was not simulated or measured. The radiation pattern of the antenna was omnidirectional in all the frequency bands of operation.

The literature on omnidirectional WLAN and WiMAX antennas illustrated that dual-band operation can be realized with various shapes and implementation. The antennas are also very small in size and easy to implement. The maximum gain achieved by the various omnidirectional antennas were less than 5 dBi.

2.2.2 Directional WLAN and WiMAX antenna

A study on directional WLAN and WiMAX antennas printed on the substrate was performed next. This study will be more in-depth than with omnidirectional antennas and focuses on antennas that are operational in the WLAN (2.4 GHz, 5.2 GHz and 5.8 GHz) and WiMAX (3.5 GHz) frequency bands with a directional radiation pattern. These antennas are summarized in the following paragraphs to understand how they operate.

A dual-band semi-circular inverted F-shaped antenna was proposed in [14]. The antenna consists of a semi-circular patch with two pairs of semi-circular F-shaped slots and a ground plane spaced 4.6 mm from the antenna. The antenna with the ground plane has an overall

size of 41.4×51.8×4.6 mm^3. The antenna covers the 2.4 GHz, 5.2 GHz and 5.8 GHz WLAN bands, due to the ground plane and has a directional radiation pattern. With a gain of 4.7 and 7.5 dBi in the lower and upper bands, respectively.

An H-shaped strip with rectangular slot and patch antenna was proposed in [15]. The antenna implements comb radiators with substrate integrated suspended line (SISL) technology to achieve a dual-band directional response and operates in the 2.4 GHz, 5.2 GHz and 5.8 GHz WLAN bands. An H-shape strip and rectangular slot was used to achieve the 2.4 GHz band, while a via were used to connect a patch to the feeding line which achieved a resonance that covered the 5.2 GHz and 5.8 GHz bands. The antenna had an overall size of 60×62×5.5 mm^3 and achieved a gain of 2.2 dBi in the lower band and 10.1 dBi in the upper band.

A dual-band triangular monopole was placed vertically on a fractal-based ground plane in [16]. The triangular monopole was 30 mm high and the size of the fractal ground plane was 104×104 mm^2. The ground plane was based on a mod-2 Sierpinski gasket and used four 90° Sierpinksi gaskets rotated 90° from each other. With the ground plane, the antenna achieved a directional radiation pattern and the gain achieved ranged from 4.1 – 5.1 dBi in the lower and upper bands, respectively.

A dual-band patch antenna with U- and T-slots was presented in [17]. The U- and T-slots were combined and underneath the T-slot, a rectangular patch is cut in the ground plane. The rectangular patch in the ground plane increased the impedance bandwidth. The antenna has dual-band characteristics in the 2.4 GHz band and the 5 GHz band for WLAN applications. The patch, as well as the ground plane, is $0.24\lambda_o \times 0.368\lambda_o$ at 2.4 GHz in size and etched on a 4 mm thick FR4 substrate. The radiation properties achieved by the antenna was directional in the 2.4 GHz band, but the radiation pattern distorts in the upper frequency band. Despite the distortion, the antenna still achieved a peak gain of 4.5 dBi and 6.5 dBi in the lower and upper frequency bands, respectively.

A high-gain dual-polarized planar etched slot array antenna, used for WLAN applications is proposed in [18]. The antenna was designed to operate at 2.4 GHz in the WLAN frequency band. Two sets of four co-linear slots were used as radiators for each polarization. A microstrip feed network using 50 Ω microstrip lines and 35 Ω quarter-wave transformers were created for each polarization. A reflector was implemented at a quarter-wavelength away from the slot array to ensure unidirectional radiation. Both substrates were cut to a finite size of $1.76\lambda_o \times 1.76\lambda_o$ at 2.4 GHz with a height of 31 mm. The final antenna achieved a gain of 14.5 dBi with a total efficiency of 85% over the WLAN frequency band.

A dual-band π-shaped slotted microstrip antenna with an aperture-coupled feed was presented in [19]. It was found that etching a π-shaped slot into a patch area generates dual resonances that cover a wide frequency band. The antenna covers the 2.4 GHz WLAN frequency band and the 3.5 GHz WiMAX frequency band. The measured gain at 2.4 GHz was 7.2 dBi and 3.5 GHz was 8.4 dBi. The proposed antenna has a multi-layered aperture-coupled feed configuration, to ensure enhanced gain and a directional radiation pattern. The overall size of the multi-layered antenna was $0.48\lambda_o \times 0.48\lambda_o$ at 2.4 GHz with a height of 11.58 mm.

A printed circular three-antenna system with dual-band applications for 2.4 GHz and 5 GHz WLAN bands is presented in [20]. The antenna consists of three circular dual loops spaced 120° from each other. Each dual-loop antenna includes a large outer loop and a small inner loop and both are operating at one-wavelength resonant mode. The antenna had a diameter of 120 mm. The antenna achieves a directional radiation pattern due to a circular reflector 8.4 mm below the three antennas. With the directional radiation pattern, the antenna achieved a gain of 7 dBi and 8.7 dBi in the lower and upper bands, respectively.

A directional strip-slot antenna for WLAN and WiMAX applications was presented in [21]. The antenna was constructed on a 0.81 mm thick Rogers RO4003C substrate with a microstrip feedline and combined a microstrip stub with a complimentary slot in the ground plane. The antenna design was based on an ultra-wideband slot radiating element in [26]. A ground plane was implemented as a reflector to achieve improved gain and directional

radiation. The antenna with the reflector had an overall size of $0.768\lambda_o \times 0.584\lambda_o$ at 2.4 GHz with a height of 14 mm. The antenna covered the 2.4 GHz, 5.2 GHz and 5.8 GHz WLAN and 3.5 GHz WiMAX frequency bands. Due to the reflecting ground plane, the realized gain at 2.4 GHz, 5.2 GHz and 5.8 GHz was measured to be 9.2 dBi, 7.0 dBi and 10.1 dBi, respectively. With an average gain of 10 dBi in the 3.5 GHz WiMAX band.

The literature study on directional antennas indicated that most of the structures implemented a reflector of some kind to achieve a directional radiation pattern. Due to the directional radiation pattern, a higher gain was also achieved by the antennas when compared to the omnidirectional antennas. A summary of the directional high-gain WLAN and WiMAX antennas found in the literature is shown in Table 2.1.

Table 2.1. Summary of directional antennas

Antenna Reference	**WLAN and WiMAX Frequency Bands [GHz]**	**Volume (L×W×H)[mm^3]**	**Average Gain [dBi]**
[14]	2.4, 5.2, 5.8	41.4×51.8×4.6	6.5
[15]	2.4, 5.8	60×62×5.5	6.2
[16]	2.4, 5.2, 5.8	104×104×30	4.6
[17]	2.4, 5.2, 5.8	30×46×4	5.4
[18]	2.4	220×220×31	14.5
[19]	2.4, 3.5	60×60×11.58	7.8
[20]	2.4, 5.2, 5.8	120×120×8.4	8.2
[21]	2.4, 3.5, 5.2, 5.8	96×73×14	9.1

2.3 LITERATURE STUDY ON ARTIFICIAL MAGNETIC CONDUCTOR (AMC) SURFACES

The design of low profile antennas are desirable for practical implementation. AMC surfaces are implemented as reflectors to reduce the overall height of the antenna. A literature study was performed to understand the implementation of AMC surfaces as reflectors. The literature study on AMC reflectors is divided into two sections, namely single- and multi-band AMC designs. The antennas in the literature study operate in the WLAN and WiMAX frequency bands. Examples of the different AMC designs are presented in each of the sections.

2.3.1 Single-band AMC design

The most important design aspects of an AMC reflector are the reflection phase of the AMC reflector and the electromagnetic bandgap (EBG) performance between the antenna and the ground plane at the bottom of the AMC [27]. The reflection phase of the AMC should ideally be 0° at the center frequency and minimal variation as a function of frequency will ensure optimum bandwidth.

A microstrip patch antenna on top of a two-layer AMC loaded substrate was investigated in [3]. The proposed antenna had a resonant frequency at 2.45 GHz with a reflection coefficient below -10 dB and a gain of 1.53 dBi. The impedance bandwidth achieved by the antenna was 100 MHz, making it adequate to satisfy the IEEE802.11b/g/n standards. Adding an AMC surface to the antenna resulted in a low profile design and the overall volume of the structure was decreased by more than 31%. The effects of various key parameters of the AMC structure was also investigated. Using larger patches and placing them further away from the substrate center resulted in a lower resonant frequency. The feeding impedance can be improved by including a quarter-wavelength transformer, which will improve the reflection coefficient.

The design of a slot antenna combined with a single-band AMC reflector was presented in [27]. The slot was etched on one side of the substrate, which caused the structure to have an omnidirectional radiation pattern. The radiation pattern can be made unidirectional by placing a perfect electric conductor (PEC) a quarter-wavelength below the slot as a reflector. The slot antenna was placed 3 mm above an AMC reflector consisting of an array of rectangular patches, a substrate, and an electrical ground plane. The simulated reflection phase of the AMC surface was 0° at 2.45 GHz with a -90° to +90° phase bandwidth from 2.28 – 2.64 GHz (14.6%), which makes it suitable for the 2.4 GHz WLAN band. The final antenna had a size of 125×100×7.662 mm^3 and an AMC with a size of 185×185 mm^2. The final antenna design had an impedance bandwidth from 2.4 – 2.5 GHz (4.1%) and the measured gain varied between 9.8 and 10.3 dBi across the frequency band. The total efficiency is better than 85% over the entire 2.4 – 2.5 GHz band, with a unidirectional radition pattern.

In [28] a single-band AMC surface was combined with a slot antenna. The simulated reflection phase of the AMC surface was 0° at 5.5 GHz with a ±90° phase bandwidth from 5.1 – 5.9 GHz (14.5%), which covers the 5.2 GHz and 5.8 GHz WLAN bands. The slot antenna combined with the AMC surface achieved a -10 dB impedance bandwidth from 4.83 – 6.25 GHz (25.6%), which covers the 5.2 GHz and 5.8 GHz WLAN bands. The gain of the antenna ranged from 5.5 – 6.1 dBi across the wide frequency bandwidth. The overall size of the slot antenna with AMC surface is 60×60×8 mm^3. The antenna achieved a directional radiation pattern with the addition of the AMC surface.

2.3.2 Multi-band AMC design

Multiple dual-band AMC antennas are presented in [22]–[24], [27], [29]–[33]. A dual-band C-slotted textile antenna suitable for wireless body area network (WBAN) applications is presented in [23]. The AMC has resonant frequencies at 2.45 GHz and 5.8 GHz. Two antennas were investigated in the paper. Antenna A was a combination of the antenna with an AMC reflector, while antenna B did not feature the AMC reflector. Antenna A achieved impedance bandwidths of 123 MHz and 714 MHz with gains of 5.26 dBi and 10.7 dBi at

2.45 and 5.8 GHz, respectively. Antenna B achieved narrower impedance bandwidths of 98 MHz and 480 MHz and gains of 1.28 dBi and 3.4 dBi at 2.45 GHz and 5.8 GHz, respectively. This indicates that the addition of the AMC reflector improved the gain of the antenna. The AMC was designed with a 3×3 diamond shaped unit cell, with a gap between each unit cell to ensure optimum radiation. The overall size of the antenna was $90\times90\times6.51mm^3$.

The technique of combining multimode resonances was applied to design a dual-wideband circularly polarized antenna, which was presented in [22]. The primary radiators are two barbed-shaped dipoles and two bowtie dipoles printed on the same substrate. The radiators were placed over a finite AMC surface, which was constructed with 6×6 square metallic plates printed on a 72×72 mm² substrate for a low profile design. The final design had an overall size of $72\times72\times20.7\ mm^3$ at 2.4 GHz and the measured impedance bandwidths were from 2 – 3 GHz (40%) and from 3.8 – 6.3 GHz (49.5%), making the antenna suitable for the 2.4 GHz, 5.2 GHz and 5.8 GHz WLAN bands. The antenna exhibited directional radiation with an average gain of 6.6 dBi and 7.4 dBi across the lower and upper bands, respectively. The antenna was fed with an SMA connector at the bottom of the AMC surface.

In [24] a V-shaped slot is etched out of a CPW-fed trapezoidal shaped monopole antenna for dual-band operation and was placed over a dual-band AMC surface operating in the WLAN frequency bands. A 3×3 unit cell AMC surface was combined with the antenna. The antenna with the AMC reflector has an overall size of $57\times57\times8\ mm^3$. A foam spacer with a height of 8 mm was used between the antenna and AMC surface in [24] and this gives the antenna to have an overall height of 12.68 mm. The proposed antenna operated from 2.23 – 2.50 GHz (11.4%) and 4.98 – 5.87 GHz (16.4%), which covers the 2.4 GHz, 5.2 GHz and 5.8 GHz WLAN frequency bands. Due to the implementation of the AMC reflector, a directional radiation pattern was achieved with a peak gain of 6.64 dBi and 7.84 dBi at 2.4 GHz and 5.5 GHz, respectively.

The design of two different dual-band antennas with an AMC surface integrated with clothing was proposed in [29] and [30]. The dual-band antenna designed in [29] operates in

the WLAN frequency bands and was integrated into clothing. The antenna consisted of a textile monopole antenna fed by a coplanar waveguide closed rectangular ring with a vertical strip. The antenna was placed over an AMC surface, which consisted of a 3×3 matrix with concentric squares. The substrate used for the AMC surface was Neltec, which has a dielectric constant of ε_r=2.2, a loss tangent of tanδ=0.0009 and a thickness of 3.15 mm. The substrate used for the antenna was cotton jeans, which was characterized with a dieletric constnat of ε_r=1.67, tanδ=0.03 and had a thickness of 2.84 mm. The antenna was placed 1.5 mm above the AMC surface. The total height of the final antenna was 7.18 mm. The overall volume of the antenna with the AMC surface is 88.5×88.5×7.18 mm^3. The final antenna operated from 2.4 – 2.56 GHz (6.5%) in the first band and from 5.5 – 6 GHz (8.7%) in the second band, making it suitable for the 2.4 GHz and 5.8 GHz WLAN bands. The gain achieved by the antenna was approximately 5.125 dBi and 3.97 dBi at 2.45 GHz and 5.8 GHz, respectively.

A low profile dual-band textile antenna with an AMC reflector for WLAN applications was proposed in [30]. The layout of a patch antenna combined with a slot dipole delivered the dual-band properties in the 2.4 GHz, 5.2 GHz and 5.8 GHz WLAN bands. The dual-band operation was a combination of the patch in the 2.4 GHz band along with a patch-etched slot dipole in the 5 GHz band. The AMC reflector was implemented to achieve a low profile design and to suppress the back-lobe radiation to minimize the electromagnetic coupling with the human body. The AMC reflector achieved a ±90° phase bandwidth from 5.04 – 5.935 GHz (16.3%). The two frequency bands obtained by the final antenna were from 2.4 – 2.484 GHz (3.4%) and from 5.04 – 5.935 GHz (16.3%), which covers the 2.4 GHz, 5.2 GHz and 5.8 GHz WLAN bands. The antenna with the AMC surface has an overall volume of 100×100×3.34 mm^3. The gain achieved by the antenna was 2.5 dBi at 2.45 GHz and between 0 dBi and 4 dBi in the higher frequency band, with a total efficiency of more than 40% throughout the whole frequency band.

A multiband-integrated AMC antenna is presented in [31]. The antenna is combined with an AMC reflector and operated from 1.5 GHz to 6 GHz. The antenna consists of a wideband

circular monopole antenna and was combined with a dual-band AMC reflector. This resulted in a low profile antenna with multiband performance. The monopole antenna was printed on a 1.6mm thick FR4 (ε_r=4.4) substrate, while the AMC was also constructed on a 3.2 mm thick FR4 (ε_r=4.4) substrate. The monopole antenna with the AMC reflector has an overall size of 88×88×7.8 mm^3. The AMC reflector achieved a 0° reflection phase at 2.0 GHz and 5.8 GHz with a ±90° phase bandwidth of 4.9% and 7.6% in the lower and upper bands, respectively. The final antenna operated over two frequency bands 1.5 – 2.7 GHz (57.1%) and 4 – 6 GHz (40%), which covers 2.4 GHz, 5.2 GHz and 5.8 GHz WLAN bands. The final gain achieved by the antenna was 5.3 dBi and 4.4 dBi at 2.0 GHz and 5.5 GHz, respectively. An investigation illustrated that the bandwidth of the antenna can be improved by increasing the height between the antenna and the AMC reflector, but a trade-off has to be made between the overall volume of the antenna and the bandwidth achieved.

The layout of a triple-band AMC structure was proposed in [34]. The AMC operates at three frequencies which are 2.3 GHz, 5.8 GHz, and 8.36 GHz and have bandwidths of 5.64%, 1.73%, and 3.58%, respectively. The AMC was designed on FR4 substrate, with a thickness of 1.6 mm. The triple-band AMC reflector was combined with a wideband monopole antenna which operated from 2.69 – 6.27 GHz (79.9%) [34]. The combination of the antenna with the AMC reflector resulted in an overall size of 62.01×62.01×3.6 mm^3. The combination of the wideband antenna with the triple-band AMC operated at 2.3 GHz, 5.11 GHz and 9.41 GHz with bandwidths of 4.2%, 21.9% and 5.1%, respectively. The gain achieved with the triple-AMC reflector was 6.16 dBi, 7.65 dBi and 6.25 dBi at 2.3 GHz, 5.11 GHz and 9.41 GHz, respectively.

The design of various directional antennas have been proposed in the literature that combine the antenna with an artificial magnetic conductor (AMC). The combination of the antenna with an AMC reflector results in a low profile design with a high gain and directional radiation. A summary on multi-band antennas with AMC reflectors in the WLAN and WiMAX frequency bands found in the literature is presented in Table 2.2.

Table 2.2. Summary of multi-band antennas with AMC reflectors

Antenna Reference	WLAN and WiMAX Frequency Bands [GHz]	Size (L×W×H)[mm^3]	Average Gain [dBi]
[23]	2.4, 5.8	90×90×6.5	8.0
[22]	2.4, 5.2, 5.8	80×80×20	7.0
[24]	2.4, 5.2, 5.8	57×57×12.68	7.2
[29]	2.4, 5.2, 5.8	88.5×88.5×7.18	4.5
[30]	2.4, 5.2, 5.8	100×100×3.34	2.0
[31]	2.4, 5.2, 5.8	88×88×7.8	4.9
[34]	2.4, 5.2, 5.8	62.01×62.01×3.6	6.7

2.4 CHAPTER SUMMARY

The literature study was performed in this chapter, where the design of various antennas for WLAN and WiMAX applications were presented. It was found that various omnidirectional antennas designs are available for WLAN applications, but low profile directional WLAN antennas are rather limited. The combination of AMC reflectors with antennas for WLAN applications and a low profile design is a growing field. The antenna summary indicated that the combination of antennas with AMC reflectors allow for a low profile antenna with high gain. The summary of the directional antennas in Table 2.1 and the antennas with AMC reflectors in Table 2.2 give a summary of the antennas found in the literature. In Table 2.1 the majority of the antennas covered the 2.4 GHz, 5.2 GHz and 5.8 GHz WLAN bands, but the only directional antenna covering the 3.5 GHz WiMAX band as well was presented in [21]. The antenna has an overall size of 96×73×14 mm^3 with an average gain of 8.8 dBi across the WLAN and WiMAX frequency bands. In Table 2.2 it was noticed that the majority of the antennas also covered the 2.4 GHz, 5.2 GHz and 5.8 GHz WLAN bands, while none of the antennas with an AMC reflector covered the 3.5 GHz WiMAX band.

CHAPTER 3 BACKGROUND

3.1 CHAPTER OBJECTIVES

In this chapter, the design of a directional strip-slot antenna as proposed in [21] will be used as a starting point. The various aspects implemented by the strip-slot antenna to achieve the WLAN and WiMAX frequency bands are investigated and discussed. The antenna consists of a substrate with a microstrip feedline, with a strip-slot pair and a short circuit termination. The antenna is then combined with a PEC reflector. The combination of the antenna with the PEC reflector, achieved a resonance in the 2.4 GHz WLAN band. This was due to the ground plane of the antenna and the PEC reflector supporting a patch mode. The upper 5.2 GHz and 5.8 GHz WLAN frequency bands were achieved by the width and length of the strip-slot pair. A background study will be presented on slot antennas, patch antennas, the strip-slot pair structure, as well as additional slot elements, to fully understand the operation and function of each component. The design of a single-, dual- and triple-band AMC reflector is also performed.

3.2 NUMERICAL MODEL

The design and analysis of antennas is done primarily with numerical approximations to Maxwell's equation. The initial implementations were restricted to very colloquial problems by using methods such as the Uniform Theory of Diffraction (UTD) and 2D formulations of the Method of Moments (MoM) [35]. The advances in computers, computational power and the improvement in the numerical techniques have resulted in the development of commercially available software packages such as FEKO, CST and HFSS. The numerical solvers utilized are discussed in the following subsections.

3.2.1 Numerical solvers

The analysis of more complex antenna geometries require the applications of numerical approximations. Various Computational Electromagnetic (CEM) techniques, which are numerical approximations to Maxwell's equations, are discussed in this section. The various

techniques have certain advantages and drawbacks and it is important to ensure that the correct technique is applied for the problem. The numerical techniques for computational electromagnetics can be divided into full-wave methods and high-frequency methods [35]. High-frequency methods are based upon asymptotic expansions or assumptions about the current and are best suited to objects that are large in size. The full-wave methods approximate Maxwell's equations numerically and includes the antenna and also the surrounding space. The full-wave method is mainly applied to objects whose size in three dimensions are within an order of magnitude or two of the wavelength. The three well-known full-wave techniques are the Method of Moments (MoM), Finite Element Method (FEM) and Finite Difference Time Domain (FDTD) and will be discussed in the following sections. The various methods are available in the commercial electromagnetic software packages CST and FEKO [25], [36]. The details of each method and the implementation of it are beyond the scope of this dissertation. A detailed discussion on the various methods are presented in [35]. The advantages and drawbacks of each method is discussed to provide background with the choice of method used in this study.

3.2.1.1 Method of Moments (MoM)

The Method of Moments method is a full-wave method, CEM technique that uses the integral based equations of Maxwell's equations in the frequency domain [35]. FEKO is a commercial electromagnetic software package that implements the MoM method. The method replaces the radiating surface of a structure with equivalent currents. Once the current distribution is known, the radiation integral can be implemented to determine the radiation patterns. The structure is first discretized into various segments and then the current over each segment is calculated. A wire structure is discretized with segments, while a surface with triangles [35].

The current over each segment is where the approximation of Maxwell's equations are applicable. Basis functions are used to determine the current dependency across a single element. The influence of the elements on each other is then calculated from the appropriate Green's function. The applications of boundary conditions is applied on each, which produces a set of linear equations that can be solved [35].

The main advantage with the MoM solver is that only surfaces are discretized and not the volume between the structures. This indicates that the solver will be highly efficient for models containing mainly conducting surfaces. The disadvantage of the MoM solver is that a large model size and wideband simulation will require a significant amount of RAM for computational purposes. The MoM operates in the frequency domain and has to recalculate the solution for each frequency point [25].

3.2.1.2 Finite Difference Time Domain (FDTD) method

The Finite Difference Time Domain method is a full-wave method, CEM technique that uses the differential formulation of Maxwell's equations [35]. The software package CST implements a variation of the FDTD method, where instead of the differential formulation the integral equations are used. This is referred to as the Finite Integration Technique (FIT) [25]. The FDTD method discretizes the structure with a 3D staggered grid. The differential equations (or integral equations) are then applied to the field quantities (*E*- and *H*-fields) of the staggered grid points in space and time [35].

The advantage of FDTD is that it is a time domain method and can be implemented for wideband responses with a single simulation, where the MoM has to solve the solution for each frequency. The computational time required for the FDTD method is slightly better than that of MoM [25]. The disadvantage of FDTD is that structure is discretized by a 3D staggered grid. This means that for curved shapes, a staircase mesh will be present and will lead to inaccuracies [37]. To overcome this problem, various approaches have been proposed with the implementation of non-orthogonal FDTD grids as well as locally conformal grids which requires a much finer division of the structure [38], [39]. This means that FDTD requires a significant amount of memory for larger scale structures, due to the discretization of the structure in three dimensions. With MoM only the conducting surfaces of the structure are used to solve the equations. This means that the FDTD requires more computational power than MoM, when the problem only consists of PEC structures.

3.2.1.3 Finite Element Method (FEM)

The Finite Element Method (FEM) is a full-wave method that implements the differential formulation of Maxwell's equations in the frequency domain [35]. With the FEM method, the problem is solved by discretizing the structure with triangles for surfaces and tetrahedrons for volumes. The FEM method solves the problem by calculating Maxwell's partial differential equations on the *E*-fields by applying boundary conditions and initial values. This produces a set of linear equations that can be solved by applying standard matrix algebra.

The advantage of the FEM method is that it is applicable to small, complex and closed region structures. The computational time required for an analysis of a model with the FEM method is slightly better than MoM for PEC structure [25]. The disadvantages of FEM is that, due to the triangular meshing of a structure, a large number of mesh elements would be required to model in three dimensions (surface meshing versus volume meshing). This makes FEM more applicable to smaller structures with complex geometries. The radiation condition is not part of the FEM formulation and boundary conditions have to be used to calculate the radiation and scattering [25].

The commercial software package used for the design and simulation of the study is CST Microwave Studio [25]. The software package has a variety of solvers available for different structures and implementations. The layout of the proposed antennas are electrically small in wavelength and rather complex and also achieve a multi-band response. The frequency domain is used due to the multi-band operation of the antennas. The advantages and disadvantages of the MoM and FEM numerical solvers in the frequency domain were analyzed. The MoM solver discretizes a surface with triangles, while the FEM solver discretizes the volume of the structure with tetrahedrons. The FEM solver requires less computational time for an analysis of the model and is also applicable to small, complex structures. The implementation of the FEM solver was used for the study as the structure is rather small in size and complex.

3.3 DIRECTIONAL STRIP-SLOT PAIR ANTENNA

The strip-slot radiating antenna proposed in [21] was used as a starting point for this study. The antenna consists of a microstrip feedline, with a slot in the ground plane and a complementary strip, which is approximately the same size as the slot. The microstrip feedline was terminated with via to the ground plane, which caused a short circuit on the feedline. The short circuit termination formed a standing wave on the feedline, which results in a high total efficiency. A high gain and directional radiation pattern was achieved by placing a PEC reflector a quarter-wavelength at 5 GHz away from the antenna. The length between the antenna and the PEC was chosen to cover the 5.2 GHz and 5.8 GHz WLAN band. The overall size of the antenna was $96\times73\times14$ mm^3 and the antenna was fed with a coaxial transmission line. The strip-slot antenna was reproduced in CST. The geometry of the strip-slot antenna without the PEC reflector is shown in Figure 3.1, while the antenna combined with the PEC reflector is shown in Figure 3.2.

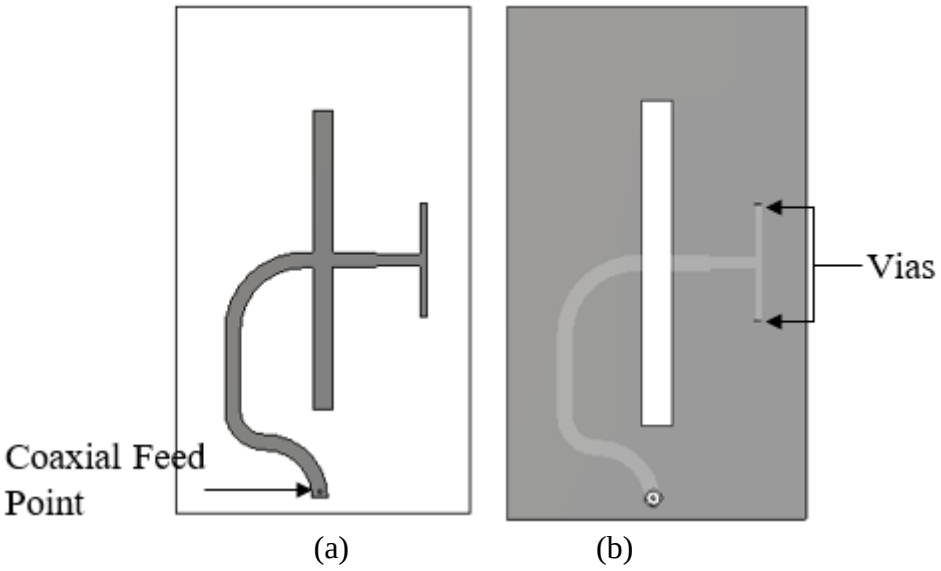

Figure 3.1. Geometry of strip-slot antenna without PEC reflector

(a) top view of antenna (b) bottom view of antenna

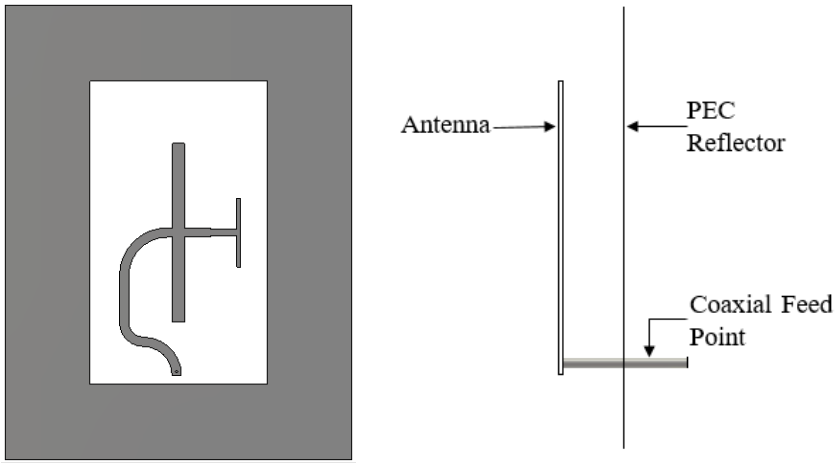

Figure 3.2. Geometry of strip-slot antenna with PEC reflector

(a) top view of antenna with PEC reflector (b) side view

The antenna was constructed in CST and simulated from 2 – 6 GHz. The simulated reflection coefficient and realized gain of the strip-slot antenna is shown in Figure 3.3 and Figure 3.4.

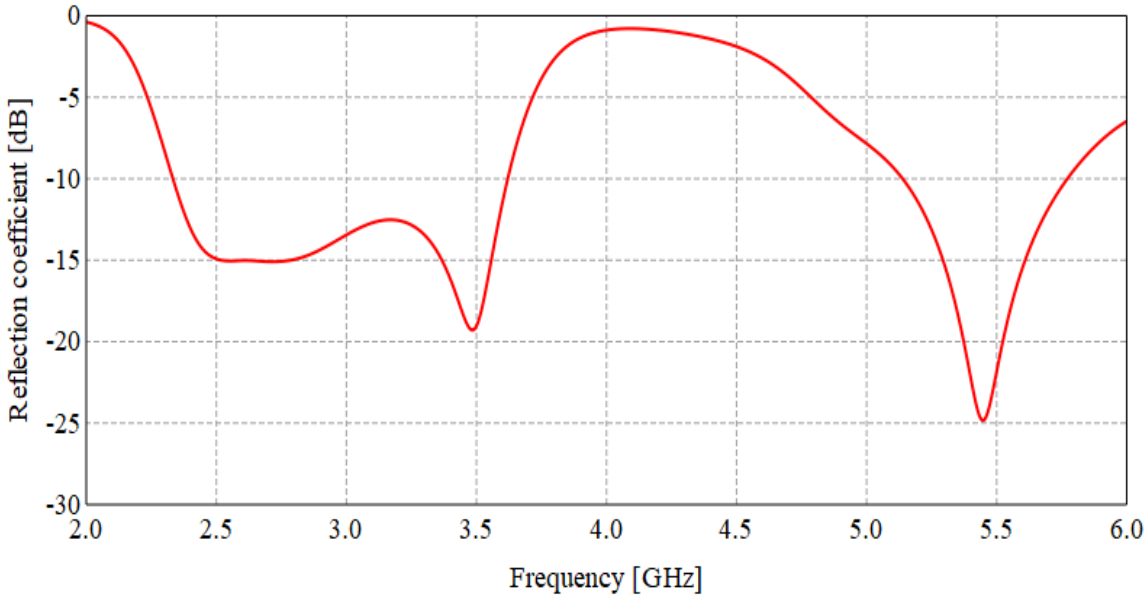

Figure 3.3. Simulated reflection coefficient of strip-slot antenna

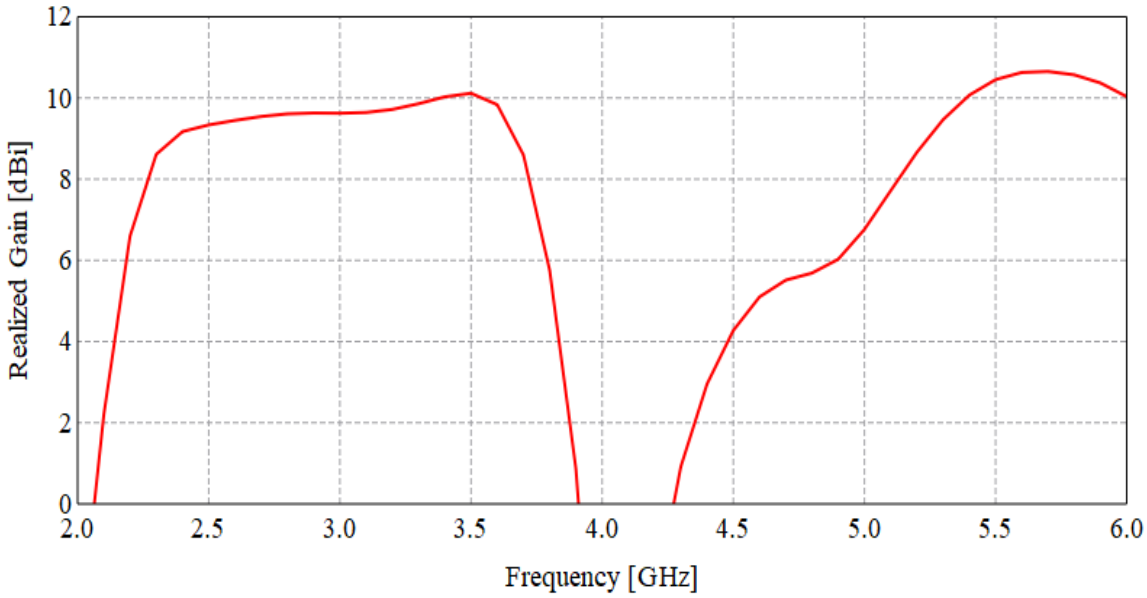

Figure 3.4. Simulated realized gain of strip-slot antenna

The simulated reflection coefficient of the strip-slot antenna achieves a -10 dB impedance bandwidth from 2.33 – 3.62 GHz (43.4%) and 5.14 – 5.77 GHz (11.5%). The antenna covers the 2.4 GHz, 5.2 GHz and 5.8 GHz WLAN and 3.5 GHz WiMAX frequency bands. The lower operating frequency at 2.4 GHz is controlled by the size of the ground plane of the antenna substrate. The reflector and the ground plane of the antenna support a radiating patch mode, with the air gap as a dielectric medium and the PEC reflector as the ground plane. The upper operating frequency is controlled by the length of the strip-slot pair. The simulated realized gain of the antenna was 9.2 dBi, 10.1 dBi, 8.7 dBi and 10.6 dBi at 2.4 GHz, 3.5 GHz, 5.2 GHz and 5.8 GHz, respectively. The strip-slot antenna achieves a high-gain across the WLAN and WiMAX frequency bands with an overall average gain of 9.1 dBi. The operation of the strip-slot antenna will be used as a basis for the proposed antenna. The lower operating resonance at 2.4 GHz resulted from the reflector and the ground plane of the antenna which excited a patch mode from the ground plane of the antenna. The individual radiators will be discussed in more detail.

3.4 PATCH ANTENNA

The design of rectangular patch antennas will be investigated for the proposed antenna. The design procedure for a patch antenna assumes that the specified information includes the dielectric constant of the substrate (ϵ_r), the resonant frequency (f_r) and the height of the antenna substrate (h) [40]. The width of the antenna is determined with the following equation

$$W = \frac{v_0}{2f_r}\sqrt{\frac{2}{\epsilon_r + 1}} \tag{3.1}$$

where the constant v_0, is the free-space velocity of light. The effective dielectric constant of a microstrip line is calculated with the following equation [27]

$$\epsilon_{eff} = \frac{\epsilon_r + 1}{2} + \frac{\epsilon_r - 1}{2}\left[1 + 12\frac{h}{W}\right]^{-1/2}. \tag{3.2}$$

The extension of the patch length, ΔL, can then be calculated by using the following equation [27]

$$\frac{\Delta L}{h} = 0.412\frac{\left(\epsilon_{eff} + 0.3\right)\left(\frac{W}{h} + 0.264\right)}{\left(\epsilon_{eff} - 0.258\right)\left(\frac{W}{h} + 0.8\right)}. \tag{3.3}$$

The extension of the patch length is used to calculate the actual length of the patch and can be determined by solving for L in the following equation [27]

$$L = \frac{1}{2f_r\sqrt{\epsilon_{eff}}\sqrt{\mu_0\epsilon_0}} - 2\Delta L. \tag{3.4}$$

Equation (3.1) to (3.4) are used to determine the width and length of a rectangular patch antenna. The calculations for the size of the patch give approximate values and the final dimensions of the patch have to be optimized to achieve the desired results. The strip-slot

antenna implemented the ground plane of the antenna with the PEC reflector as a radiating patch mode. The design of a patch antenna will then be implemented to determine the size of the ground plane of the antenna.

3.5 SLOT ANTENNA

The strip-slot antenna in [21] incorporates a full-wavelength slot in the ground plane.The operation of full- and half-wavelength slot antennas will be investigated in this subsection. The slot antennas will be simulated on Rogers RO4003C, which has a dielectric constant of 3.38, a loss tangent of 0.0027 and a thickness of 0.81 mm. The length of the slot is used for the frequency of operation. The impedance of the slot increases with an increase in the width of the slot. The length of the slots will be designed to operate at 5.4 GHz. The slot wavelength, λ_s, can be calculated by the following equations [41]

$$\lambda_0 = \frac{v_0}{f} \tag{3.5}$$

$$\lambda_s = \frac{\lambda_0}{\sqrt{\epsilon_{eff}}} \tag{3.6}$$

where the constant v_0, is the free-space velocity of light, f is the frequency of operation and λ_0 is the free-space wavelength. The dielectric constant for the slot, ϵ_{eff}, is determined by the dielectric constant of the substrate, ϵ_r, as well as the air as medium for transmission. The effective dielectric constant for the slot, if the slot width, W_S, is much smaller than the free-space wavelength, λ_0, can be calculated by the average of the two mediums in the following equation [41]

$$\epsilon_{eff} = \frac{\epsilon_r + 1}{2}. \tag{3.7}$$

In this case, λ_s=37.54 mm at a frequency of 5.4 GHz, which is a full-wavelength slot. The design of various slot antennas are presented in literature [42]–[45]. Slot antennas offer the advantage of being easy to fabricate with the possible realization of higher order modes. The

drawback of slot antennas is that they are relatively lossy compared to other lines and that they cannot be used for broadband applications.

The operation of a single microstrip feedline with a slot in the ground plane was simulated on a substrate with a size of 65×65 mm^2. The length of the slot s λ_s=40.63 mm, which is close to a full-wavelength, and the slot width is w_s=1.79 mm. The slot in the ground plane of the antenna is excited by the proximity coupling of the magnetic fields from the microstrip line [46]. The layout of the full-wavelength slot antenna is shown in Figure 3.5.

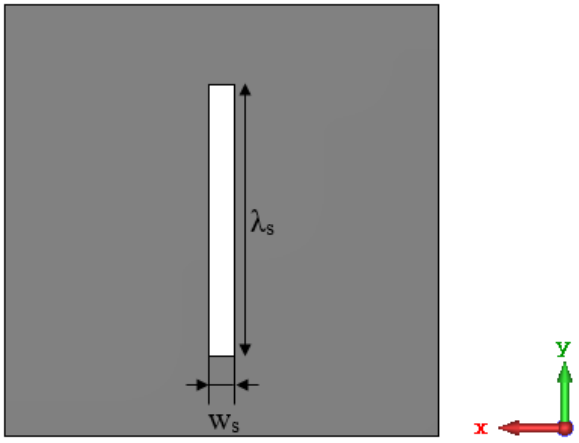

Figure 3.5. Layout of microstrip fed full-wavelength slot in the ground lane

The E_x-fields of the full-wavelength slot antenna was simulated on the ground plane of the antenna at 5.4 GHz, to illustrate the field distribution of the slot. The simulated E_x-field of the full-wavelength slot antenna is shown in Figure 3.6 (a). The simulated *E*-vector fields were also simulated at 5.4 GHz as shown in Figure 3.6 (b). This illustrates that the slot operates at a full-wavelength.

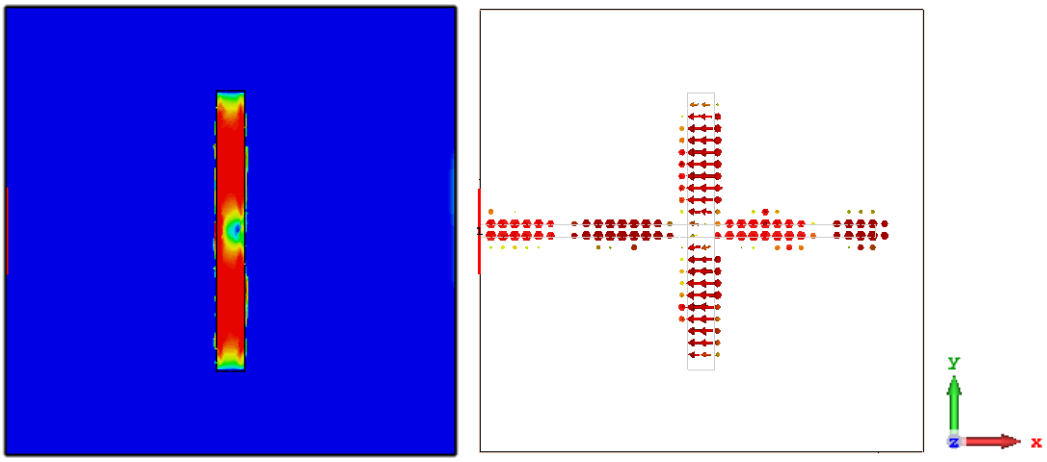

(a) (b)

Figure 3.6. Simulated fields of full-wavelength slot antenna at 5.4 GHz

(a) E_x-fields (b) E-vector fields

The simulated E_x-fields illustrate that a maximum electric field is present in the top and bottom half of the slot, corresponding to two half-wavelength resonant structures. The arrows on the simulated E-vector fields indicate that the field distribution in the top and bottom halves of the slot are in phase. The simulated fields indicate that the slot operates as two half-wavelength resonant slots, which radiate in phase at 5.4 GHz.

The operation of a half-wavelength slot was also investigated by using equations (3.5) to (3.7) and dividing the length of the slot by 2. The calculated length of the half-wavelength slot was λ_s=18.77 mm, while the slot has a width of w_s=1.8 mm. The layout of the slot antenna with a half-wavelength slot at 5.4 GHz is shown in Figure 3.7.

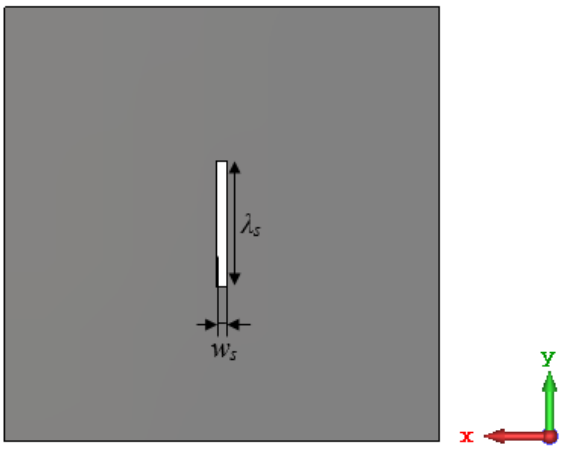

Figure 3.7. Layout of microstrip fed half-wavelength slot in the ground lane

The E_x-fields were simulated on the ground plane of the antenna at 5.4 GHz, to illustrate the distribution of the fields. The simulated E_x-fields of the half-wavelength slot are shown in Figure 3.8 (a). The simulated *E*-vector fields were also simulated at 5.4 GHz and is shown in Figure 3.8 (b).

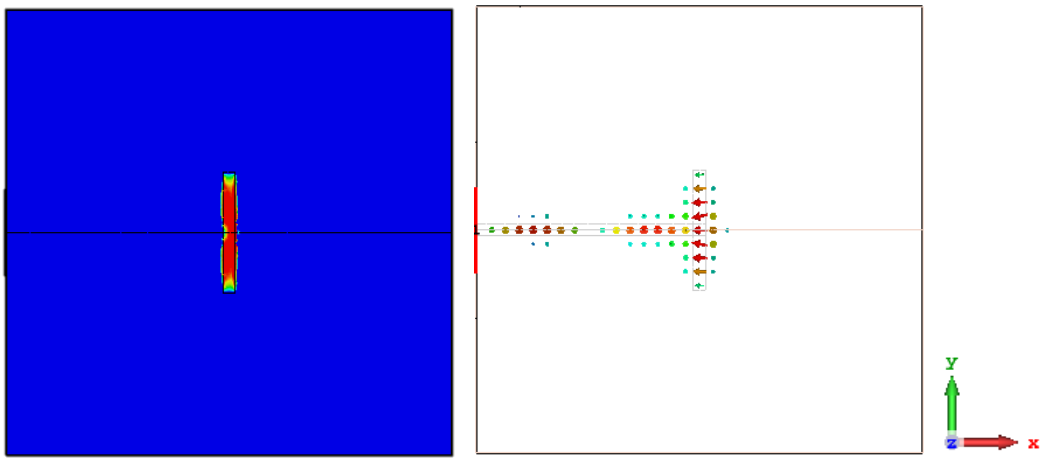

(a) (b)

Figure 3.8. Simulated fields of half-wavelength slot antenna at 5.4 GHz

(a) E_x-field (b) *E*-vector fields

The simulated E_x- and *E*-vector fields at 5.4 GHz for this slot antenna illustrates that a typical half-wavelength resonant standing wave field distribution is present in the slot. This indicates that a full-wavelength as well as a half-wavelength slot can be realized.

3.5.1 Double slot

The impedance bandwidth achieved by a slot antenna is not wide enough to cover the entire 5.2 GHz and 5.8 GHz WLAN bands. The impedance bandwidth of a slot antenna can be improved by including an additional slot element close to the slot in the ground plane. The structure of a dipole array with parasitic dipole elements was implemented in [47]. The combination of the parasitic dipoles with the original dipoles increased the impedance bandwidth from 2.8% to 5.8% with a center frequency of 9.5 GHz. This method is implemented for the slot antenna to increase the impedance bandwidth of a single slot by placing a secondary slot-element in close proximity to it.

The effect of a secondary slot-element was implemented to achieve dual resonances and cover the 5.2 GHz and 5.8 GHz WLAN bands. The length and width of the first slot is L_{s1} = 50.79 mm and w_{s1} = 4.93 mm, respectively. The length and width of the secondary slot is L_{s2} = 56.07 mm and w_{s2} = 5.44 mm. The center of the secondary slot element was placed 6 mm away from the original slot. The layout of the substrate consisted of a microstrip feedline being terminated by a three-quarter wavelength (25.506 mm) open circuit at 5.4 GHz with a slot and secondary slot in the ground plane as shown in Figure 3.9.

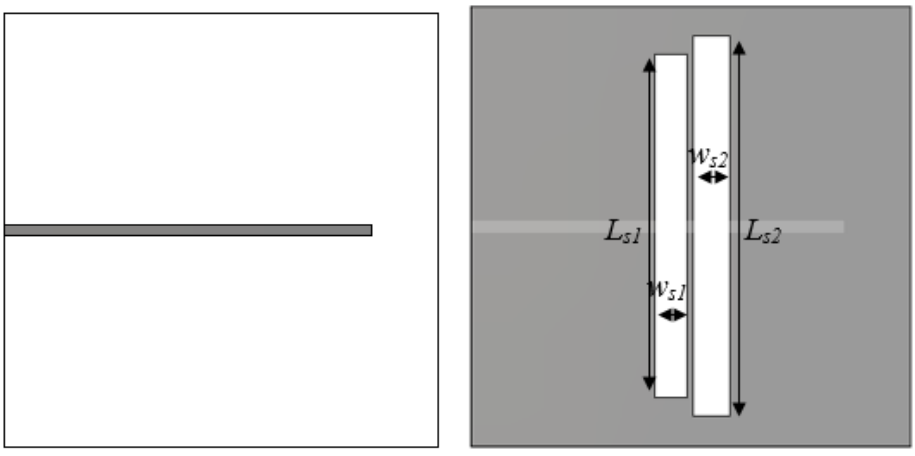

(a) (b)

Figure 3.9. Layout of slot antenna with a secondary slot-element

(a) top view (b) bottom view

The design of the slot with a secondary slot element was simulated and compared to the microstrip line with only a single slot in the ground plane. The simulated reflection coefficient is shown in Figure 3.10.

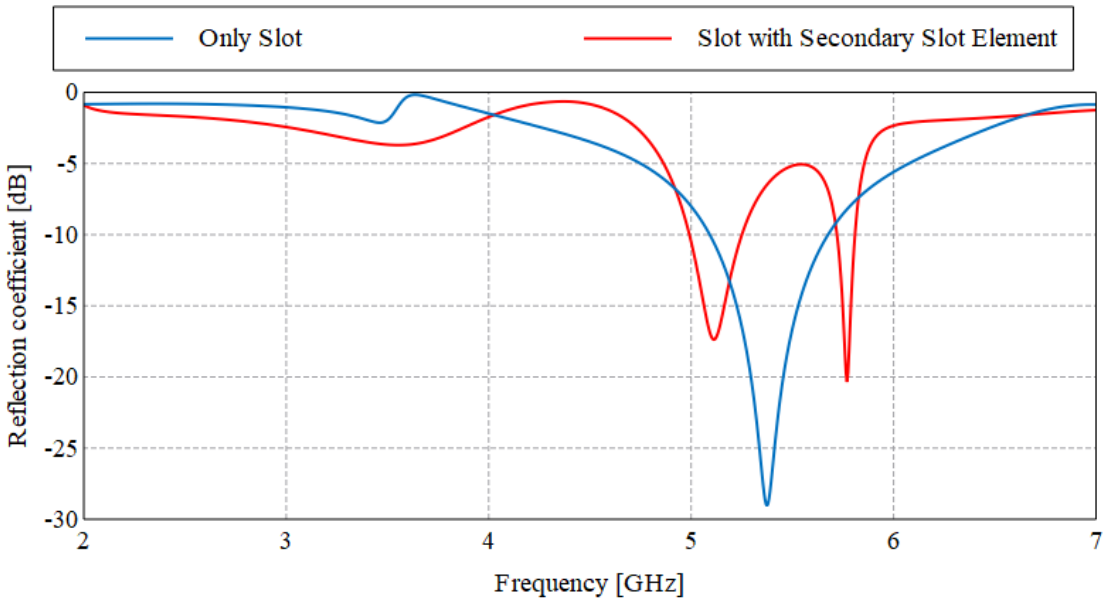

Figure 3.10. Simulated reflection coefficient of slot with secondary slot element

The simulated reflection coefficient illustrates that the addition of the secondary slot produced a second resonance in the upper frequency band. The -10 dB impedance bandwidths achieved by the two resonances are from 4.99 – 5.25 GHz (5.08%) and from 5.72 – 5.81 GHz (1.56%). The first resonance covers the entire 5.2 GHz WLAN frequency band, but the second resonance does not cover the entire 5.8 GHz WLAN frequency band. The results illustrate that the addition of the secondary slot produced the second resonance close to the original and this principle can be used increase the impedance bandwidth and cover the entire 5.2 GHz and 5.8 GHz WLAN bands.

3.6 STRIP-SLOT PAIR

The strip-slot antenna in [21] implements the design of a complementary microstrip-slot pair. The design and analysis of the complementary strip-slot structure is based on the ultra-wideband slot radiating element in [26]. In [26] an even- and odd-mode analysis of a single

microstrip-slot coupled subsection was performed and the electric field distribution between the two modes were investigated. The coupled line configuration between the microstrip and the slotline, resulted in bandwidth enhancement. The investigation also found that in the odd-mode, the electric field was focused in the gap and exhibits a distribution that is similar to the response of a slot. With the even-mode analysis, the distribution of the electric field was focused around the strip, which was similar to the response of a microstrip line [26]. The even- and odd-modes in [26] are referred to as quasi-strip and quasi-slot modes for the even- and odd-modes, respectively. The following equations can be used to achieve an estimate of the even- and odd-mode parameters [26]

$$Z_{0e} \approx 2Z_M;\ \ \varepsilon_{eff,e} \approx \varepsilon_{eff,M} \tag{3.10}$$

$$Z_{0o} \approx \frac{Z_S}{2};\ \ \varepsilon_{eff,o} \approx \varepsilon_{eff,S}. \tag{3.11}$$

The parameters Z_{0e} and Z_{0o} are the even- and odd-mode characteristic impedances of the strip-slot structure. The parameters Z_M and Z_S, are the characteristics impedances for the microstrip line and slotline, respectively. The parameter ε_{eff}, is the effective permittivity of the even- and odd-modes for the microstrip line and slotline, respectively. The image impedance can be calculated from the characteristic impedances for the even- and odd-modes, with the following equation [26]

$$Z_{im} = \sqrt{Z_{0e}.Z_{0o}.\cot(\theta_e)\,.\,\cot(\theta_o)}. \tag{3.12}$$

The parameters θ_e and θ_o are the electrical lengths of the even- and odd-mode, respectively. By neglecting the losses, the electrical lengths can be expressed in terms of the microstrip and slot lengths with the following equations [26]

$$\theta_e = \sqrt{\varepsilon_{eff,M}} \times L_M \tag{3.13}$$

$$\theta_o = \sqrt{\varepsilon_{eff,S}} \times L_S. \tag{3.14}$$

The length, L_M, is the length of the microstrip from the feedline and the length, L_S, is half the length of the slot. When the electrical lengths of the even- and odd-modes are equal to each other ($\theta_e=\theta_o$), the characteristic impedance of the microstrip feedline can be calculated as [26]

$$Z_0=\frac{1}{2}\sqrt{Z_{0e}.Z_{0o}} \tag{3.15}$$

which is also used as a design condition to achieve impedance matching with the microstrip feedline. The structure of the strip-slot pair can be expressed by the four parameters w_M, w_S, L_M and L_S, which represent the widths and lengths of the microstrip and slotline.

The design equations of the strip-slot pair were implemented. The length of the microstrip, L_M, was calculated to be 17.84 mm from the feedline and the width of the strip, w_M was 2.51 mm. The length of the slot, L_S, was calculated to be 20.32 mm from the center of the slot, with a slot width, w_S, of 3.94 mm. The length of the open circuit termination from the strip-slot pair, g = 25.506 mm. The layout of the microstrip feedline with a strip-slot pair is shown in Figure 3.11. The simulated reflection coefficient of the strip-slot pair is compared to the slot antenna and is presented in Figure 3.12.

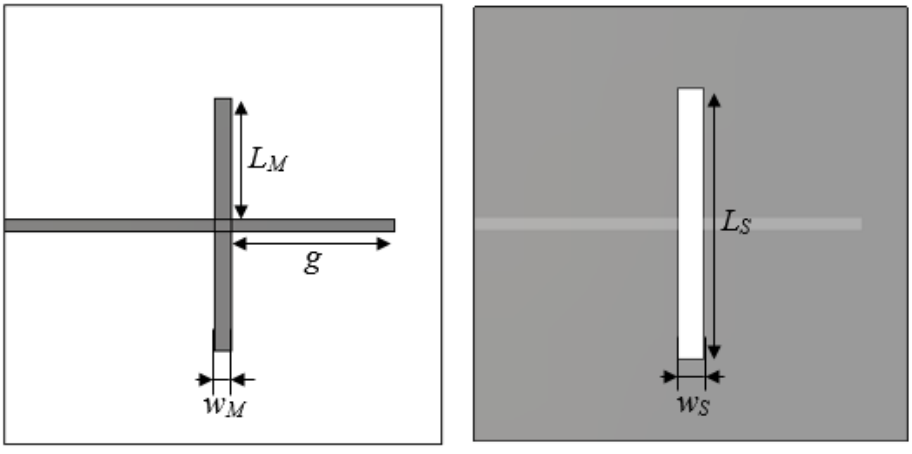

(a) (b)

Figure 3.11. Layout of strip-slot pair with three-quarter open circuit termination

(a) top view (b) bottom view

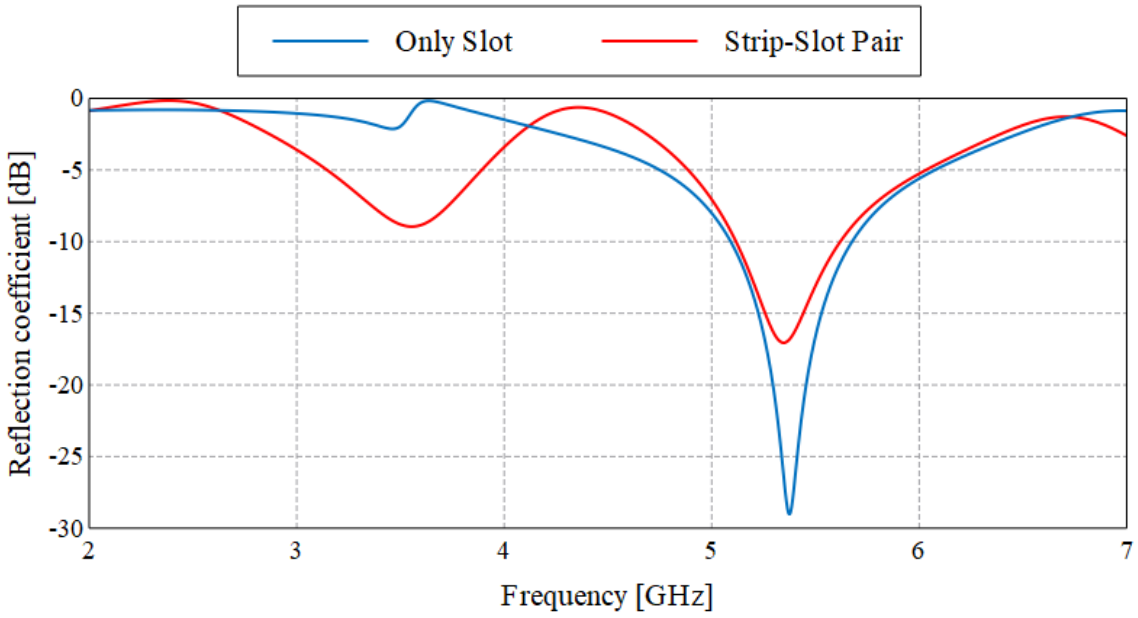

Figure 3.12. Simulated reflection coefficient between a strip-slot pair and only slot antenna

The simulated reflection coefficient of the strip-slot pair illustrates that the structure still achieves a resonance at 5.4 GHz. The -10 dB impedance bandwidth is from 5.12 – 5.62 GHz (9.3%), which does not cover the entire 5.2 GHz and 5.8 GHz WLAN bands. The addition of a secondary slot element in the ground plane is considered in the following sub-section, to try and improve the -10 dB impedance bandwidth.

3.7 STRIP WITH DOUBLE SLOT

The bandwidth achieved by a single strip-slot pair is too narrow to cover the entire 5.2 GHz and 5.8 GHz WLAN frequency bands. The combination of the strip-slot pair with an additional slot in the ground plane was performed to increase the impedance bandwidth of the antenna. The introduction of the additional slot-element and the size of the strip-slot pair had to be optimized and the dimensions are summarized in Table 3.1. The layout of the strip-slot pair with a secondary slot in the ground plane and an open circuit termination is shown in Figure 3.13. The simulated reflection coefficient of the structure is shown in Figure 3.14.

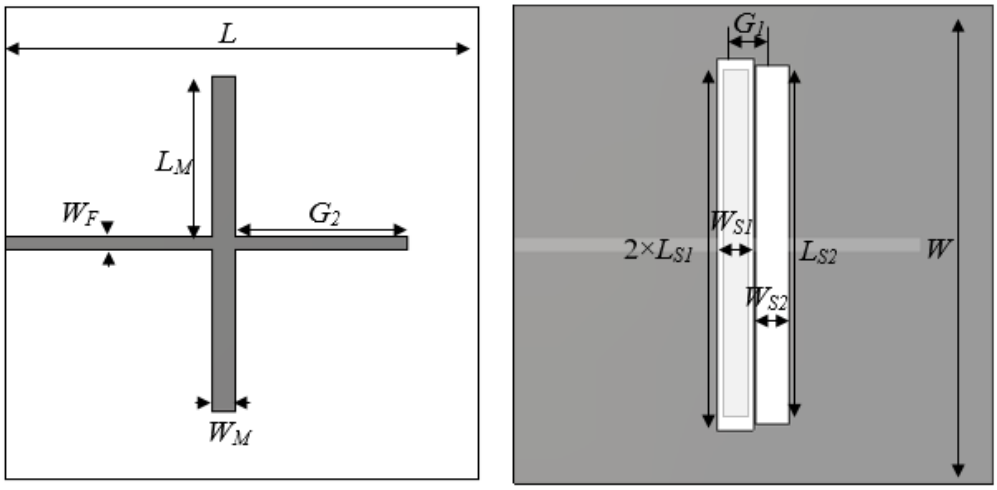

(a) (b)

Figure 3.13. Layout of strip-slot pair with additional slot-element

(a) top view (b) bottom view

Table 3.1. Parameters of strip-slot pair, with additional slot-element

Dimension	Length (mm)	Parameter
L	65.00	Substrate length
W	65.00	Substrate width
$2\times L_{S1}$	50.79	Slot length
W_{S1}	4.93	Slot width
L_{S2}	48.76	Secondary slot length
W_{S2}	4.73	Secondary slot width
G_1	5.00	Gap between slots
L_M	22.30	Strip length
W_M	3.14	Strip width
G_2	23.94	Gap length
W_F	1.80	Feedline width

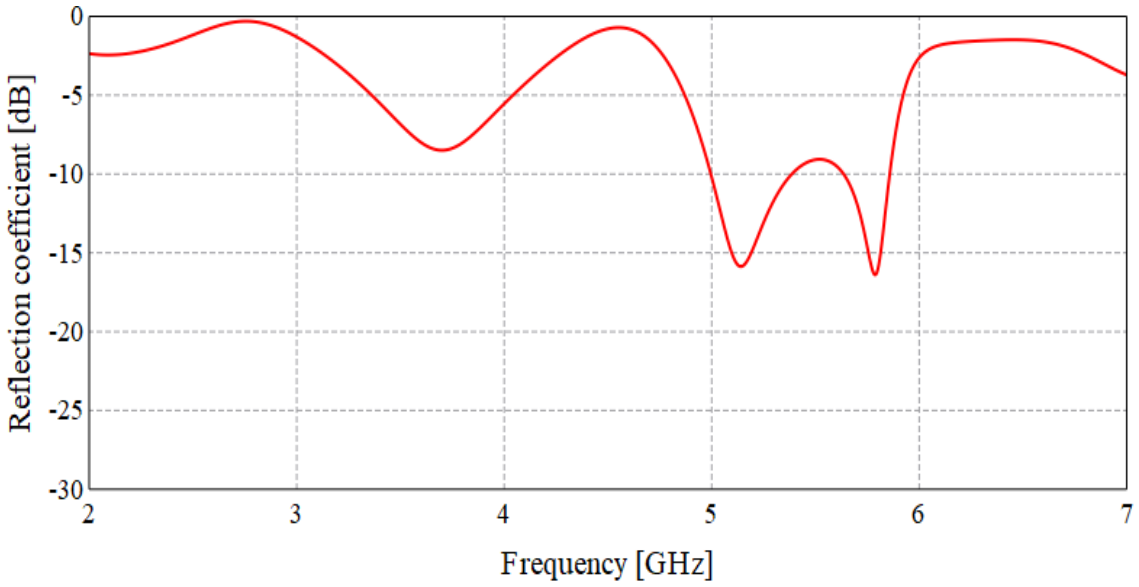

Figure 3.14. Simulated reflection coefficient of the strip-slot pair with a secondary slot-element

The simulated reflection coefficient indicates that the -10 dB bandwidth achieved is from 5.00 – 5.39 GHz (7.5%) and from 5.64 – 5.86 GHz (3.83%). The two resonances obtained covered the WLAN frequency bands (5.15 – 5.25 GHz and 5.725 – 5.825 GHz). The combination of the secondary slot with the strip-slot pair has introduced another resonance close to the original and allowed both 5.2 GHz and 5.8 GHz WLAN bands to be covered.

3.8 DESIGN OF AMC REFLECTOR

One of the objectives is to design a low profile antenna with a directional radiation pattern. Various techniques have been proposed to achieve a low profile antenna and enhance the gain and radiation properties of an antenna. One technique is to incorporate a perfect electric conductor (PEC) reflector behind the antenna. The PEC reflector needs to be placed a quarter-wavelength ($\lambda_o/4$) away from the antenna to achieve optimum unidirectional radiation [24]. The reflection phase for a PEC reflector is 180° for a normally incident plane wave, while the reflection phase for a perfect magnetic conductor (PMC) is 0° [27].

When an antenna is placed close to a PEC, the antenna current cancels with its image current and poor radiation is achieved. By employing a PMC reflector close to the antenna, the current is in-phase with its image current and does not degrade the radiation of the antenna

[48]. The concept of a PMC does not exist in nature, which resulted in an artificial magnetic conductor (AMC) surface to be introduced [3]. The implementation of an AMC as a reflector was investigated. The reflected plane waves from an AMC surface have 0° phase shift. This unique characteristic allows the AMC to be placed close to the antenna to achieve a low profile, high-gain and directional radiation pattern. In this section, the design of a single-, dual- and triple-band AMC reflector is discussed.

3.8.1 Single-band AMC

The simulation tool used to design and simulate the AMC reflector was CST Microwave Studio [25]. The simulation tool has various different solvers that can be implemented, for example the Finite Integration Technique (FIT) based Time Domain Solver (TDS) and the Finite-Element Method (FEM) based Frequency Domain Solver (FDS). The AMC reflector was simulated with the FDS and a tetrahedral mesh. The design of a single-band AMC unit cell was based on the single-band AMC in [27]. The performance of an infinite repetition of the unit cell was simulated by applying the proper boundary conditions. The planes normal to the polarization of the incident field was chosen as PEC, while the planes parallel to the polarization of the incident field was chosen as PMC [27]. The AMC unit cell with the boundary conditions are shown in Figure 3.15. The blue sides are magnetically grounded, while the green sides are electrically grounded. The purple side represents free-space and the unit cell is excited with a waveguide port from this side. The simulated reflection phase of the AMC unit cell is used to determine the resonant frequency at 0° and the operating bandwidth from -90° to +90°.

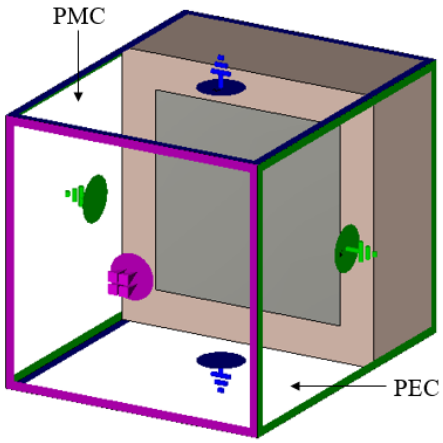

Figure 3.15. Layout of unit cell with boundary conditions

The AMC reflector was designed to operate 6 mm away from the antenna. The unit cell was excited with a waveguide port, 6 mm away from the top of the unit cell. The AMC reflector consists of a ground plane backed dielectric substrate with an array of patches. The substrate used for the AMC reflector is FR4, which has a dielectric constant of 4.4, a loss tangent of 0.02 and a thickness of 3.2 mm. The dimensions of the square AMC unit cell are A = 7.5 mm, B = 5.5 mm and T = 3.2 mm. The layout of the single-band AMC unit cell is shown in Figure 3.16. The simulated reflection phase of the single-band AMC unit cell is shown in Figure 3.17.

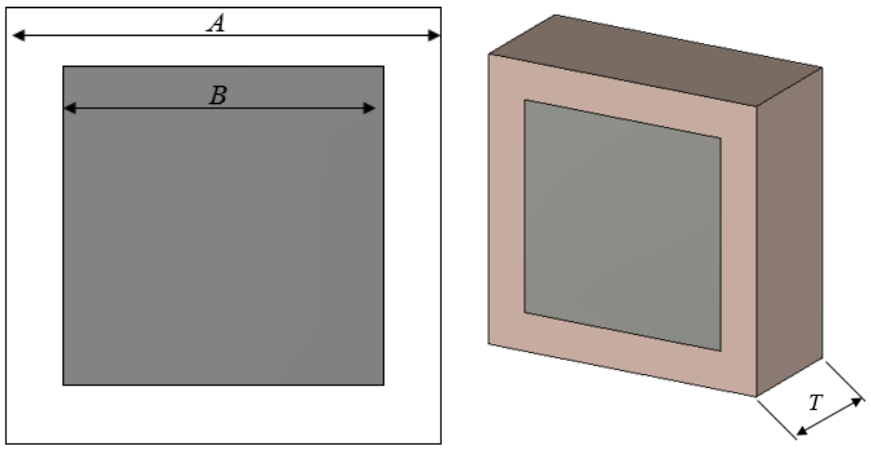

Figure 3.16. Layout of single-band AMC unit cell

(a) top view (b) 3D view

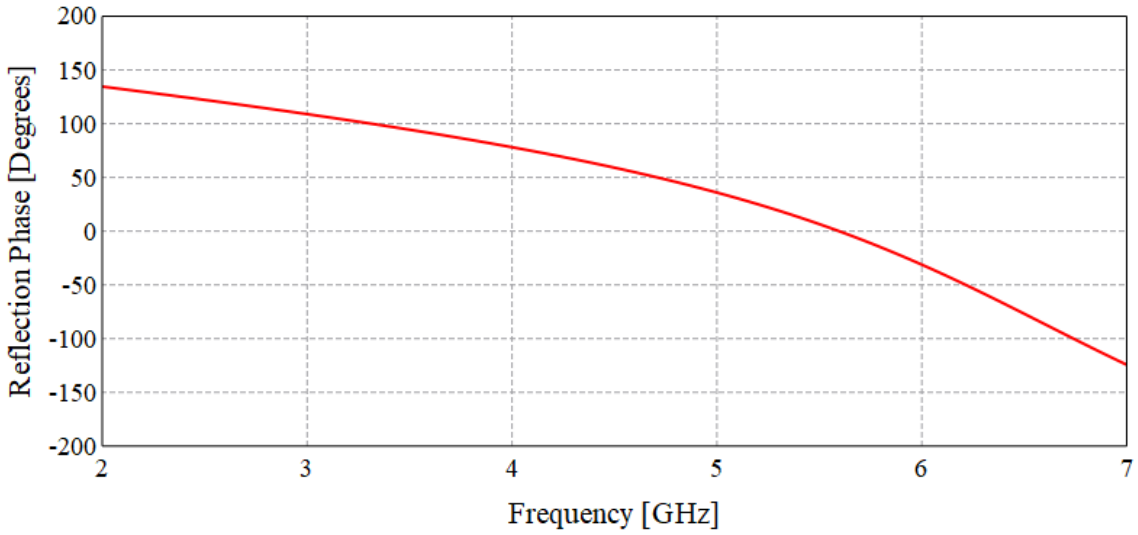

Figure 3.17. Simulated reflection phase for a single-band AMC unit cell

The simulated reflection phase of the single-band AMC unit cell is 0° at 5.6 GHz and has a ±90° reflection phase bandwidth from 3.64 GHz to 6.64 GHz (58.4%). The frequency bandwidth covered by the AMC unit cell covers both WLAN frequency bands. Dimension *B* was varied from 4.5 mm to 6.5 mm and Figure 3.18 shows how a slight change in the dimension influences the position of the 0° reflection phase frequency.

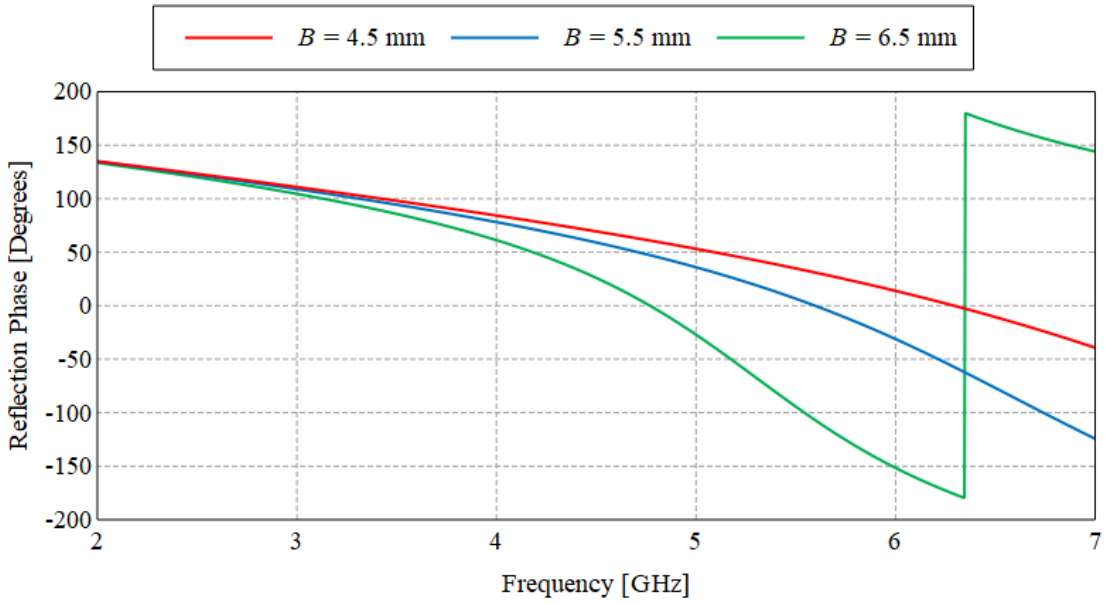

Figure 3.18. Simulated reflection phase of single-band AMC unit cell with a change in length of dimension *B*

The simulation results illustrate that the length of dimension *B* can be adjusted to shift the 0° reflection phase frequency. By decreasing the length of dimension *B*, the 0° reflection phase frequency shifts to a higher frequency. The length of dimension *A* can also be varied to move the 0° reflection phase frequency, but does not affect the 0° reflection phase frequency as significantly as the length of dimension *B*.

3.8.2 Dual-band AMC

The same procedure with the single-band AMC unit cell was used to design a dual-band AMC. The design of a dual-band AMC unit cell consisted of the single-band AMC unit cell with an additional cut out square patch. The substrate used was the same 3.2 mm thick FR4. The dimensions of the dual-band AMC unit cell are A = 17 mm, B = 12.35 mm, C = 12 mm, D = 10.60 mm and T = 3.2 mm. The layout of the dual-band AMC unit cell is shown in Figure 3.19. The same simulation as with the single-band AMC unit cell was performed and the simulated reflection phase of the dual-band is shown in Figure 3.20.

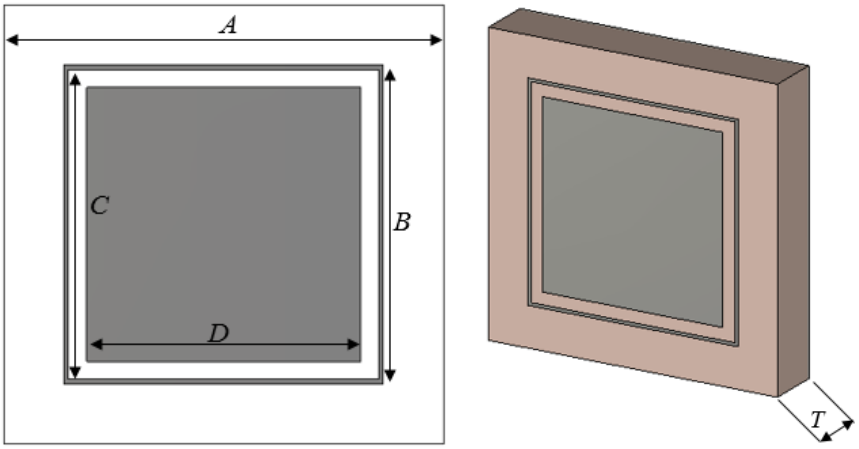

Figure 3.19. Layout of dual-band AMC unit cell

(a) top view (b) 3D view

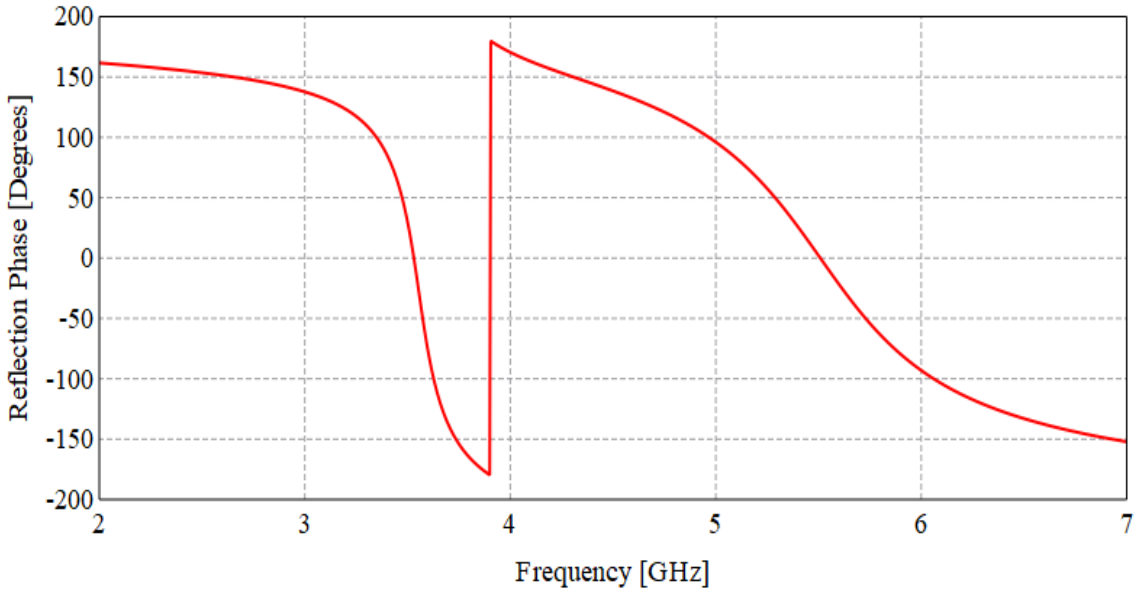

Figure 3.20. Simulated reflection phase for dual-band AMC unit cell

The simulated reflection phase of the dual-band AMC unit cell achieves two 0° reflection phase points at 3.53 GHz and 5.51 GHz. The ±90° phase bandwidth is from 3.38 – 3.61 GHz (6.6%) and from 5.05 – 5.98 GHz (16.9%), which indicates that the 3.5 GHz WiMAX band and 5.2 GHz and 5.8 GHz WLAN bands are covered.

3.8.3 Triple-Band AMC

The one objective of the study is to operate in the 2.4 GHz, 5.2 GHz and 5.8 GHz WLAN frequency bands as well as the 3.5 GHz WiMAX frequency band. The design of a triple-band AMC unit cell is performed to cover the 2.4 GHz WLAN band. The design of the triple-band AMC unit cell builds upon the design of the single- and dual-band AMC unit cells. The FR4 substrate used was now increased from 3.2 mm to 4.8 mm to achieve the correct response. The addition of another rectangular cut patch is placed around the dual-band AMC design to cover the 2.4 GHz WLAN band. The layout of the triple-band AMC unit cell is shown in Figure 3.21. The dimensions for the triple-band AMC unit cell are A = 20.5 mm, B = 16 mm, C = 15.8 mm, D = 13.32 mm, E = 11.4 mm, F = 4.28 mm, G = 1.25 mm, H = 1.25 mm and T = 4.8 mm. The simulated reflection phase of the triple-band AMC unit cell is shown in Figure 3.22.

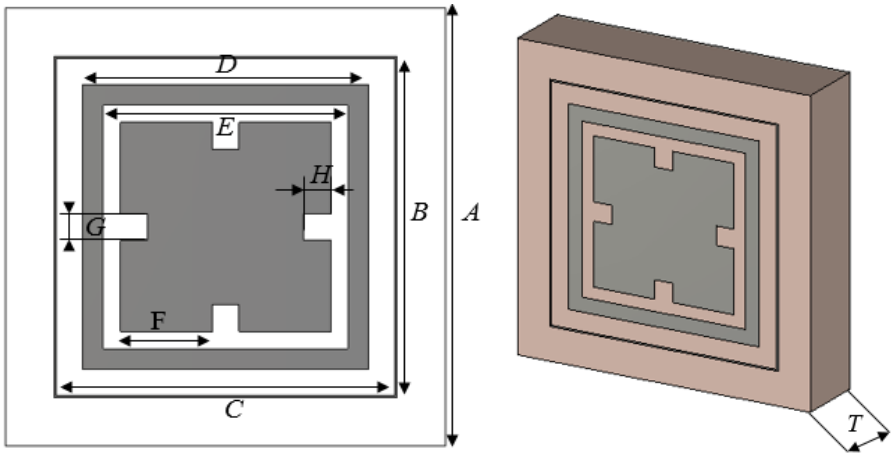

Figure 3.21. Layout of triple-band AMC unit cell

(a) top view (b) 3D-view

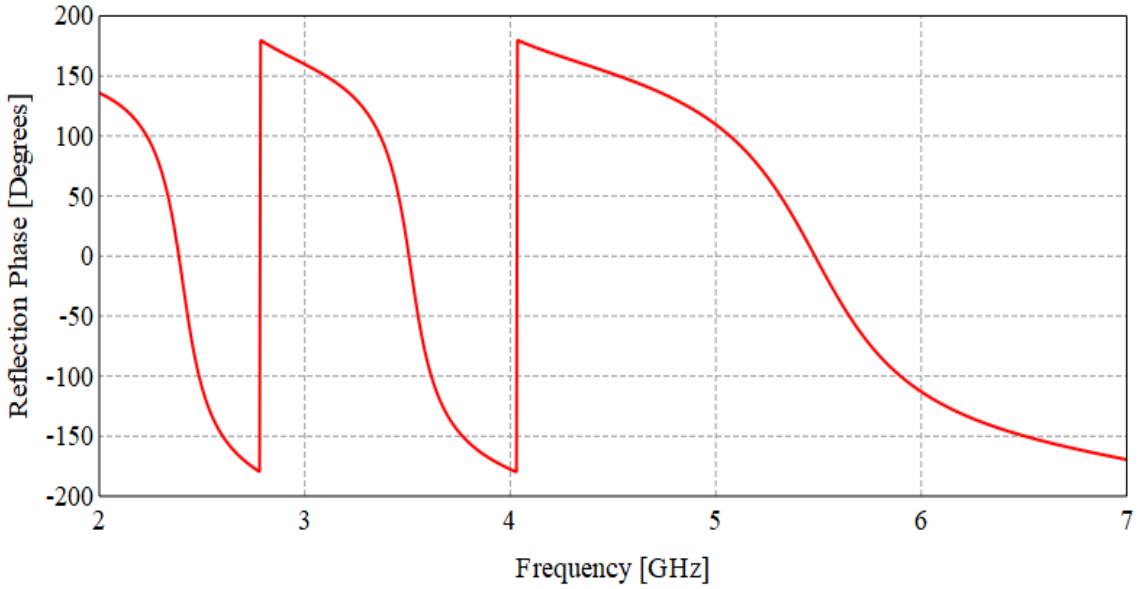

Figure 3.22. Simulated reflection phase for triple-band AMC unit cell

The simulated reflection phase of the triple-band AMC unit cell achieves three resonances at 0° with frequencies 2.42 GHz, 3.52 GHz and 5.29 GHz. The ±90° phase bandwidth achieved at each band is from 2.27 – 2.48 GHz (8.8%), 3.39 – 3.60 GHz (6.0%) and 5.13 – 5.84 GHz (12.9%), which covers the respective WLAN and WiMAX frequency bands. The design of the three different AMC unit cells can be used to combine with the slot radiating

antenna to achieve a low profile design. The combination of the slot antenna with an AMC reflector is presented in the following section.

3.9 SLOT ANTENNA WITH AMC REFLECTOR

The strip-slot pair antenna with the secondary slot-element in Figure 3.13 is now placed over a single-band AMC reflector. The combination of the antenna was also considered with the dual- and triple-band AMC reflectors. The operation of the strip-slot pair and secondary slot element only covered the upper 5.2 GHz and 5.8 GHz WLAN bands, which resulted in the combination of the antenna with the single-band AMC reflector delivering the best results. The size of the AMC reflector must be larger than the size of the antenna to ensure that the power radiated from the antenna is reflected by the AMC. The antenna in Figure 3.23 has a substrate size of 65×65 mm^2. The size of the AMC reflector was increased to an overall size of 82.5×82.5 mm^2. The AMC consists of an 11×11 array of rectangular patches. The AMC unit cell was designed to have a 0° reflection phase at a height of 6 mm. This means that the gap size between the antenna and the AMC reflector has to be 6 mm, giving the structure an overall height of 10.01 mm. The antenna with the AMC reflector is shown in Figure 3.23.

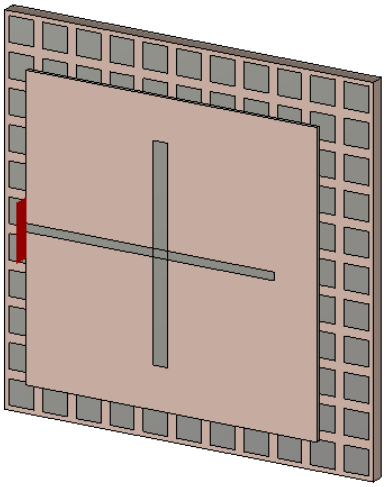

Figure 3.23. Layout of slot antenna with single-band AMC reflector

The structure was simulated and the reflection coefficient and realized gain achieved by the antenna with and without the single-band AMC reflector are compared. The simulated reflection coefficient and gain are shown in Figure 3.24 and Figure 3.25, respectively.

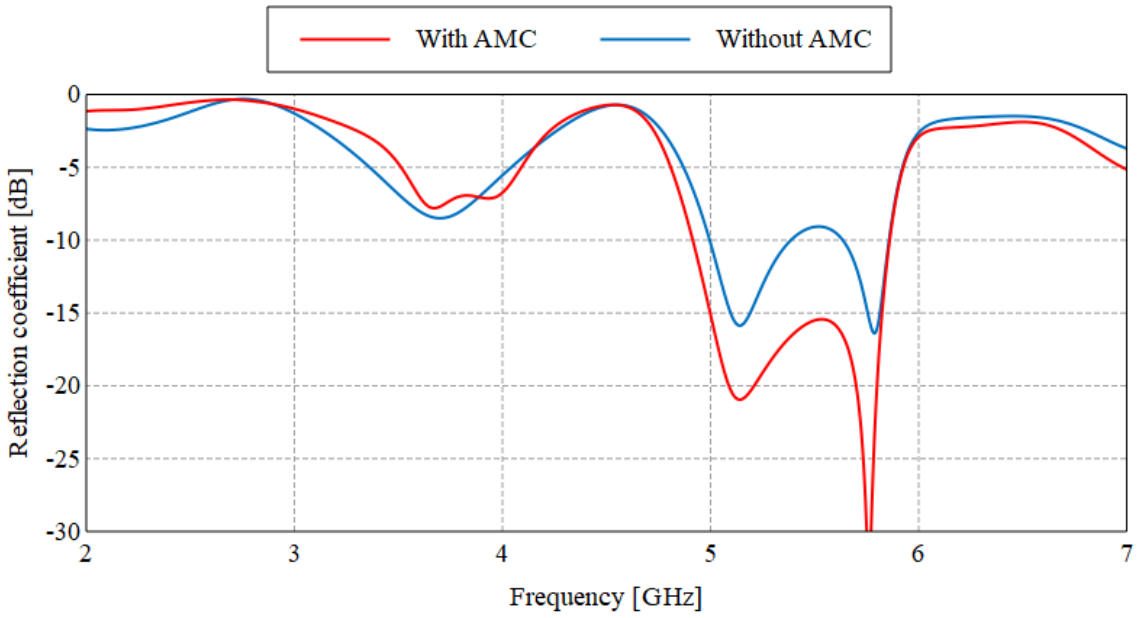

Figure 3.24. Simulate reflection coefficient of slot antenna with and without AMC reflector

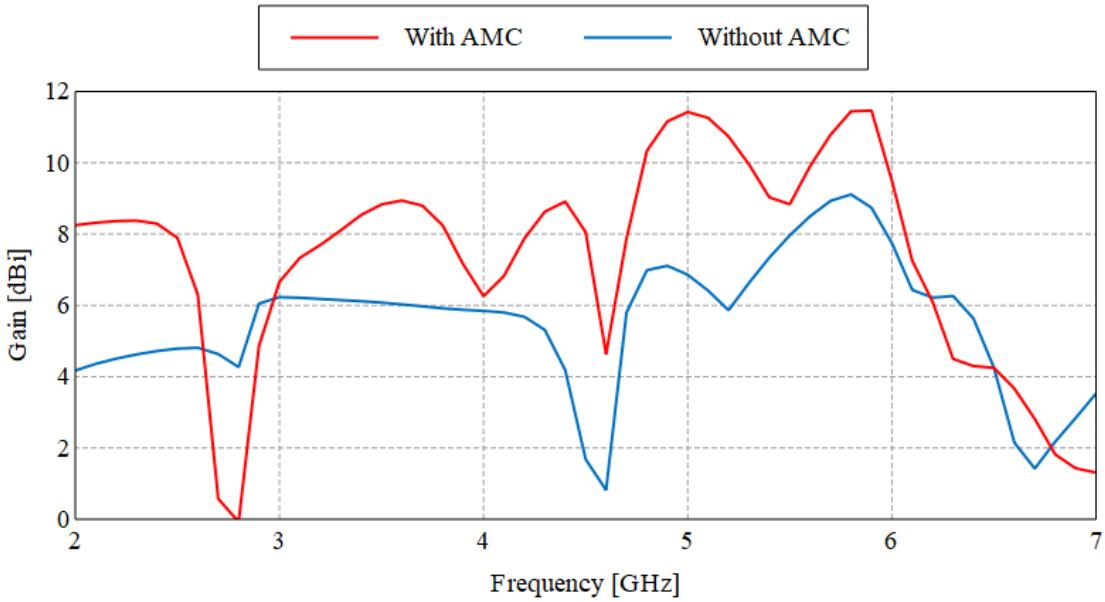

Figure 3.25. Simulated gain of slot antenna with and without AMC reflector

The -10 dB impedance bandwidth achieved by the slot antenna with the AMC reflector is from 4.91 – 5.86 GHz (17.6%), which covers both 5.2 GHz and 5.8 GHz WLAN bands. The realized gain illustrates that the combination of the slot antenna with the AMC reflector has increased the gain across the frequency bands of operation. The realized gain has increased from 6.23 dBi to 10.4 dBi at 5.2 GHz and from 9.11 dBi to 11.4 dBi at 5.8 GHz. This increase in gain is due to the radiation pattern of the antenna being reflected by the AMC and changing the pattern from omnidirectional to unidirectional. The slot antenna was also combined with the dual- and triple-band AMC reflector, but was found that the single-band AMC reflector delivered the best results. This is due to the antenna only operating in the 5.2 GHz and 5.8 GHz bands and not in the 2.4 GHz and 3.5 GHz bands.

3.10 PRACTICAL IMPLEMENTATION

The practical implementation of the antenna will require the connection of a coaxial connector to the feed line. The connection of a coaxial connector on the side of the substrate will influence the radiation patterns of the antenna. In order to try and minimize the effect of the feed point on the radiation pattern of the antenna an alternative approach was required. The coaxial connector is connected perpendicularly to the ground plane of the antenna. A hole was drilled through the antenna substrate, which has the same size as the inner conductor of the coaxial cable. The inner conductor extended through the substrate and was connected to the microstrip feedline. A hole as large as the outer conductor, of the coaxial connector, is etched in the ground plane of the antenna. The outer conductor of the coaxial connector is soldered to the ground plane of the antenna.

The AMC reflector is placed behind the antenna, which requires the coaxial connector to go through the reflector. To accommodate the coaxial connector through the AMC reflector a hole, slightly larger than the outer conductor of the connector, has to be made in the reflector. The outer conductor of the coaxial connector is also soldered to the ground plane of the AMC reflector.

The size of the antenna is made more compact by including a T-junction split for the open circuit termination. The width of the microstrip feedline is 1.80 mm to achieve a 50Ω impedance. By introducing a T-junction split the impedance has to be made 100Ω, which relates to a microstrip width of 0.38 mm on the Rogers RO4003C substrate with a thickness of 0.81 mm. The layout of the coaxial connector and T-junction split for the open circuit termination is presented in Figure 3.26.

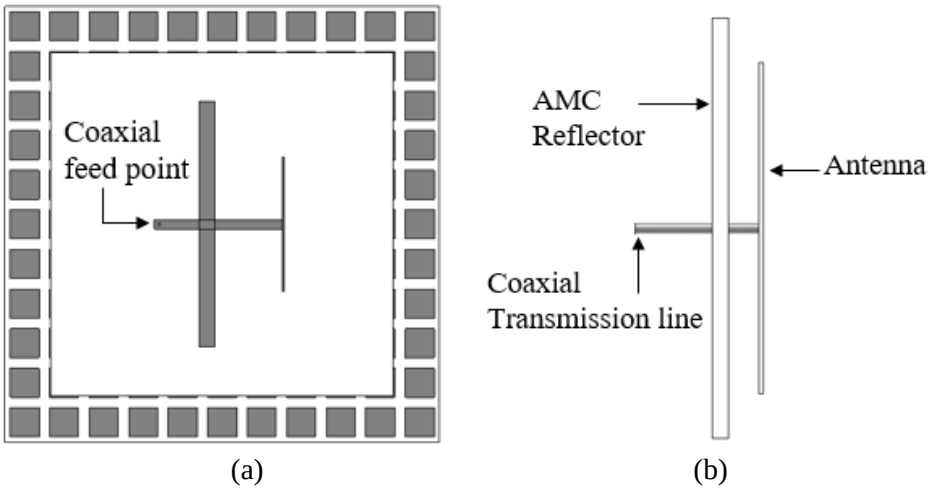

Figure 3.26. Layout of slot antenna with a coaxial connector and T-junction split

(a) top view (b) side view

The antenna was simulated and the results before and after the implementation of the coaxial connector and the T-junction split is compared to each other. The simulated reflection coefficient is presented in Figure 3.27.

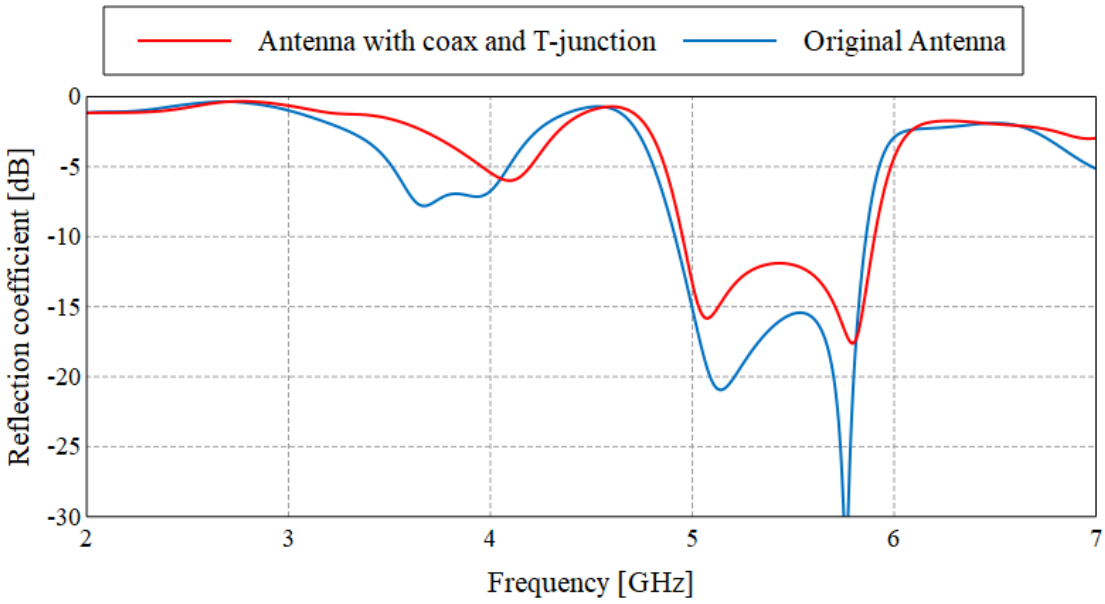

Figure 3.27. Simulated reflection coefficient of antenna with coaxial connector and T-junction split

The overall size of the antenna has decreased with the implementation of the coaxial connector and the T-junction split at the open circuit termination. The -10 dB impedance bandwidth is from 4.95 – 5.9 GHz (17.5%) with the implementation of the coaxial connector and T-junction split. The impedance bandwidth is wide enough to cover the entire 5.2 GHz and 5.8 GHz WLAN bands. With the decreased microstrip feedline length and open circuit termination length, the size of the antenna substrate can be decreased to achieve a smaller overall size antenna.

3.11 PATCH MODE

The strip-slot antenna in [21] combined the ground plane of the antenna with the PEC reflector to support a radiating patch mode and achieve the lower 2.4 GHz WLAN band. The same principle will be implemented with the ground plane of the antenna, acting as a patch antenna and the AMC reflector as the ground plane of the patch. The dielectric medium of the patch antenna is the air gap, which has a dielectric constant of 1. The width and length of the patch antenna is calculated by applying the design equations for a patch antenna as described in section 3.4. The dielectric constant, ϵ_r, is the air gap which is 1 and the resonant frequency, f_r, is 2.4 GHz. The ground plane of the patch antenna is a combination of the air

gap between the ground plane of the antenna and a combination of the AMC reflector substrate and ground plane. The height of the substrate, *h*, was chosen to be the spacing between the antenna and the AMC reflector, which is 6 mm. Equations (3.1) to (3.4) were used and the width and length of the patch antenna were calculated to be $W = 62.5$ mm and $L = 54.26$ mm, respectively.

The width and length of the antenna substrate was then optimized and decreased to 60×40 mm^2. The size of the AMC reflector was also decreased from 82.5×82.5 mm^2 to 68×53 mm^2. The size of the AMC array was decreased from an 11×11 array to a 9×7 array with the decrease in reflector size. The layout of the antenna with a decreased overall size is shown in Figure 3.28.

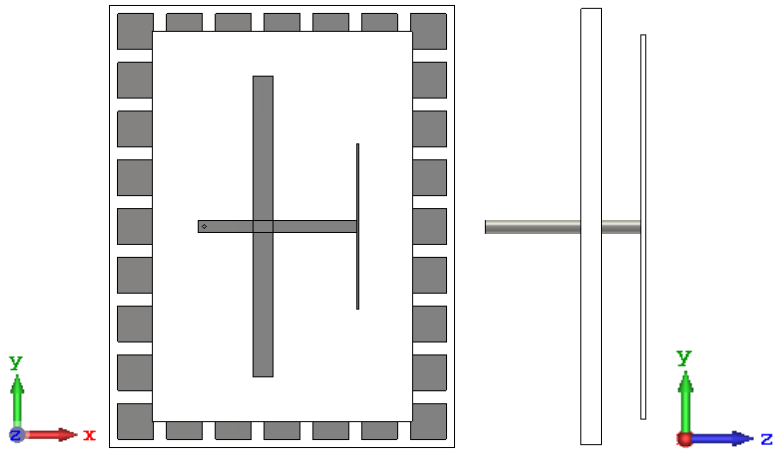

(a) (b)

Figure 3.28. Layout of antenna with AMC reflector and decreased substrate size

(a) top view (b) side view

The simulated reflection coefficient of the original and decreased size antenna and AMC are compared. The simulated reflection coefficient for the change in size is shown in Figure 3.29.

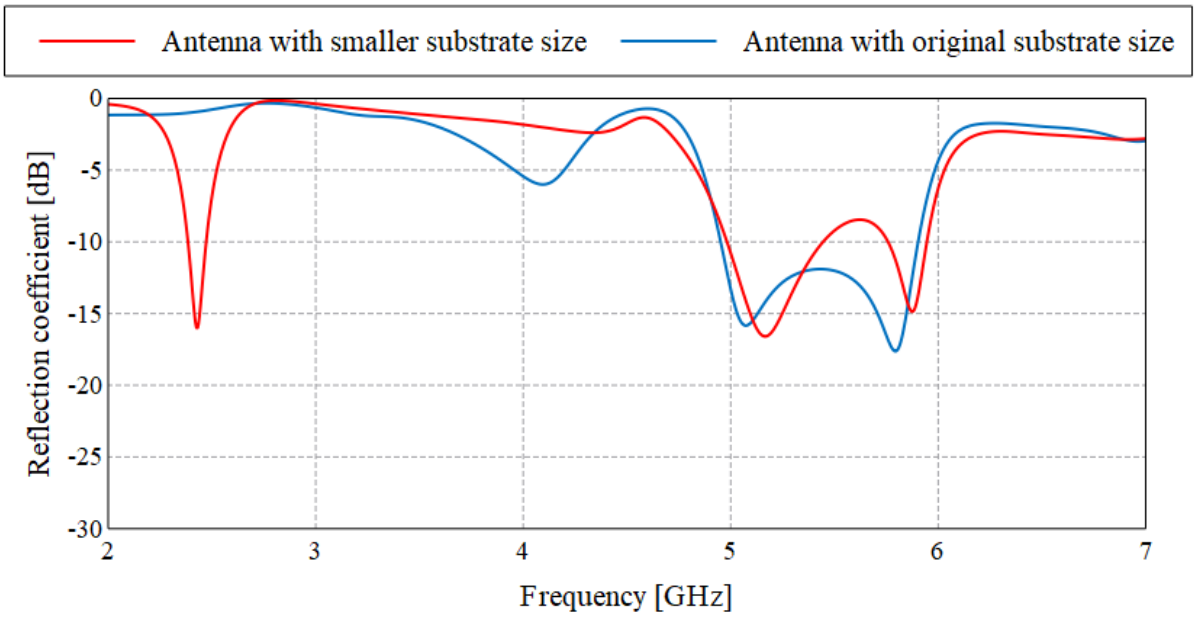

Figure 3.29. Simulated reflection coefficient of slot antenna between different substrate sizes

The matching of the antenna has been affected and the -10 dB impedance bandwidth is from 4.98 – 5.45 GHz (9.0%) and from 5.76 – 5.95 GHz (3.2%), which covers the 5.15 – 5.25 GHz WLAN frequency band but not the entire 5.725 – 5.825 GHz frequency band. The structure has to be optimized to achieve a wide enough impedance bandwidth to cover the entire 5.2 GHz and 5.8 GHz WLAN frequency band. The decrease in antenna and AMC reflector substrate size has produced a resonance at 2.43 GHz. The -10 dB impedance bandwidth in the lower frequency band is from 2.38 – 2.47 GHz (3.7%), which partially covers the 2.4 – 2.483 GHz WLAN band. The lower frequency band can be altered by adjusting the length and width of the antenna ground plane.

3.12 CHAPTER SUMMARY

The design of a strip-slot antenna with a reflector was used as a starting point for this study. The strip-slot antenna in [21] was used as a starting point due to it being the only directional, high gain antenna being able to operate in the 2.4 GHz, 5.2 GHz and 5.8 GHz WLAN bands as well as the 3.5 GHz WiMAX band. The various aspects that caused the strip-slot antenna to operated in the WLAN and WiMAX frequency bands were determined and a background

study was performed on them. The background study was performed on slot antennas, patch antennas, as well as microstrip with complementary slot structure. The addition of a secondary slot-element to the strip-slot structure produces a resonance close to the original and allows for an improved frequency bandwidth. The strip-slot antenna implemented a PEC reflector and to achieve a low profile design a background study was also done on the operation of AMC reflector. The addition of the AMC reflector to the antenna achieved a directional antenna with high gain and a low profile design. The background study will be used to design the final proposed antennas in the following chapter.

CHAPTER 4 ANTENNA DESIGN

4.1 CHAPTER OVERVIEW

This chapter contains the design of the final proposed triple- and quad-band antennas. The background study performed in the previous chapter presented an overview of the different aspects and were combined to design the final proposed antennas. The final design and assembly of the proposed triple- and quad-band antennas are presented as well as the antenna functionality is described. The manufactured antennas of the proposed final design are also presented.

4.2 TRIPLE-BAND ANTENNA WITH AMC REFLECTOR

The substrate used for the antenna was Rogers RO4003C, which has a dielectric constant of 3.38, a loss tangent of 0.0027 and a thickness of 0.81 mm. The size of the antenna substrate was determined by applying the design equations for a patch antenna and optimized, with the "Nelder Mead Simplex Algorithm" in CST, to achieve a resonance at 2.4 GHz. The antenna substrate has a size of 56.93×40.28 mm^2. The antenna consists of a strip-slot pair with a secondary slot element. The width and length of the strip-slot pair was designed along with the secondary slot element to cover the upper 5.2 GHz and 5.8 GHz WLAN frequency bands.

The substrate used for the AMC reflector was FR4, which has a dielectric constant of 4.3, a loss tangent of 0.025 and a thickness of 3.2 mm. The AMC reflector has a size of 68.00×53.00 mm^2. The AMC reflector was designed to operate 6 mm away from the antenna, resulting in an overall height of 10.01 mm. The antenna is fed with a 50Ω coaxial transmission line, which has an outer conductor diameter of 2.2 mm and an inner conductor diameter of 0.51 mm. The coaxial transmission line is connected to the 1.8 mm wide microstrip feedline, which excites the antenna. The feed point of the antenna was placed close to the strip-slot pair, due to the current distribution of the antenna being affected negatively when it is fed from the edge of the substrate.

4.2.1 Antenna dimensions of triple-band antenna

The layout of the antenna without the AMC reflector is shown in Figure 4.1. While the layout of the triple-band antenna with the AMC reflector is shown in Figure 4.2.

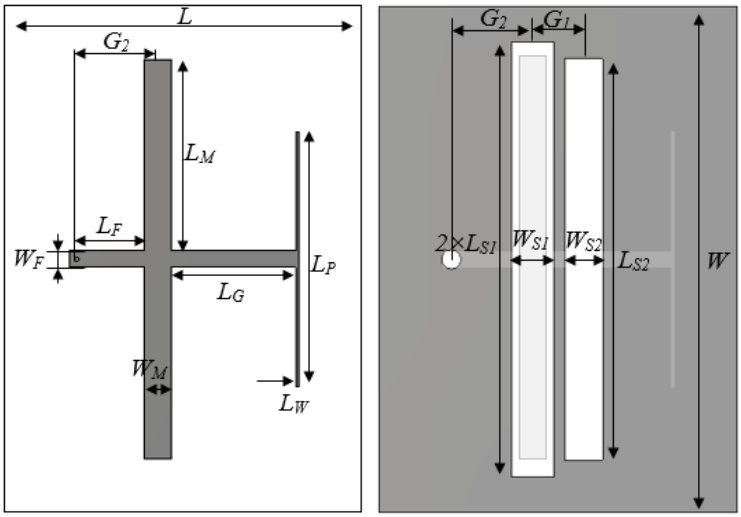

Figure 4.1. Layout of triple-band antenna without AMC reflector

(a) top of antenna (b) bottom of antenna

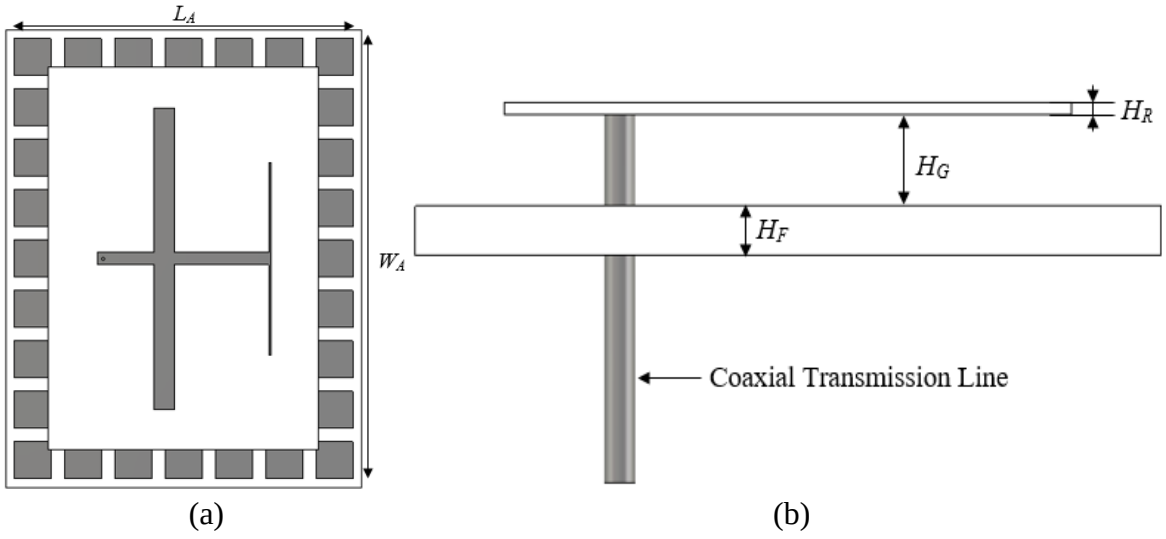

Figure 4.2. Layout of triple-band antenna with AMC reflector

(a) top view (b) side view

The dimensions of the optimized triple-band antenna with the AMC reflector are summarized in Table 4.1.

Table 4.1. Dimensions of triple-band antenna

Dimension	Length (mm)	Parameter
L	40.28	Substrate length
W	56.93	Substrate width
$2\times L_{S1}$	49.02	Slot length
W_{S1}	4.75	Slot width
L_{S2}	45.15	Secondary slot length
W_{S2}	4.23	Secondary slot width
G_1	5.76	Gap between slots
G_2	9.35	Feed point distance
L_M	21.53	Strip length
W_M	3.03	Strip width
L_G	14.05	Gap length
L_P	28.72	Split length
L_W	0.38	Split width
L_F	8.49	Feedline length
W_F	1.80	Feedline width
H_R	0.81	Rogers RO4003C height
H_G	6.00	Gap size
H_F	3.20	FR4 substrate height
L_A	68.00	AMC length
W_A	53.00	AMC width

The antenna was designed and simulated in CST Microwave Studio [25]. In the CST simulations, the antenna was fed with a coaxial transmission line below the AMC reflector. The coaxial connector was excited with a waveguide port. This was an approximate

representation of a coaxial connector that will feed the antenna once it was manufactured. The inner conductor of the coaxial transmission line was connected to the microstrip feedline, while the outer conductor is connected to the ground plane of the antenna, as well as the ground plane of the AMC reflector.

4.2.2 Simulation results of triple-band antenna

The antenna achieved an impedance bandwidth of less than -10 dB and a gain of more than 6.5 dBi in the respective WLAN bands. The simulated reflection coefficient, realized gain and total efficiency is shown in Figure 4.3 to Figure 4.5. The normalized radiation patterns in the *E*- and *H*-planes of the triple-band antenna with the AMC reflector are presented in Figure 4.6 and Figure 4.7, respectively.

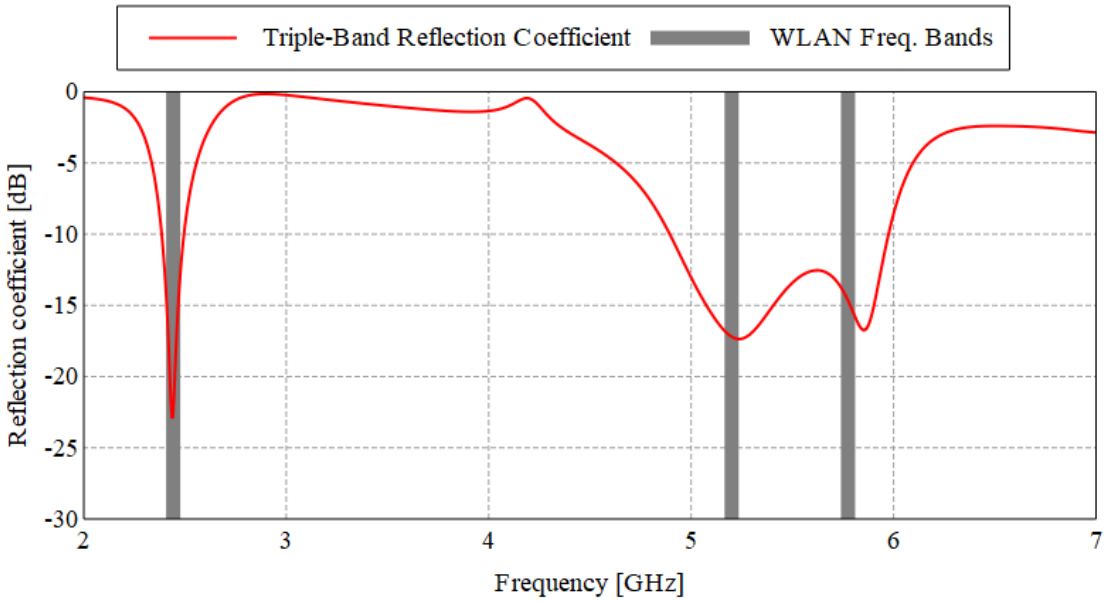

Figure 4.3. Simulated reflection coefficient of triple-band antenna

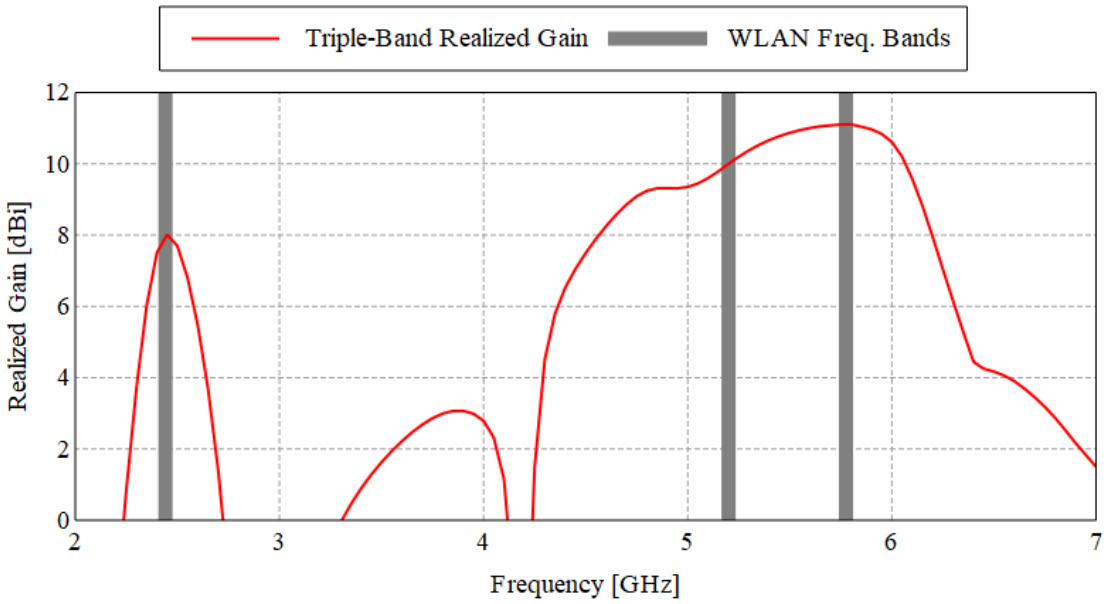

Figure 4.4. Simulated realized gain of triple-band antenna

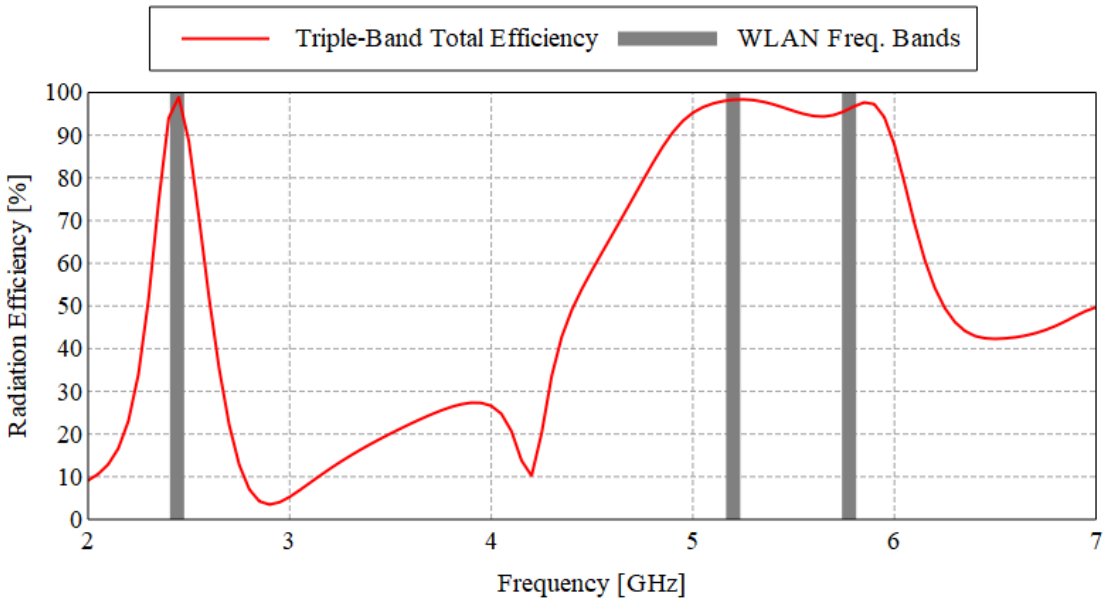

Figure 4.5. Simulated total efficiency of triple-band antenna

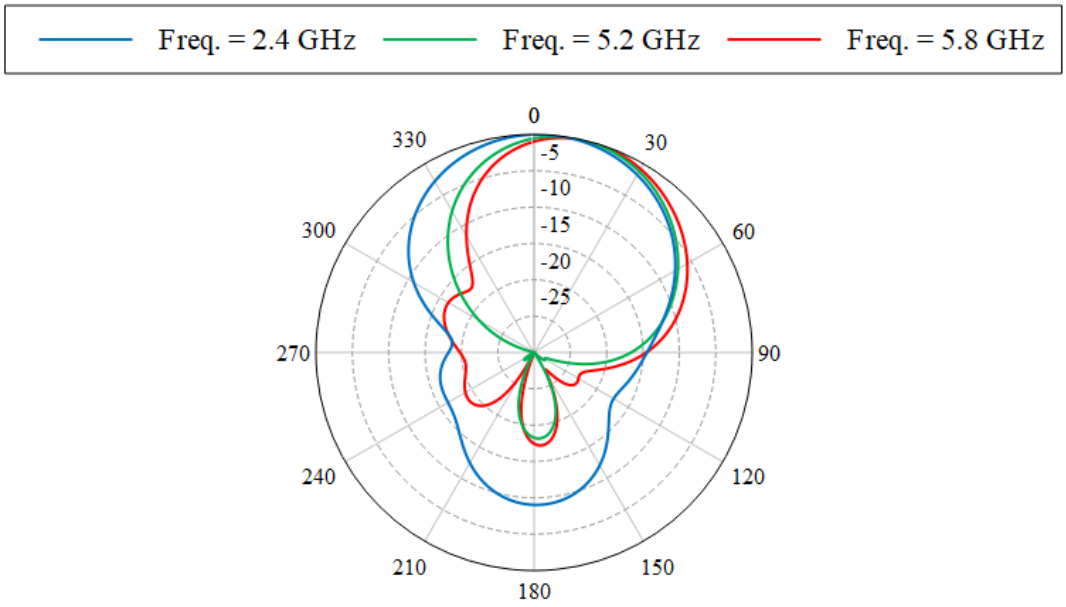

Figure 4.6. Simulated *E*-plane co-polarization radiation patterns of the triple-band antenna

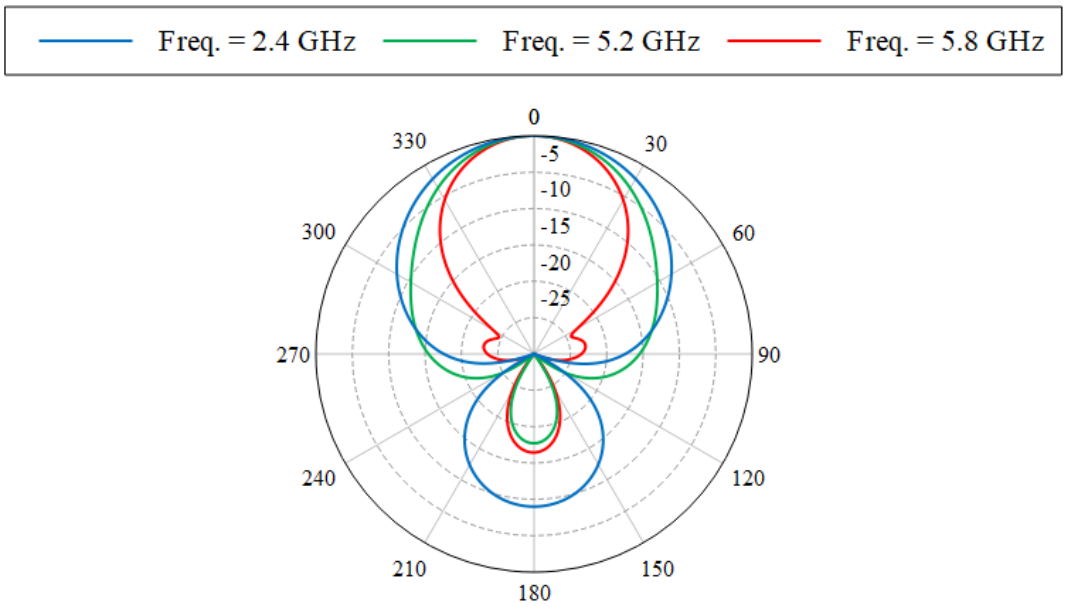

Figure 4.7. Simulated *H*-plane co-polarization radiation patterns of the triple-band antenna

The simulation results indicate that the antenna achieved a -10 dB impedance bandwidth from 2.39 – 2.50 GHz (4.50%) and from 4.89 – 5.98 GHz (20.1%), which covers the respective WLAN bands. The realized gain of the antenna is more than 7 dBi across the three frequency bands. The peak gain achieved at the three frequency bands are 7.59 dBi, 10.0 dBi

and 11.1 dBi at 2.45 GHz, 5.2 GHz and 5.8 GHz, respectively. The simulated total efficiency of the antenna was more than 90% across all three frequency bands. The radiation patterns achieved by the antenna are all directional with a front-to-back ratio, except for the *E*-plane at 2.4 GHz which has a lower front-to-back ratio than the other frequency bands. The results from the simulated radiation patterns are summarized in Table 4.2.

Table 4.2. Summarised simulated radiation pattern results of triple-band antenna

Plane	***E*-Plane**			***H*-Plane**		
Frequency	2.45 GHz	5.2 GHz	5.75 GHz	2.45 GHz	5.2 GHz	5.75 GHz
3-dB beam-width	70.3°	56.4°	54.5°	70.9°	54.2°	45.1°
Main beam direction	3.0°	12.0°	13.0°	0.0°	0.0°	0.0°
Max Side-lobe level	-10.2 dB	-18.1 dB	-17 dB	-10.2 dB	-17.7 dB	-17 dB
Front-to-back ratio	10 dB	18 dB	17 dB	10 dB	18 dB	17 dB
Max Cross-polarization	-49 dB	-43 dB	-41 dB	-6.8 dB	-12 dB	-11 dB

The 3-dB beamwidth of the antenna at 2.45 GHz in the *E*-plane is 70.3°, while at 5.2 GHz and 5.8 GHz it is 56.4° and 54.5°. This indicates that the pattern at 2.45 GHz is broader than the upper 5.2 GHz and 5.8 GHz WLAN bands. In the *E*-plane, at 5.2 GHz and 5.8 GHz, the radiation pattern squints at an angle of 12.0° and 13.0°, respectively. The front-to-back ratios at the respective frequency bands are 10, 18 and 17 dB at 2.45 GHz, 5.2 GHz and 5.8 GHz, respectively.

4.2.3 Antenna functionality of triple-band antenna

The antenna is excited by the coaxial transmission line, while the end of the feedline is terminated with an open circuit termination which produces a standing wave on the feedline.

The strip-slot pair forms a single element with an almost constant impedance over a wide frequency range. The secondary slot produces a resonance close to the resonance from the strip-slot pair and achieves a wide impedance bandwidth to cover the 5.2 GHz and 5.8 GHz WLAN bands.

The AMC reflector is designed to have a 0° reflection phase at 6 mm with a ±90° reflection phase bandwidth from 3.64 – 6.64 GHz (58.4%), which covers the entire 5.2 GHz and 5.8 GHz WLAN frequency band. The radiation from the strip-slot pair and parasitic slot-element is omnidirectional and due to the AMC reflector a directional radiation pattern is achieved. The AMC reflector reflects the radiated energy in the frequency band it is designed for.

The simulated reflection coefficient in Figure 4.3 illustrates that the 2.4 GHz, 5.2 GHz and 5.8 GHz WLAN bands are covered. To illustrate which part of the antenna resonates at the respective resonance, the *E*-fields were simulated 1.2 mm below the antenna substrate, which is between the antenna substrate and AMC reflector. The *E*-fields were simulated in the Z-axis at 2.4 GHz and in the X-axis at 5.2 GHz and 5.8 GHz. The *E*-fields were simulated at 2.4 GHz, 5.2 GHz and 5.8 GHz and is shown in Figure 4.8.

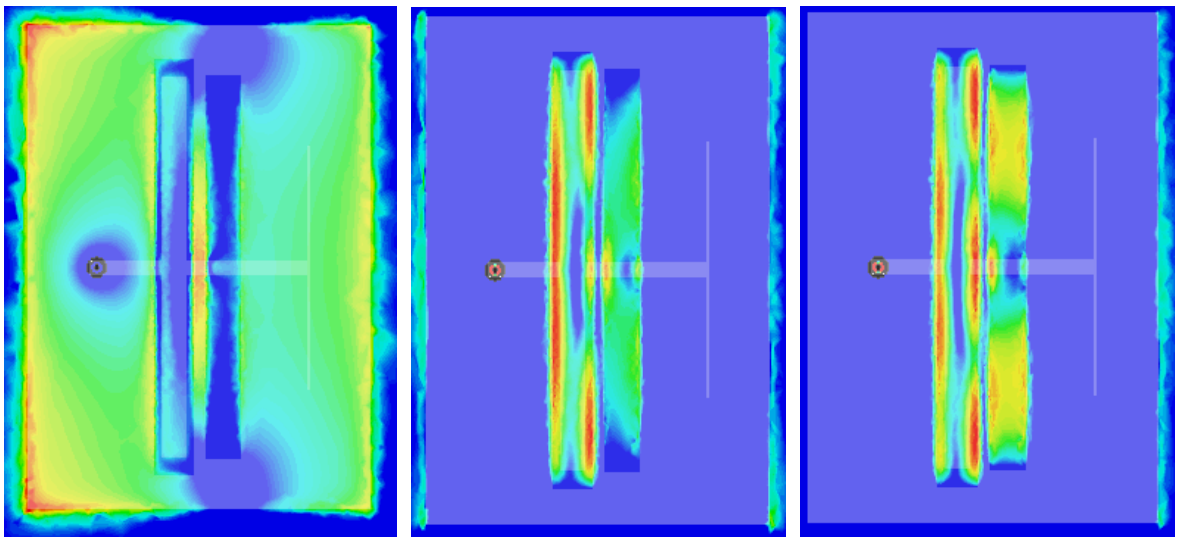

(a) (b) (c)

Figure 4.8. Simulated *E*-fields at 1.2 mm below the antenna ground plane of triple-band antenna at (a) 2.4 GHz (b) 5.2 GHz (c) 5.8 GHz

The simulated E_z-fields at 1.2 mm below the antenna show that the lower operating resonance at 2.4 GHz is primarily controlled by the length of the ground plane of the antenna substrate. The AMC surface and the ground plane of the antenna support a radiating patch mode, as can be seen by the high value fields at the two vertical edges of the antenna ground plane in Figure 4.8(a). At 5.2 GHz the E_x-fields are concentrated around the strip-slot pair. At 5.8 GHz the simulated E_x-fields indicated that the resonance is a combination between the strip-slot pair and the secondary slot element.

4.2.4 PARAMETER STUDY

The design of the triple-band antenna in simulation software assumes perfect operating conditions for the antenna. The effect of tolerances with regards to manufacturing and assembly is investigated. A parameter study was performed to determine the effect of a different dielectric constant. A parameter study was also performed on the position of the coaxial feed and also the gap size between the antenna and the AMC reflector.

4.2.4.1 Parameter study of substrate dielectric constant

The substrate used for the antenna was Rogers RO4003C and has a dielectric constant of 3.38 at 10 GHz. The datasheet for Rogers RO4003C states that for simulation, the dielectric constant is 3.55 for microstrip applications. The antenna was designed and simulated in CST Microwave Studio, which has a material library with the characteristics for Rogers RO4003C having a dielectric constant of 3.38. To illustrate what effect a difference in dielectric constant has on the performance of the antenna, the dielectric constant of the antenna was varied and simulated with a dielectric constant of 3.38 and 3.55, respectively. The simulated reflection coefficient for the change in dielectric constant is presented in Figure 4.9.

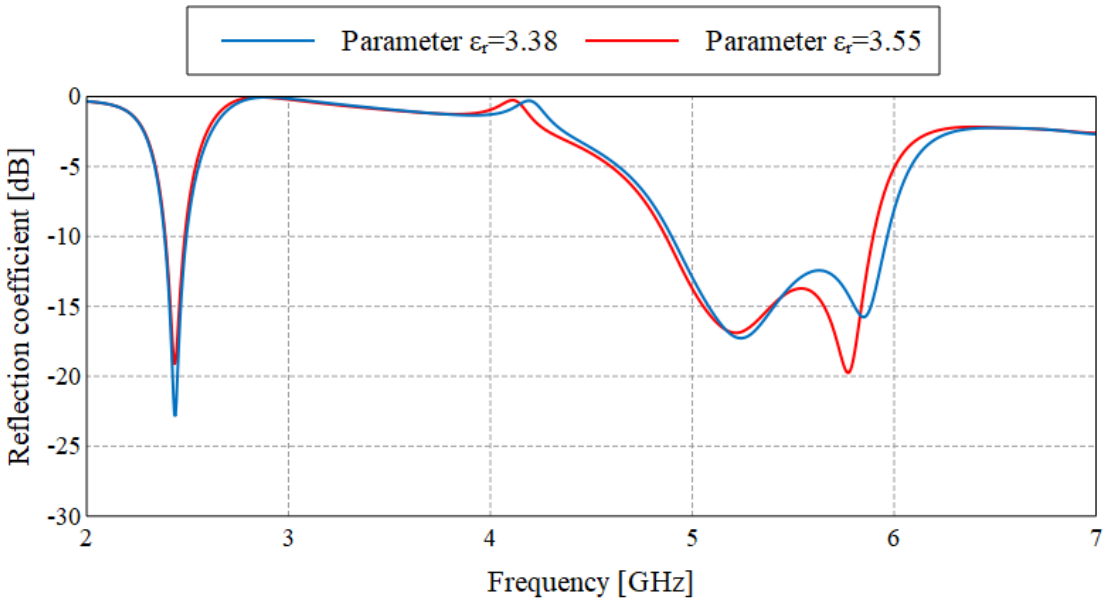

Figure 4.9. Parameter study for change in dielectric constant of triple-band antenna

The simulated reflection coefficient illustrates that the small change in dielectric constant has shifted the matching of the higher frequency band. The bandwidth of the higher frequency band decreased with an increase in dielectric constant. This was the expected result due to a larger dielectric constant the wavelength decreases which resulted in the resonance being reached at a lower frequency. With regards to the lower frequency band, it was clear that the change in dielectric constant did not influence the frequency bandwidth.

4.2.4.2 Parameter study of coaxial connector position

As the antenna is manufactured the microstrip feedline has to be connected to the coaxial transmission line afterward. A parameter study on the position of the coaxial connector with the microstrip feedline is investigated. The position of the coaxial connector is varied with 0.5 mm to the left and right of the original position. The simulated reflection coefficient for the position of the coaxial connector at -0.5, 0 and 0.5 mm is presented in Figure 4.10.

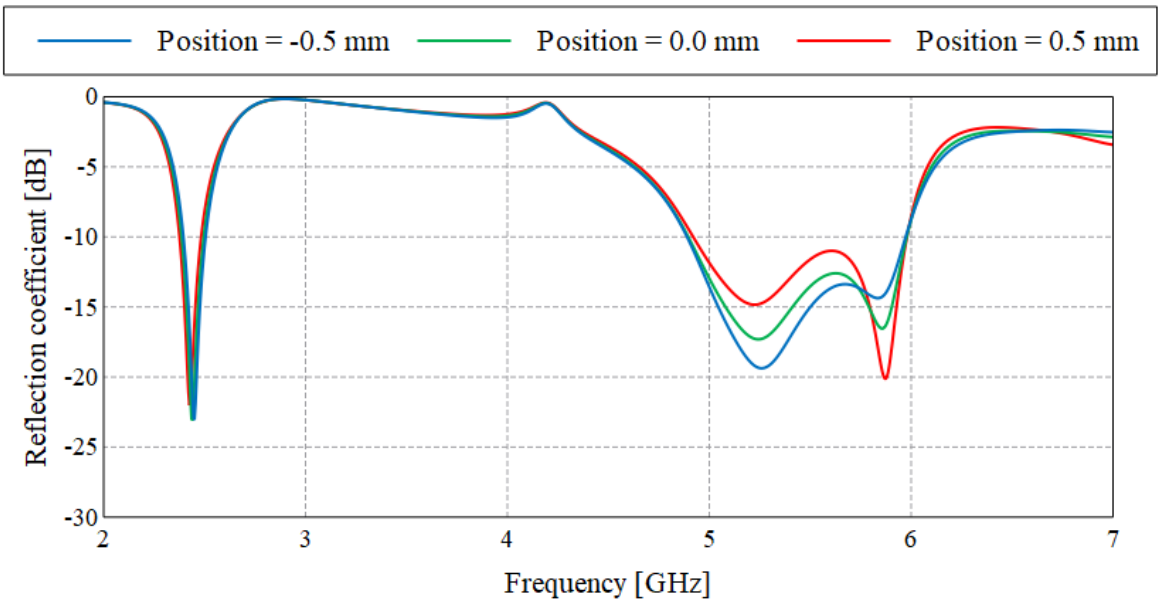

Figure 4.10. Parameter study for change in coaxial connector position of triple-band antenna

The change in coaxial connector position has a significant influence on the matching of the upper frequency band. When the position of the coaxial connector was closer to the edge of the microstrip feedline (-0.5 mm), the matching of the resonance at 5.25 GHz improved. When the position of the coaxial connector was moved further away from the edge of the microstrip feedline (0.5 mm), the matching of the resonance at 5.85 GHz improved while the matching at 5.25 GHz decreased. The position of the coaxial connector on the feedline is, therefore, important with regards to the matching of the antenna. The position of the coaxial connector influences the matching of the resonance in the lower WLAN band. This is due to the current distribution of the ground plane being affected by the change in the coaxial connector position.

4.2.4.3 Parameter study of gap size between antenna and AMC reflector

The distance between the antenna and the AMC reflector is a vital part in the matching of the antenna. The AMC reflector was designed to have a 0° reflection phase at 6 mm and a change in height can influence the matching of the antenna. A parameter study is performed on the gap size between the antenna and AMC reflector. The simulation results for the gap size is investigated at 4, 6 and 8 mm from the antenna and presented in Figure 4.11.

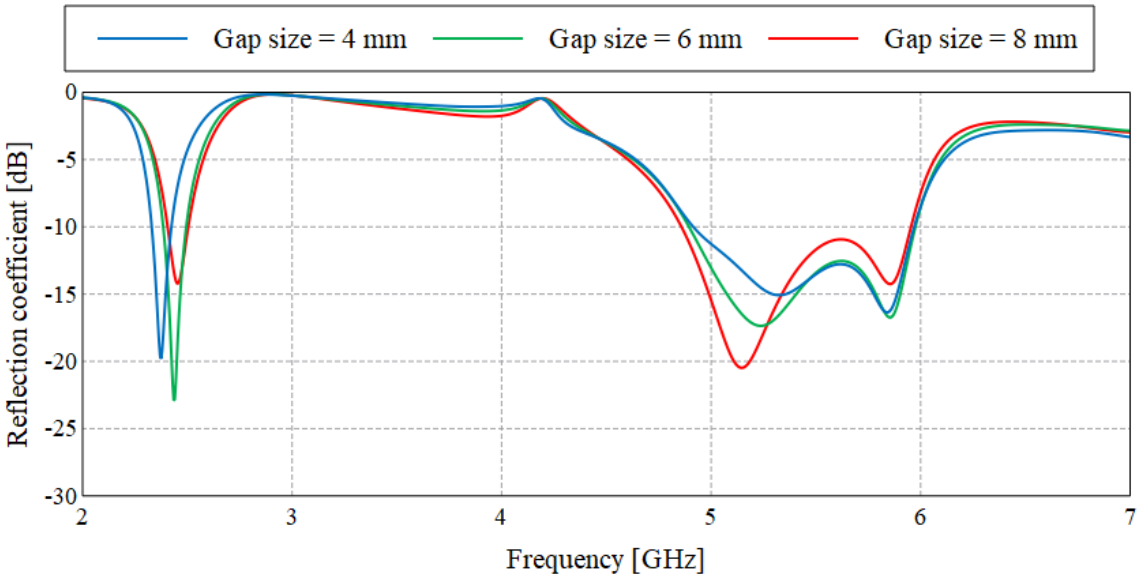

Figure 4.11. Parameter study change in gap size of triple-band antenna

The change in gap size illustrates that the lower frequency band has shifted when the gap size is decreased from 4 to 6 mm. The 2.4 GHz resonance is dependent on the gap size between the antenna and the AMC reflector, due to the air gap being the substrate for the patch mode. With regards to the upper-frequency band, it is clear that the frequency bandwidth remains similar when the gap size is varied. It is noticed that as the gap size is increased to 8 mm, the matching has improved at the 5.15 GHz resonance, but decreased at the 5.62 GHz resonance. The AMC reflector was designed to achieve a 0° at 5.6 GHz and by varying the gap size, the resonant frequency of the AMC reflector is affected. The change in gap size will then have an influence on the upper-frequency bands. The gap size between the antenna substrate and the AMC reflector is therefore an important parameter when the antenna is manufactured and assembled.

4.3 DESIGN OF QUAD-BAND ANTENNA

The design of the triple-band antenna was used as a starting point and the design of strip-slot pair and the additional slot was used from the background study. The size of the secondary slot-element from the triple-band antenna was decreased to half the size. By

decreasing the size of the secondary slot, an additional resonance was achieved at 3.5 GHz in the WiMAX frequency band (3.4 – 3.6 GHz). The resonance was due to the coupling between the strip-slot pair and secondary slot-element.

The same procedure as with the triple-band antenna was implemented. The ground plane was implemented as a patch antenna to operate at 2.4 GHz and the strip-slot pair was now adjusted to operate at 5.8 GHz. The antenna has an optimized substrate size of 37.50×64.74 mm^2 on Rogers RO4003C, while the AMC reflector has a substrate size 53×68 mm^2 on FR4. The spacing between the antenna and AMC reflector is 6 mm. The three-quarter wavelength open circuit termination at 5.4 GHz was reduced in size by including a T-junction split at the end of the feedline. With regard to the quad-band antenna, the design of the T-junction split was removed and the feedline was curved, which resulted in improved performance. The quad-band antenna was also fed with a coaxial transmission line from below, which went through the AMC reflector and antenna substrate. The layout and detailed dimensions for the quad-band antenna are presented in the following subsection.

4.3.1 Antenna dimensions of quad-band antenna

The layout of the quad-band antenna without the AMC reflector is shown in Figure 4.12. The layout of the optimized quad-band antenna with the single-band AMC reflector is shown in Figure 4.13. The dimensions of the quad-band antenna with the AMC reflector are summarized in Table 4.3.

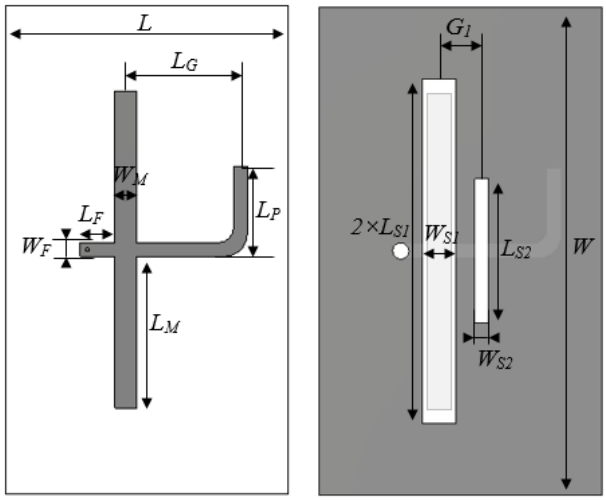

(a) (b)

Figure 4.12. Layout of quad-band antenna without AMC reflector

(a) top view of antenna (b) bottom view of antenna

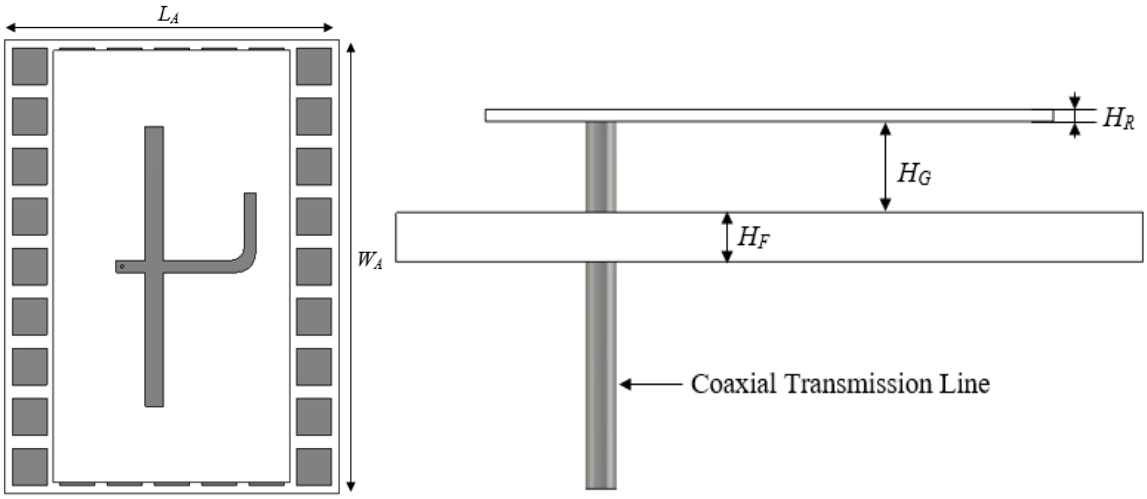

(a) (b)

Figure 4.13. Layout of optimized quad-band antenna with AMC reflector

(a) top view of antenna with AMC reflector (b) side view

Table 4.3. Dimensions of optimized quad-band antenna

Dimension	Length (mm)	Parameter
L	37.50	Substrate length
W	64.74	Substrate width
$2 \times L_{S1}$	45.72	Slot length
W_{S1}	4.43	Slot width
L_{S2}	19.11	Additional slot length
W_{S2}	1.79	Additional slot width
G_1	5.59	Gap between slots
L_M	20.08	Strip length
W_M	2.82	Strip width
L_G	15.19	Gap length
L_P	11.90	Curve Length
L_F	4.62	Feedline length
W_F	1.80	Feedline width
H_R	0.81	Rogers RO4003C height
H_G	6.00	Gap size
H_F	3.20	FR4 substrate height
L_A	53.00	AMC length
W_A	68.00	AMC width

In the simulation, the quad-band antenna was excited with a coaxial transmission line below the AMC reflector. This was a close approximation of how the antenna will be fed after manufacturing. The inner connecter of the coaxial transmission line was connected to the microstrip feedline, while the outer conductor was connected to the ground plane of the antenna, as well as the ground plane of the AMC reflector.

4.3.2 Simulation results of quad-band antenna

The quad-band antenna was simulated and the reflection coefficient, realized gain and total efficiency are shown in Figure 4.14 to Figure 4.16. The radiation patterns of the antenna were also simulated and the normalized radiation patterns in the *E*- and *H*-planes are shown in Figure 4.17 and Figure 4.18, respectively.

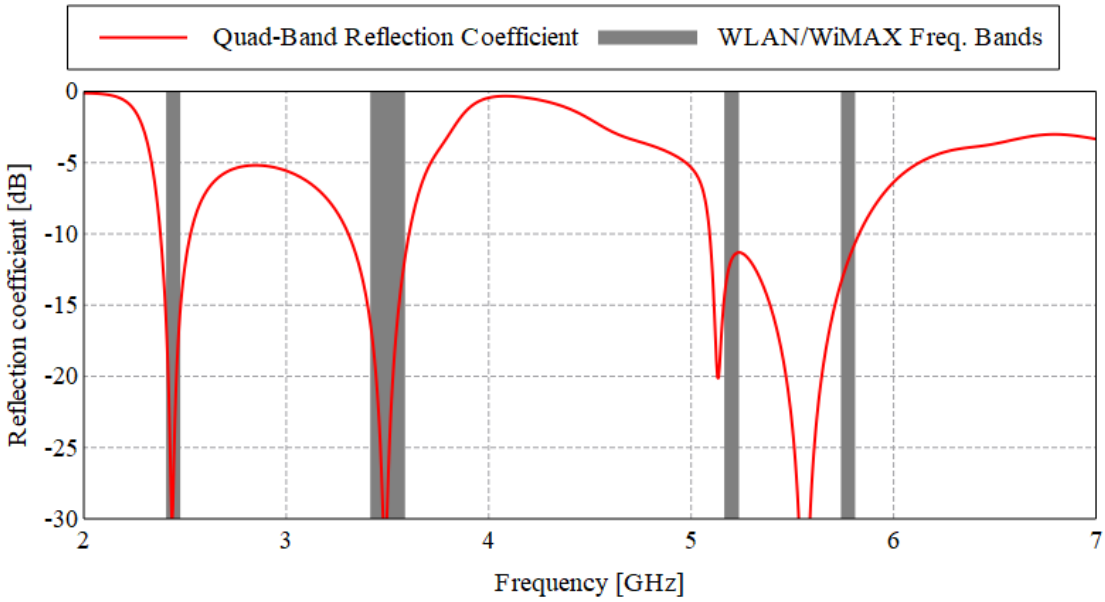

Figure 4.14. Simulated reflection coefficient of quad-band antenna

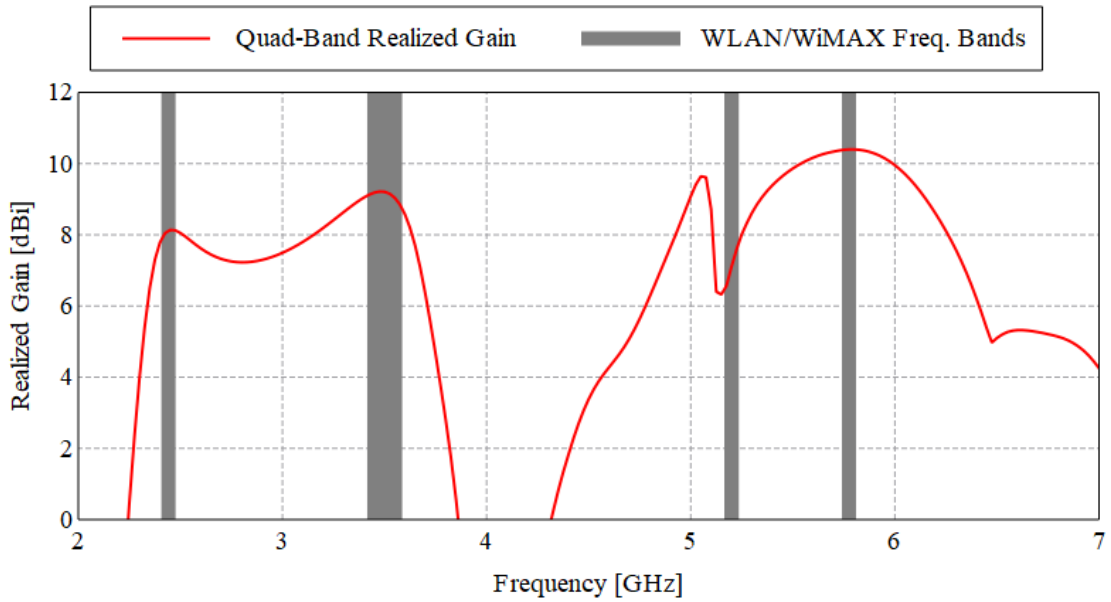

Figure 4.15. Simulated realized gain of quad-band antenna

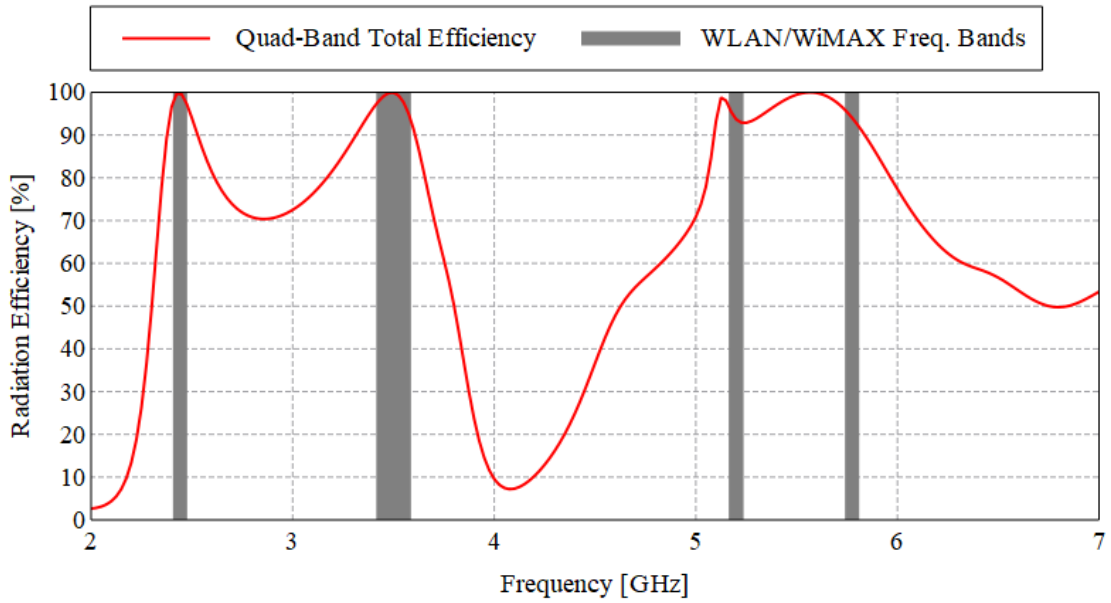

Figure 4.16. Simulated total efficiency of quad-band antenna

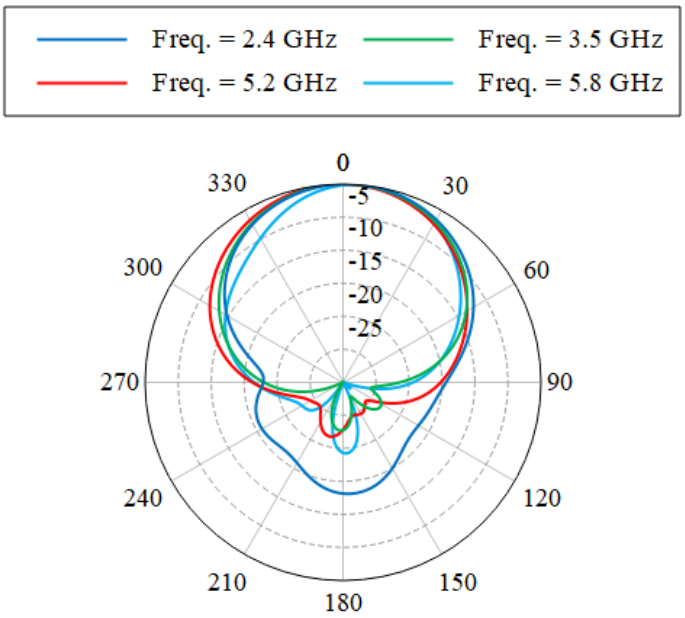

Figure 4.17. Simulated *E*-plane co-polarization radiation patterns of the quad-band antenna

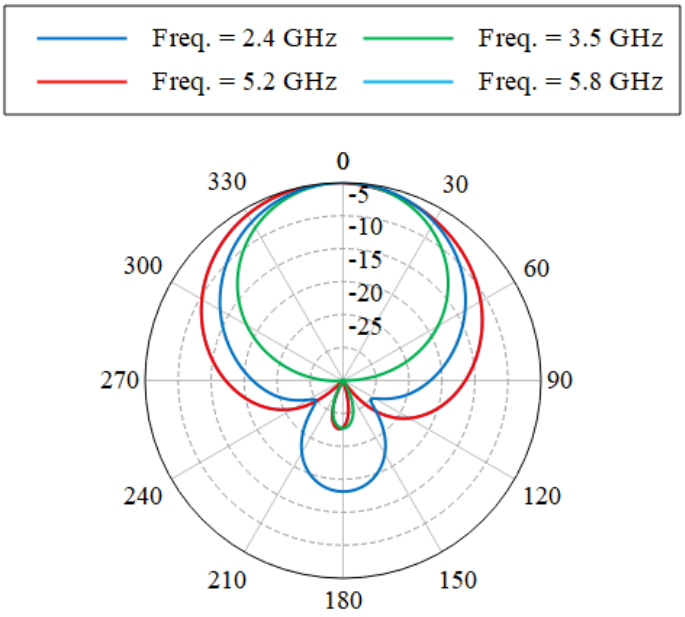

Figure 4.18. Simulated *H*-plane co-polarization radiation patterns of the quad-band antenna

The simulated reflection coefficient illustrates that a quad-band response was realized by the antenna. The -10 dB impedance bandwidth at each of the resonances are from 2.38 – 2.53 GHz (6.11%), 3.31 – 3.61 GHz (8.67%) and from 5.09 – 5.83 GHz (13.6%). This indicates that the antenna was well matched in the respective WLAN and WiMAX frequency bands.

The realized gain achieved by the quad-band antenna was above 7 dBi across all three resonances. The peak gain achieved at the center of each band were 7.94 dBi, 9.21 dBi, 7.07 dBi and 10.4 dBi at 2.45 GHz, 3.5 GHz, 5.2 GHz and 5.8 GHz, respectively. The simulated total efficiency of the antenna was also above 90% across the respective WLAN and WiMAX bands. The normalized radiation patterns achieved by the antenna are all directional and the results from the simulated radiation patterns are summarized in Table 4.4.

Table 4.4. Summarised simulated radiation pattern results of quad-band antenna

Plane	***E*-Plane**				***H*-Plane**			
Frequency [GHz]	2.45	3.5	5.2	5.75	2.45	3.5	5.2	5.75
3-dB beam width	73.0°	71.3°	73.8°	55.5°	68.6°	56.7°	85.9°	49.2°
Main beam direction	2.0°	1.0°	-2.0°	7.0°	0.0°	0.0°	0.0°	0.0°
Side-lobe level [dB]	-14	-23	-22	-20	-14	-23	-23	-20
Front-to-back ratio [dB]	14	23	23	20	14	23	23	20
Max Cross-polarization [dB]	-30	-28	-9	-26	-7	-6	-7	-16

The *E*-plane radiation patterns at the respective resonances illustrates that the quad-band antenna also achieves a directional radiation pattern. The 5.2 GHz resonance achieved by the quad-band antenna is due to the smaller secondary slot-element. The radiation pattern results also show that the maximum cross-polarization, in the *E*-plane at 5.2 GHz, is larger than the other resonances. The 3-dB beamwidth in the *H*-plane at 5.2 GHz, is 85.9° and is much broader when compared to the 3-dB beamwidth of the other resonances in the *H*-plane. The front-to-back ratios of the antenna are 14 dB, 23 dB, 23 dB and 20 dB at 2.4 GHz, 3.5 GHz, 5.2 GHz and 5.8 GHz, respectively.

4.3.3 Antenna functionality of quad-band antenna

The quad-band antenna is excited by the coaxial transmission line, while the end of the feedline is terminated with an open circuit termination, which produces a standing wave on the feed line. The antenna also consists of a strip-slot pair with a secondary slot element in the ground plane of the antenna. The size of the secondary slot had an important role in the operation of the quad-band antenna. The coupling between the slot, from the strip-slot pair, and the secondary slot, produced a resonance at 3.5 GHz which was not possible with the triple-band antenna.

The strip-slot antenna on its own has an omnidirectional radiation pattern and to make the antenna unidirectional, the AMC reflector was placed 6 mm behind the antenna. The AMC reflector has a ±90° phase bandwidth from 3.64 GHz to 6.64 GHz (58.4%), which covers the 5.2 GHz and 5.8 GHz WLAN frequency bands. The AMC reflector and the ground plane of the antenna excited a radiating patch mode, which caused the 2.4 GHz resonance to be achieved.

The simulated reflection coefficient of the quad-band antenna in Figure 4.14 illustrates that the 2.4 GHz, 5.2 GHz and 5.8 GHz WLAN and 3.5 GHz WiMAX frequency bands are covered. The *E*-fields were simulated 1.2 mm below the antenna ground plane, which is between the antenna and AMC reflector. This was to determine what aspect of the quad-band antenna resonated at the respective resonances. The *E*-fields were simulated in the Z-axis at 2.4 GHz and 3.5 GHz and in the X-axis at 5.2 GHz and 5.8 GHz. The *E*-fields were simulated at 2.4 GHz, 3.5 GHz, 5.2 GHz and 5.8 GHz and is shown in Figure 4.19.

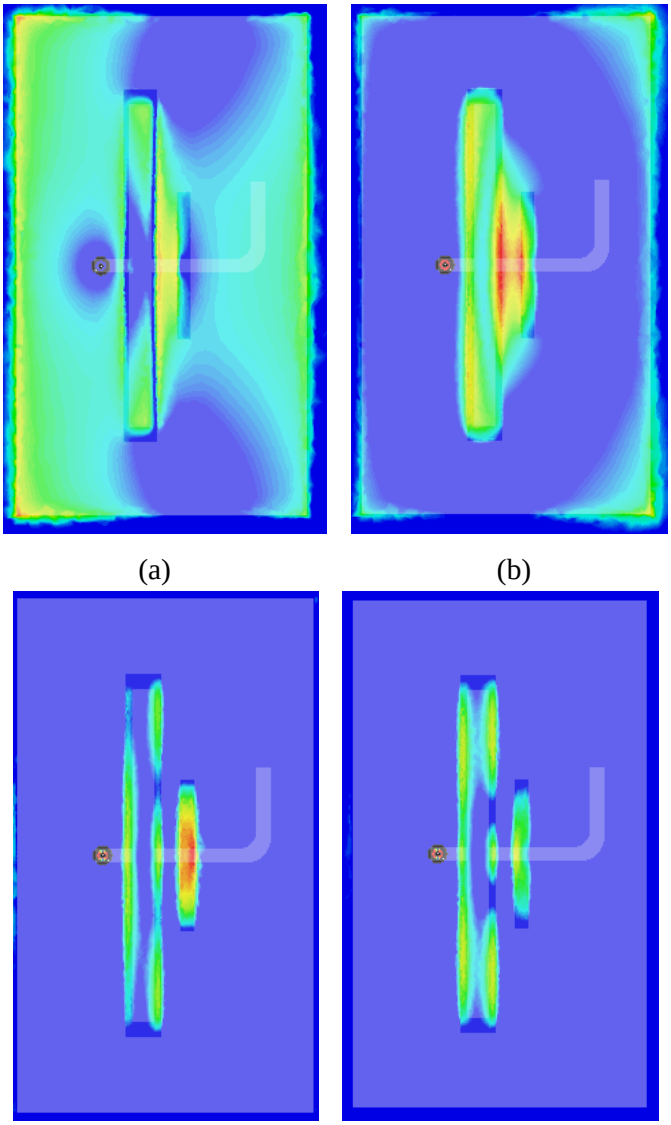

(a) (b)

(c) (d)

Figure 4.19. Simulated *E*-field at 1.2 mm below antenna ground plane of quad-band antenna at (a) 2.4 GHz (b) 3.5 GHz (c) 5.2 GHz (c) 5.8 GHz

The simulated *E*-fields at 1.2 mm below the ground plane of the quad-band antenna illustrates where the fields are concentrated at the respective resonant frequencies. The lower operating resonance at 2.4 GHz is primarily controlled by the length of the ground plane of the antenna substrate. The AMC surface and the ground plane of the antenna support a radiating patch mode, as can be seen by the high value fields at the two vertical edges of the antenna ground plane in Figure 4.19(a). The 3.5 GHz resonance is produced by the coupling

between the strip-slot pair and the secondary slot element. The design of the strip-slot pair with the smaller secondary slot-element allows for the 3.5 GHz WiMAX frequency band to be achieved. At 5.2 GHz it can be seen that the E_x-fields are concentrated around the smaller secondary slot-element. The simulated E_x-fields at 5.8 GHz illustrate that the fields are concentrated among the strip-slot pair. The combination of the strip-slot pair with the secondary slot and the size of the antenna ground plane, resulted in a quad-band antenna covering the respective 2.4 GHz, 5.2 GHz and 5.8 GHz WLAN bands as wells as the 3.5 GHz WiMAX band.

4.3.4 Improved front-to-back ratio

The simulated radiation patterns of the quad-band antenna show that at 2.45 GHz the radiation pattern had a smaller front-to-back ratio when compared to the other bands. The size of the AMC ground plane was varied to try and improve the front-to-back ratio of the antenna at the 2.4 GHz band. The initial size of the AMC ground plane was 53×68 mm^2. In simulation, it was found that increasing the size of the AMC ground plane to 100×100 mm^2, reduced the gain in the upper 5.2 GHz and 5.8 GHz bands by 1.5 dB. This indicated that a trade-off had to be made between the overall size of the antenna and the gain in the upper 5.2 GHz and 5.8 GHz bands. The size of the AMC ground plane was increased to a size of 80×80 mm^2. The layout of the quad-band antenna with a larger AMC ground plane is shown in Figure 4.20.

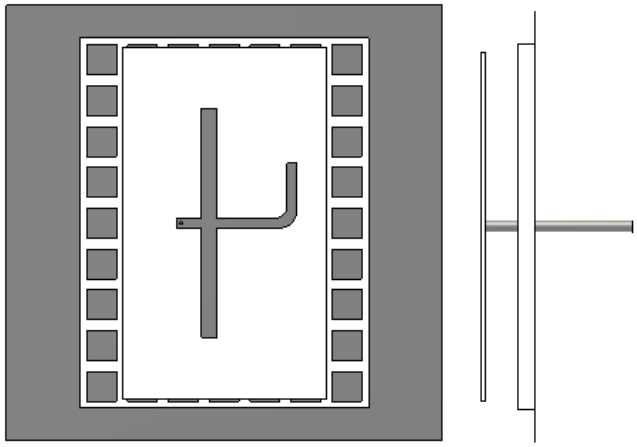

(a) (b)

Figure 4.20. Layout of quad-band antenna with a larger AMC ground plane

(a) top view (b) side view

The quad-band antenna with a larger ground plane was simulated and compared to the original quad-band antenna. The simulated reflection coefficient and realized gain between the two antennas are shown in Figure 4.21 and Figure 4.22.

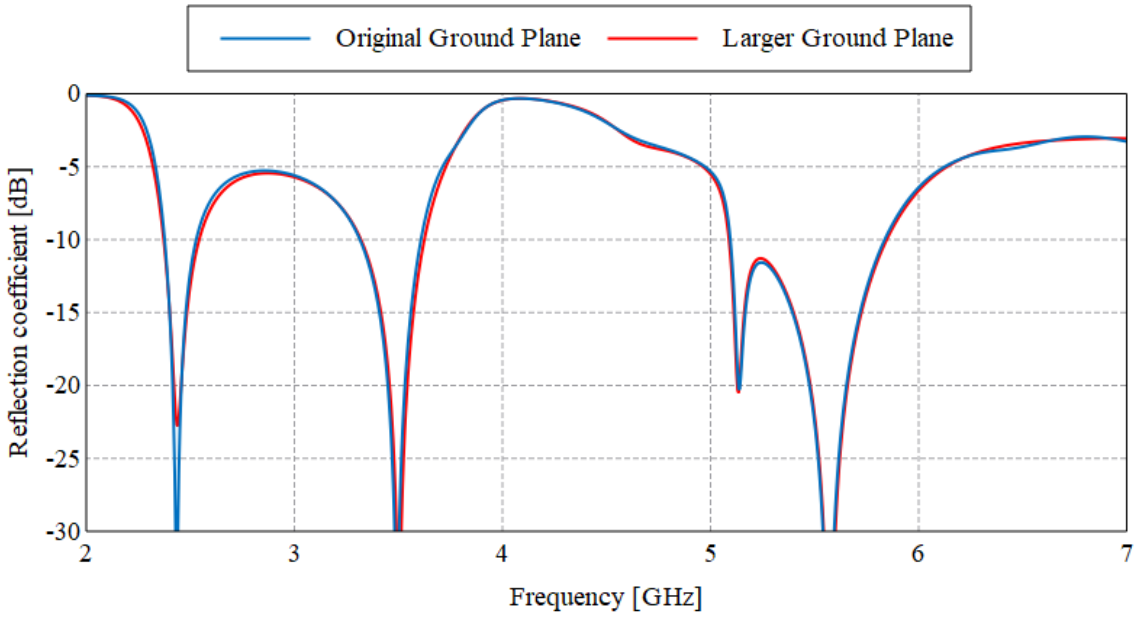

Figure 4.21. Simulated reflection coefficient of quad-band antenna with and without larger AMC ground plane

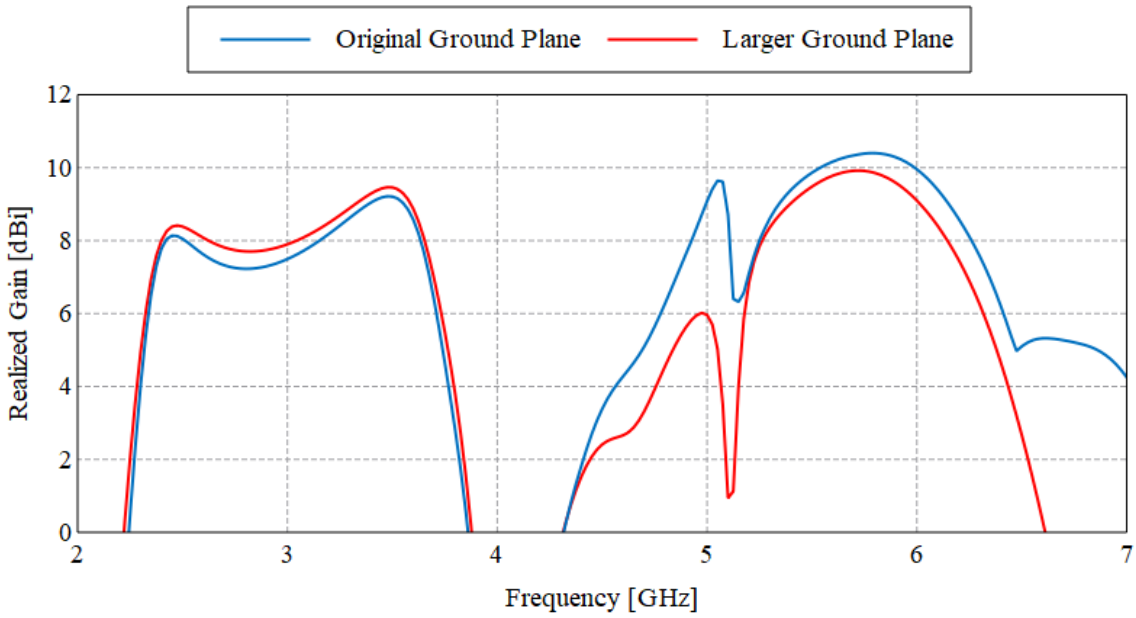

Figure 4.22. Simulated realized gain of quad-band antenna with and without larger AMC ground plane

The simulated reflection coefficient illustrates that the addition of the larger AMC ground plane did not influence the matching of the quad-band antenna. The simulated realized gain results illustrate that the increase in the ground plane did have an influence. The simulated realized gain in the lower 2.45 GHz and 3.5 GHz bands achieved a gain increase of 0.2 dBi and 0.25 dBi, respectively. In the upper 5.2 GHz and 5.8 GHz bands, the realized gain was affected much more. The simulated gain at 5.2 GHz remained the same, but the gain at 5.8 GHz decreased by 0.54 dBi. The radiation patterns were simulated at 2.45 GHz, to determine what influence the larger ground plane has on the front-to-back ratio of the antenna. The simulated *E*- and *H*-plane radiation patterns at 2.45 GHz between the original and larger ground plane are shown in Figure 4.23 and Figure 4.24, respectively.

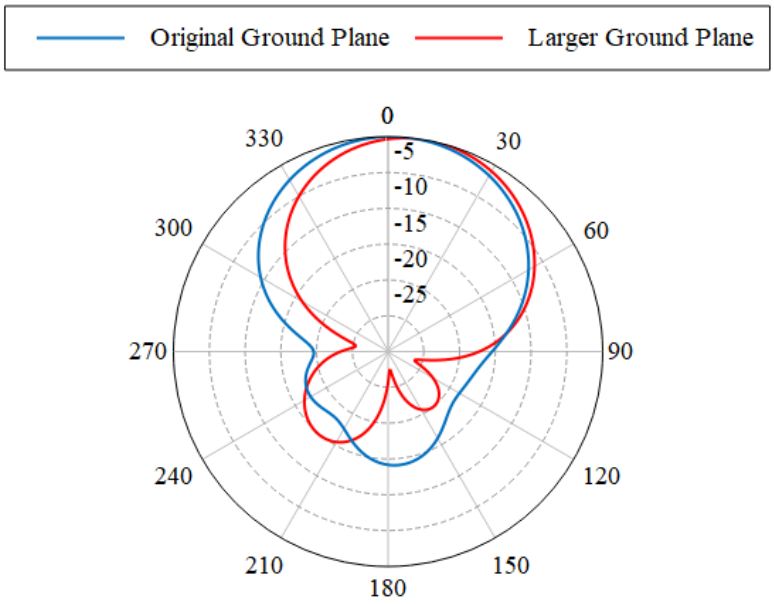

Figure 4.23. Simulated *E*-plane radiation pattern at 2.45 GHz of quad-band antenna with and without larger AMC ground plane

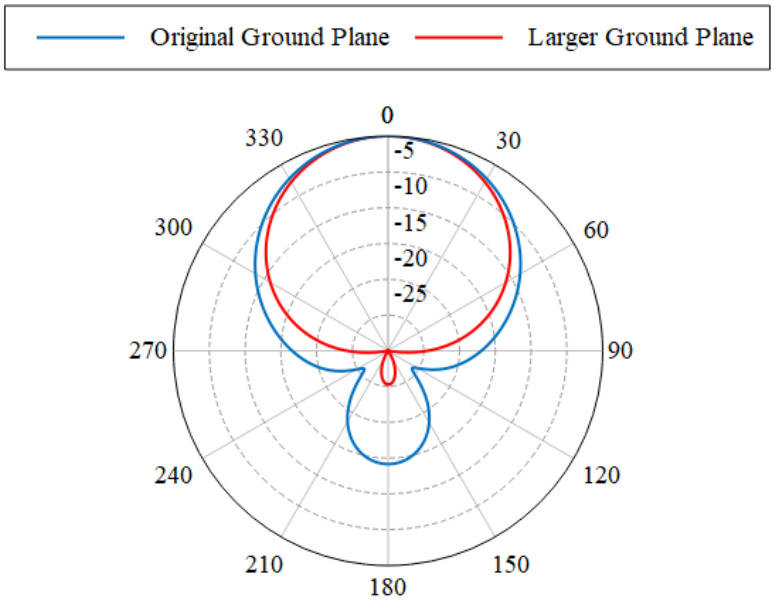

Figure 4.24. Simulated *H*-plane radiation pattern at 2.45 GHz of quad-band antenna with and without larger AMC ground plane

The simulated radiation patterns at 2.45 GHz show that a significant improvement in the front-to-back ratio of the antenna was achieved with the larger AMC ground plane. The

front-to-back ratio improved from 13.3 dB to 24.3 dB, which is an increase of 11 dB. The improved gain in the 2.4 GHz and 3.5 GHz bands is also due to the improved front-to-back ratio. The implementation of a larger AMC ground plane can be incorporated to achieve a better front-to-back ratio, but the overall size of the antenna will then be increased.

4.3.5 PARAMETER STUDY

The effect of tolerances on the performance of the antenna was determined by performing a parameter study. The same procedure as with the triple-band antenna was followed. The effect of a change in dielectric constant, coaxial feed position and a change in gap size between the antenna and AMC reflector was simulated in the following subsections.

4.3.5.1 Parameter study of substrate dielectric constant

The substrate used for the antenna was Rogers RO4003C, which has a dielectric constant of 3.38 at 10 GHz. According to the Rogers RO4003C datasheet, the dielectric constant is 3.55 for simulation. The antenna was designed and simulated in CST Microwave Studio, which has a material library with the characteristics for Rogers RO4003C. The dielectric constant was simulated with a dielectric constant of 3.38 and 3.55, to determine what influence a slight change in the dielectric constant might have on the matching of the antenna. The simulated reflection coefficient for the change in the dielectric constant of the antenna substrate is shown in Figure 4.25.

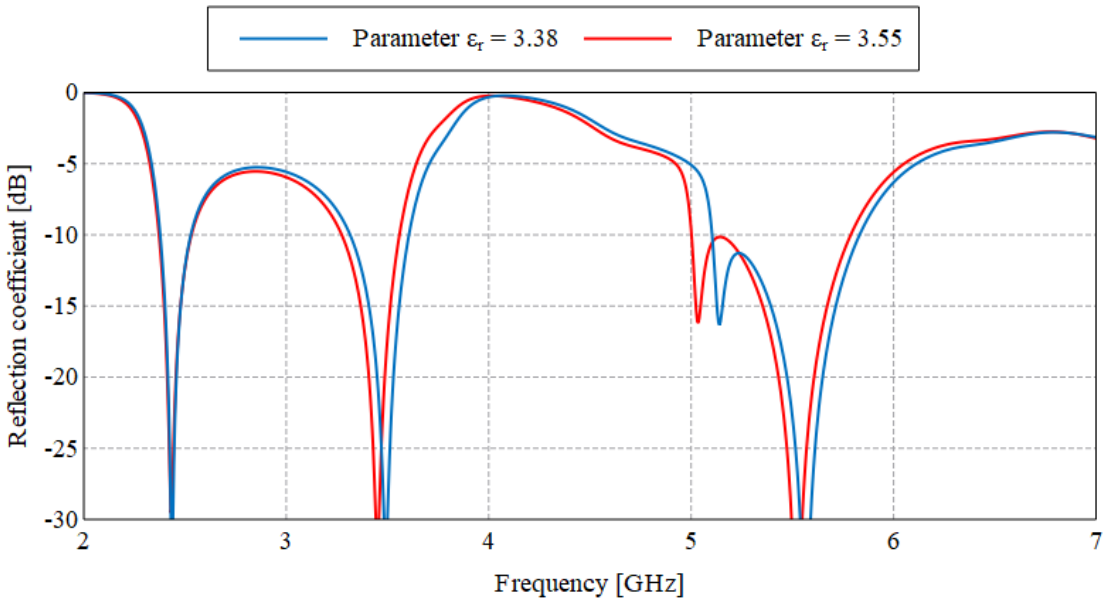

Figure 4.25. Parameter study for change in dielectric constant of quad-band antenna

The simulated reflection coefficient illustrates that a slight change in the dielectric constant has an effect on the matching of the antenna. The matching of the resonances in the WiMAX and upper WLAN frequency bands are affected by the change in dielectric constant and shift to a lower frequency as the dielectric constant increases to 3.55. The lower WLAN frequency band resonance was not affected by the change in dielectric constant, because the dielectric medium for the patch mode is the air gap between the ground plane of the antenna and the AMC reflector. The results achieved illustrate that a change in dielectric constant can influence the impedance bandwidth of the antenna at the respective WiMAX and upper WLAN bands.

4.3.5.2 Parameter study of coaxial connector position

The pin of the coaxial transmission line has to be connected to the microstrip feedline. The position of the coaxial connector on the microstrip feedline was varied to determine what influence it has on the matching of the antenna. The position of the coaxial transmission line connector pin was varied with 0.5 mm to the left and right of the original position. The simulated reflection for the change in coaxial connector position is shown in Figure 4.26.

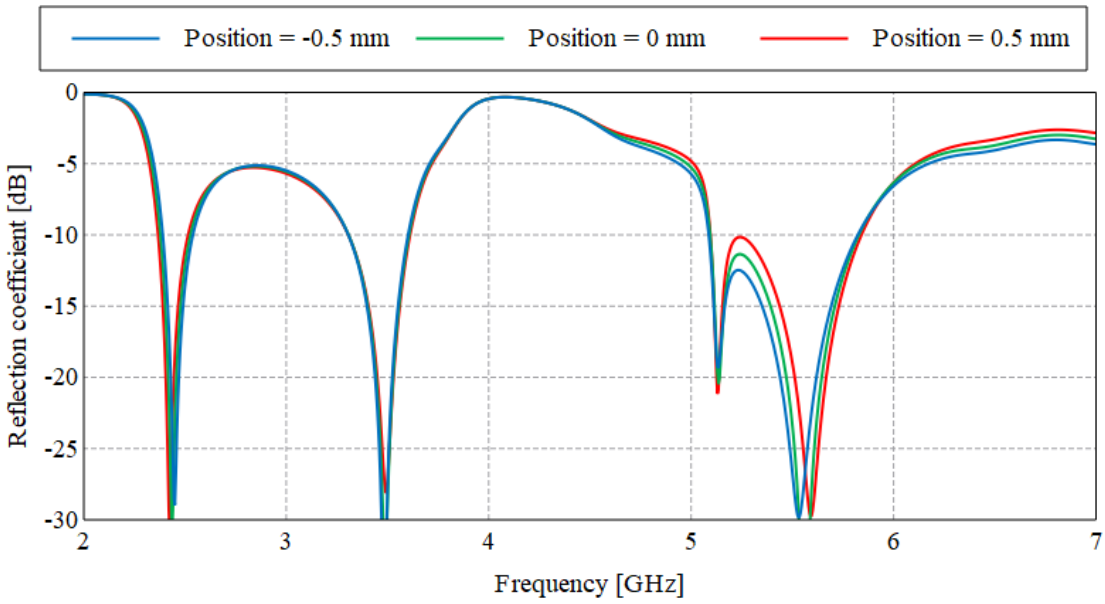

Figure 4.26. Parameter study for change in coaxial connector position of quad-band antenna

The simulated reflection coefficient illustrates that the slight change in the coaxial connector position has an effect on the matching of the antenna. As the coaxial connector position was varied 0.5 mm left and right of the original position (0 mm), the matching in the upper (5.2 GHz and 5.8 GHz) WLAN band was influenced. The microstrip-slot pair achieves a resonance at 5.56 GHz and as the coaxial pin connector was moved to the left (-0.5 mm) and closer to the edge of the feedline, the resonance shifted to the left. When the coaxial connector pin was moved to the right (0.5 mm), the resonance shifted to the right. The simulation results illustrate that if the coaxial connector is moved further away from the edge, the resonance achieved by the strip-slot pair will shift to a higher frequency. This will cause the -10 dB impedance bandwidth to break and not cover the entire upper WLAN frequency band. The placement of the coaxial connector pin has an important influence on the matching of the quad band antenna.

4.3.5.3 Parameter study of gap size between antenna and AMC reflector

The distance between the antenna and the AMC reflector is an important aspect in terms of the matching of the antenna. The AMC reflector was designed achieve a 0° reflection phase 6 mm away from the antenna. The antenna and AMC reflector will have to be assembled by

hand after manufacturing. The effect for a change in spacing between the antenna and reflector is investigated. The gap size between the antenna and AMC reflector is varied and investigated at a gap size of 4 mm, 6 mm and 8 mm. The simulated reflection coefficient for the change in gap size is shown in Figure 4.27.

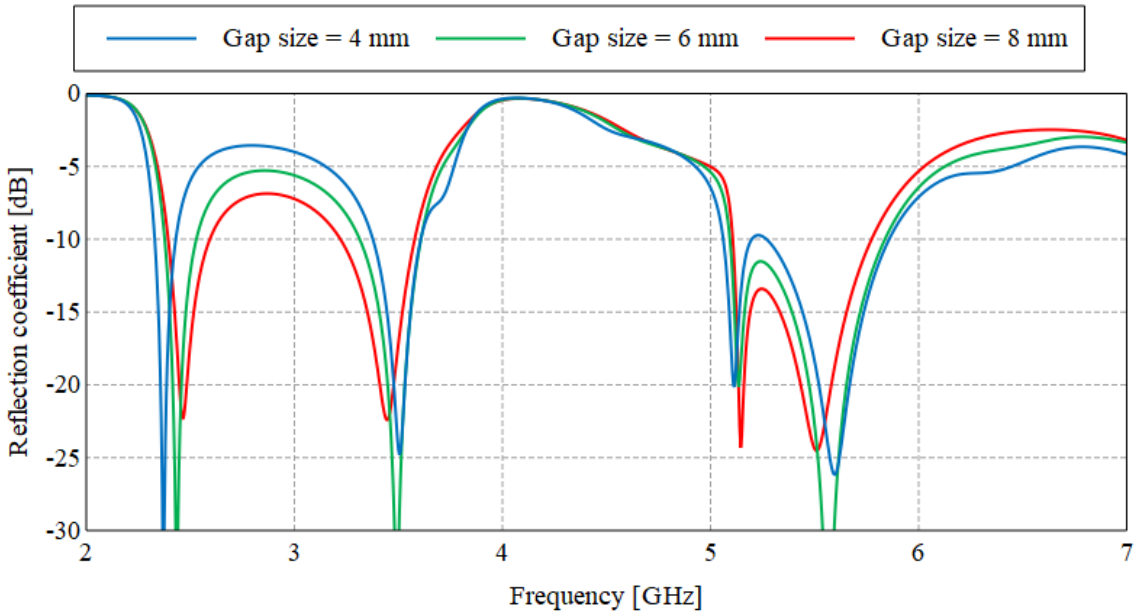

Figure 4.27. Parameter study for change in gap size between antenna and AMC reflector of quad-band antenna

The simulated reflection coefficient illustrates that the change in gap size between the antenna and AMC reflector has a significant effect on the matching. When the gap size was increased from 6 mm to 8 mm, the lower WLAN and WiMAX frequency bandwidth increased, while the upper WLAN frequency bandwidth decreased. This was as expected as the AMC reflector was designed to operate with a gap size of 6 mm. As the gap size was decreased from 6 mm to 4 mm, the opposite occurred and the bandwidth of the lower WLAN and WiMAX frequency bands decreased, while the bandwidth in the upper WLAN frequency band increased. The simulation results indicate that when the antenna is assembled, the gap size has to be accurate to achieve the correct results. The gap size can also be used as a tuning parameter to obtain a better bandwidth in the lower WLAN and WiMAX frequency bands.

4.4 PROTOTYPE ANTENNA

The triple- and quad-band antennas were manufactured on the respective substrates. The holes for the coaxial transmission line through the antenna and AMC reflector were drilled by hand. The spacing between the antenna and AMC reflector was controlled by including M3 nylon screws and nuts. The holes were also drilled by hand for the spacers to be included. The coaxial cable was fed through the AMC reflector and antenna substrate. The inner connecter of the coaxial transmission line was soldered to the feedline and the outer conductor of the coaxial cable was also soldered to the ground plane of the antenna, as well as the ground plane of the AMC reflector.

The assembled prototype triple- and quad-band antennas are shown in Figure 4.28 and Figure 4.29. In Figure 4.28 the antennas are shown from the top, which shows the soldered coaxial center pins on the feedline and also the top of the nylon screws and nuts. In Figure 4.29 the side-view of the prototype triple-band antenna is shown and the quad-band antenna was connected in the same manner.

Figure 4.28. Top view of prototype antennas

(a) triple-band antenna (b) quad-band antenna

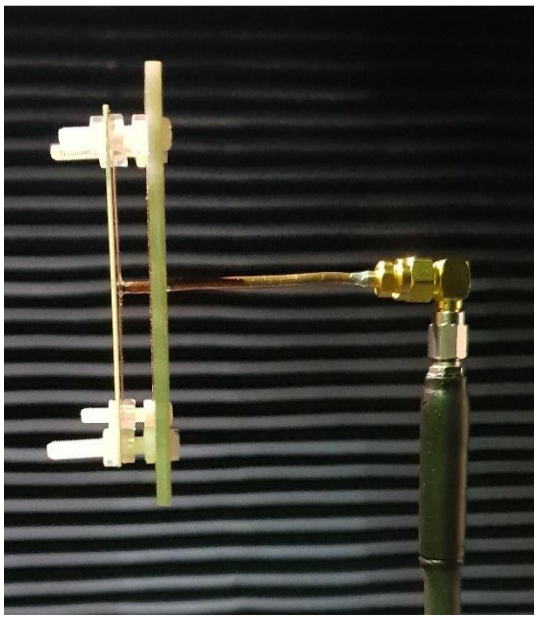

Figure 4.29. Side view of prototype triple-band antenna

4.5 CHAPTER SUMMARY

The final design of the proposed triple- and quad-band antennas were performed in this chapter. The antenna geometries were designed from the knowledge gained from the background study and the strip-slot antenna in [21]. The triple-band antenna consisted of a strip-slot pair, a secondary slot element in the ground plane and a single-band AMC reflector. The secondary slot element increased the impedance bandwidth achieved by the antenna and the antenna operated in the 2.4 GHz, 5.2 GHz and 5.8 GHz WLAN frequency bands. The quad-band antenna was designed and also consisted of a strip-slot pair with a smaller secondary slot in the ground plane and a single-band AMC reflector. The only difference between the triple- and quad-band antennas is the size of the secondary slot. The quad-band antenna achieved a -10 dB impedance bandwidth in the 2.4 GHz, 5.2 GHz and 5.8 GHz WLAN frequency bands as well as the 3.5 GHz WiMAX frequency band. The antennas achieved a low profile design, with a high gain and directional radiation pattern. The final prototype triple- and quad-band antennas were manufactured and assembled.

CHAPTER 5 RESULTS AND DISCUSSION

5.1 CHAPTER OVERVIEW

In this chapter, the manufactured triple- and quad-band antennas were measured and compared to the simulation results. The antennas were measured in the compact antenna range at the University of Pretoria. The setup of the triple- and quad-band antennas for measurements are shown in Figure 5.1.

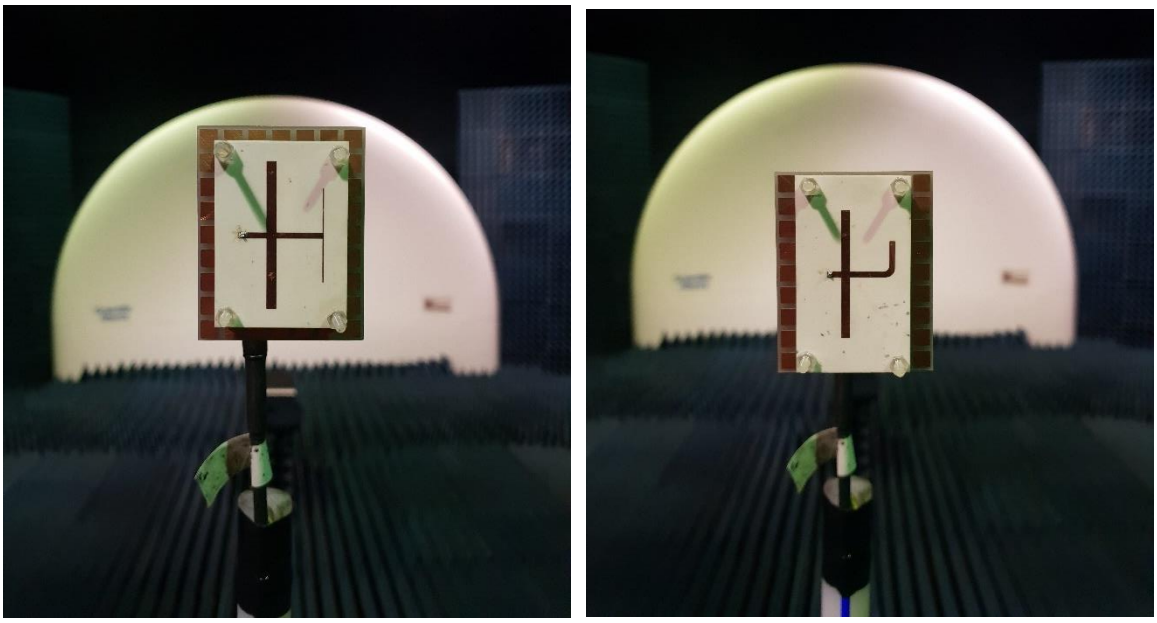

(a) (b)

Figure 5.1. Manufactured antennas in the compact antenna range

(a) triple-band antenna (b) quad-band antenna

5.2 TRIPLE-BAND ANTENNA

5.2.1 Reflection Coefficient

The reflection coefficient measurement after the triple-band antenna was assembled as shown in Figure 5.2. The antenna was measured with a calibrated Hewlett Packard HP8510 Vector Network Analyzer (VNA). It can be seen that the results obtained from the

measurements correspond very well to the simulated results. The -10 dB impedance bandwidth achieved by the measured results are from 2.39 – 2.49 GHz (4.1%) and from 4.90 – 5.94 GHz (19.2%). The antenna was well matched in the WLAN frequency bands and covered the entire 2.4 GHz, 5.2 GHz and 5.8 GHz WLAN bands.

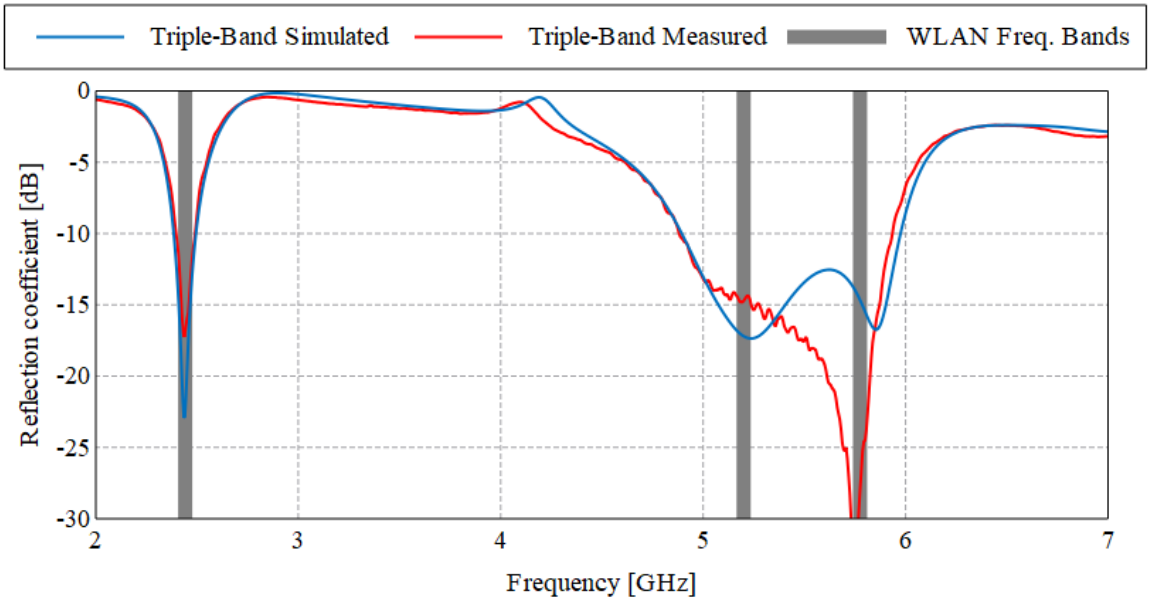

Figure 5.2. Simulated and measured reflection coefficient of triple-band antenna

5.2.2 Radiation Patterns

The radiation patterns of the triple-band antenna were measured in the compact antenna range at the University of Pretoria. In the simulation of the proposed triple-band antenna, it was found that the front-to-back ratio achieved at 2.45 GHz was 10 dB. It was larger in comparison to the front-to-back ratio achieved at 5.2 GHz and 5.8 GHz, which was 18 dB and 17 dB, respectively. The radiation patterns of the manufactured triple-band antenna and the same results were achieved.

The size of the AMC ground plane was increased to improve the front-to-back ratio of the triple-band antenna. The initial size of the AMC ground plane was 53×68 mm^2 and was increased to a size of 80×80 mm^2 in simulation. The ground plane of the manufactured AMC

reflector was increased to the size and measured. The triple-band antenna with the larger AMC ground plane for measurements is shown in Figure 5.3.

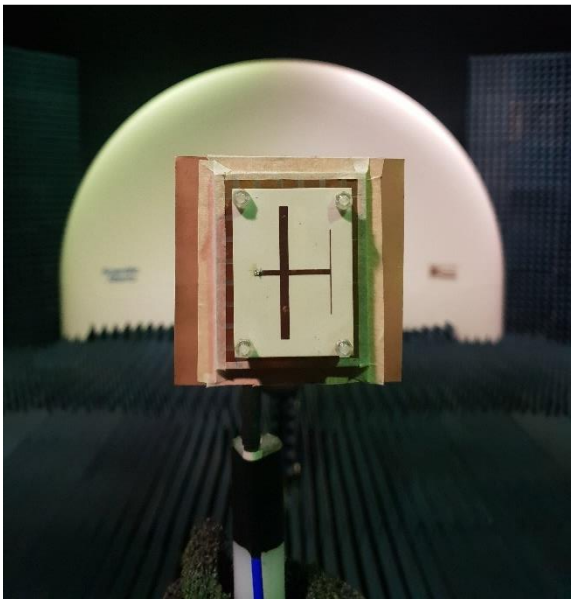

Figure 5.3. Triple-band antenna with larger AMC ground plane

The radiation patterns were measured at the center frequency of each of the WLAN bands. The simulated radiation patterns in the *E*- and *H*-planes are compared to the measured results and shown in Figure 5.4 to Figure 5.9.

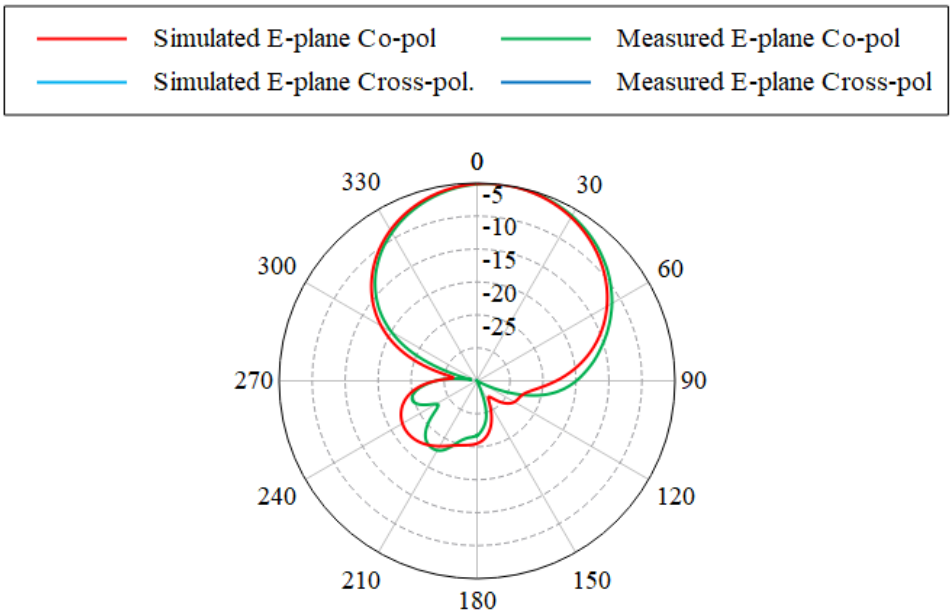

Figure 5.4. Simulated and measured radiation pattern in the *E*-plane at 2.45 GHz of triple-band antenna with the larger ground plane

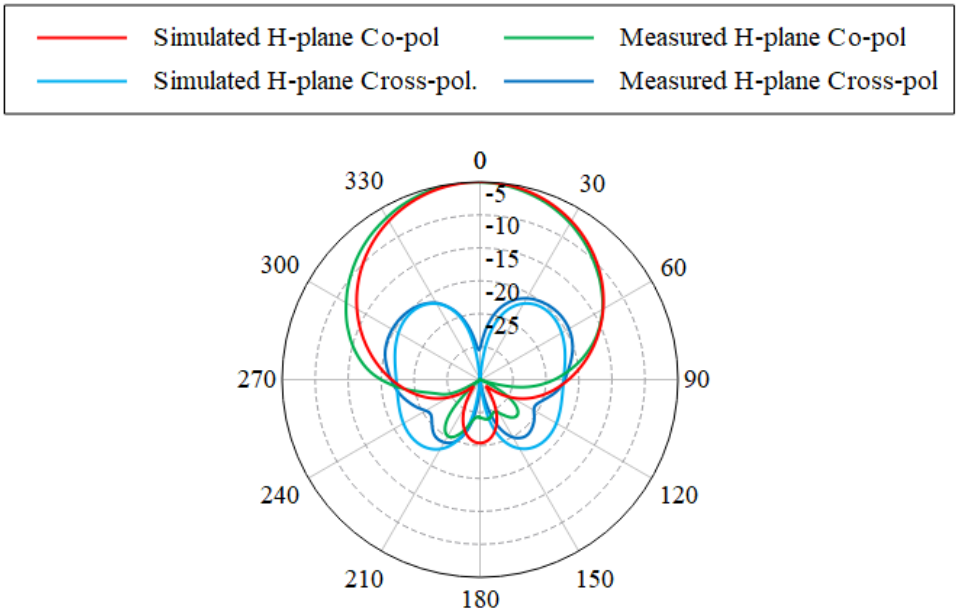

Figure 5.5. Simulated and measured radiation patterns in the *H*-plane at 2.45 GHz of triple-band antenna with the larger ground plane

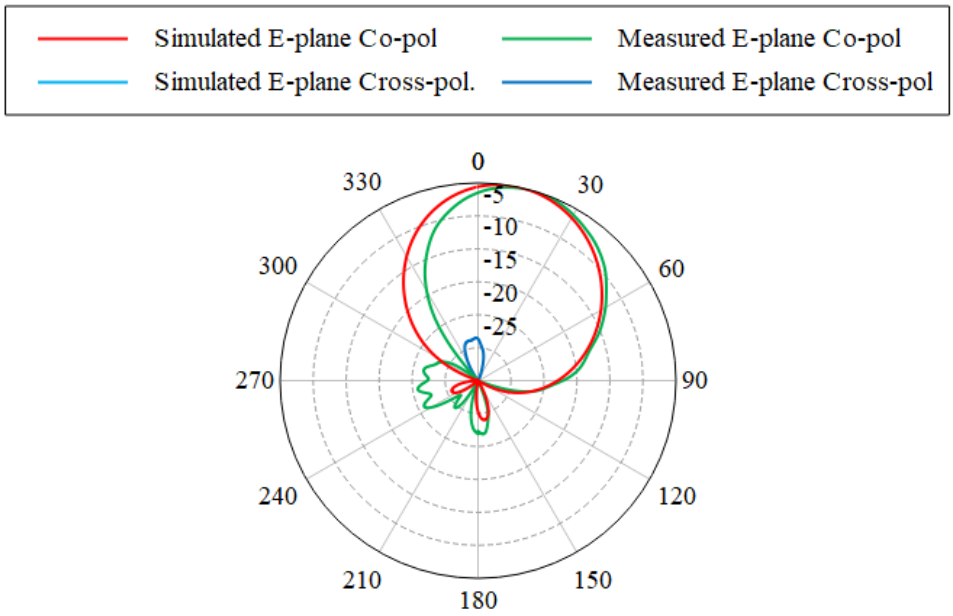

Figure 5.6. Simulated and measured radiation patterns in the *E*-plane at 5.2 GHz of triple-band antenna with the larger ground plane

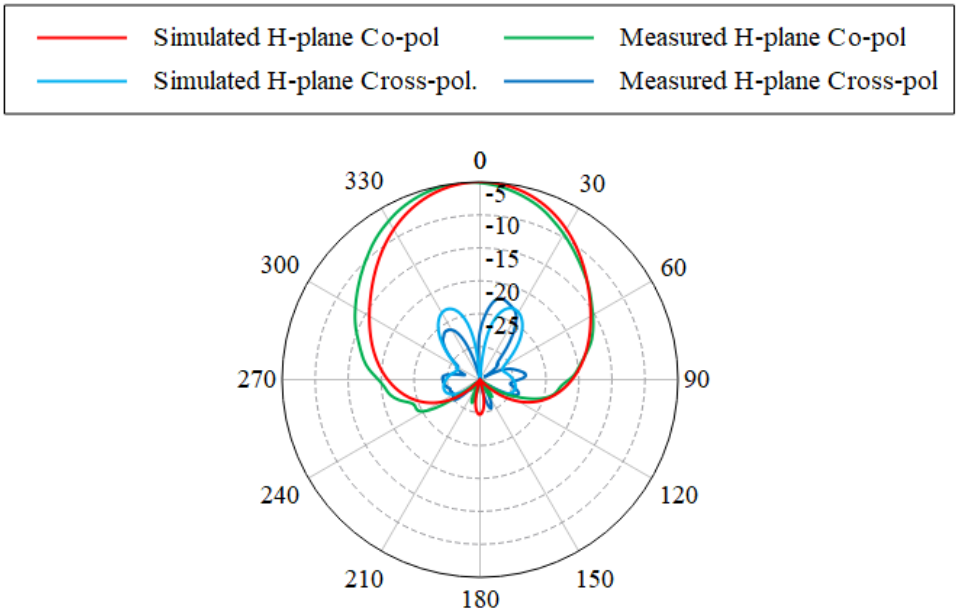

Figure 5.7. Simulated and measured radiation patterns in the *H*-plane at 5.2 GHz of triple-band antenna with the larger ground plane

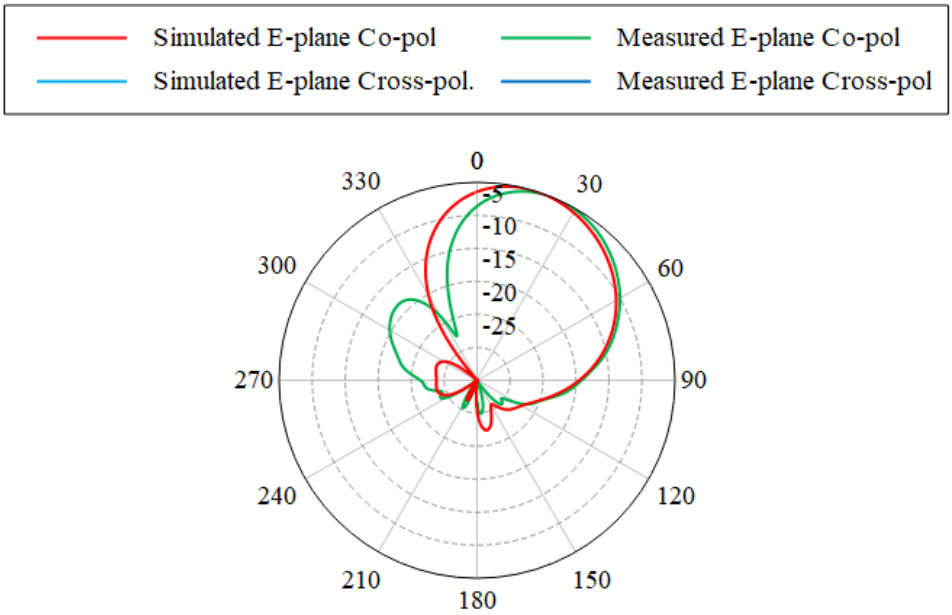

Figure 5.8. Simulated and measured radiation patterns in the *E*-plane at 5.75 GHz of triple-band antenna with the larger ground plane

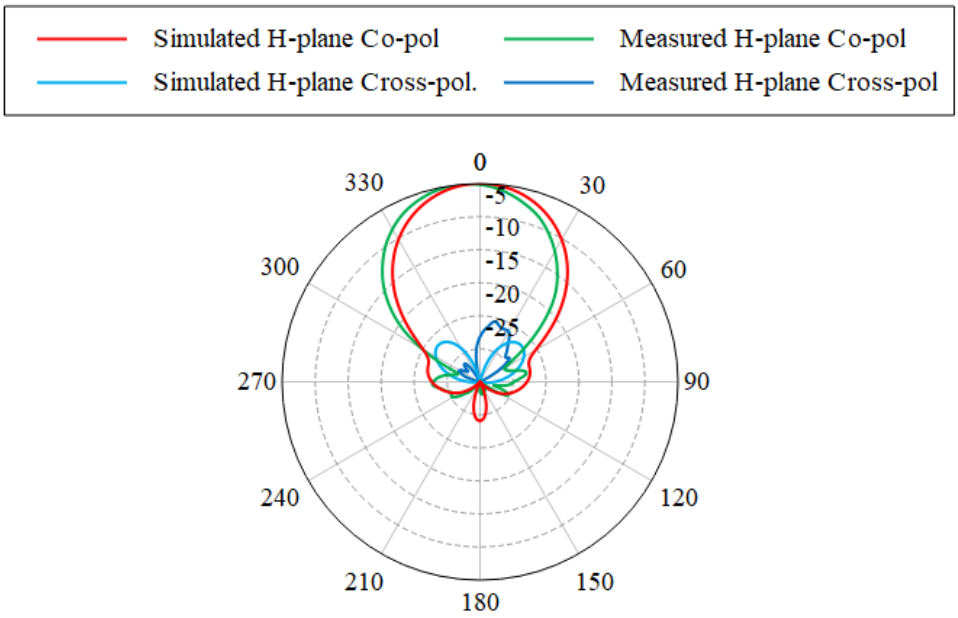

Figure 5.9. Simulated and measured radiation patterns in the *H*-plane at 5.75 GHz of triple-band antenna with the larger ground plane

The measured radiation patterns achieved by the triple-band antenna exhibit good agreement with the simulated results in the three WLAN frequency bands of operation. The parameters for the measured radiation patterns of the triple-band antenna with a larger ground plane are summarized in Table 5.1.

Table 5.1. Measured triple-band antenna radiation pattern parameters

Plane	***E*-Plane**			***H*-Plane**		
Frequency	2.45 GHz	5.2 GHz	5.75 GHz	2.45 GHz	5.2 GHz	5.75 GHz
3-dB beam-width	68.1°	49.0°	52.9°	72.7°	56.9°	46.3°
Main beam direction	6°	17°	23°	0°	0°	0°
Max side-lobe level	-18 dB	-21 dB	-14 dB	-20 dB	-26 dB	-23 dB
Front-to-back ratio	24 dB	28 dB	29 dB	24 dB	28 dB	29 dB
Max cross-polarization	-25 dB	-24 dB	-30 dB	-14 dB	-17 dB	-21 dB

The radiation pattern in the *E*-planes show that the antenna squints in the 2.45 GHz frequency bands. The current distribution of the ground plane is not symmetrical, due to the feed point of the antenna, which causes the antenna to squint in the 2.4 GHz band. The radiation patterns achieved by the triple-band antenna in the respective resonances are directional and have a very good front-to-back ratio. The front-to-back ratio achieved at 2.45 GHz is 24 dB, which is better than the front-to-back of 10 dB with the original ground plane of the AMC reflector. The increase in the AMC ground plane has improved the radiation pattern of the antenna. The measured *E*-plane radiation pattern at 5.75 GHz indicated a side-lobe, which was not experienced with the simulation. The side-lobe was investigated by varying various aspects of the triple-band antenna that could have caused it. Such as the alignment between the antenna and the AMC reflector, the bent coaxial connecter, as well as small variations in

the manufacturing of the antenna. The simulations indicated that the various changes in the antenna alignment and manufacturing did not have an influence on the *E*-plane radiation pattern at 5.75 GHz.

The measured *E*-plane radiation patterns were also measured at three frequencies in the respective 2.4 GHz, 5.2 GHz and 5.8 GHz WLAN bands. The measured *E*-plane radiation patterns are shown in Figure 5.10 to Figure 5.12.

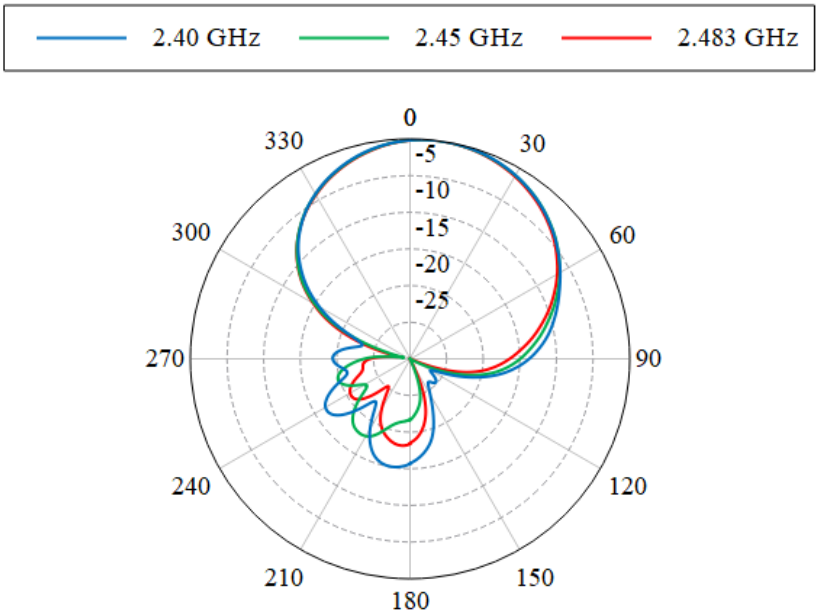

Figure 5.10. Measured radiation patterns in the *E*-plane of triple-band antenna with larger AMC ground plane in 2.4 GHz WLAN frequency band

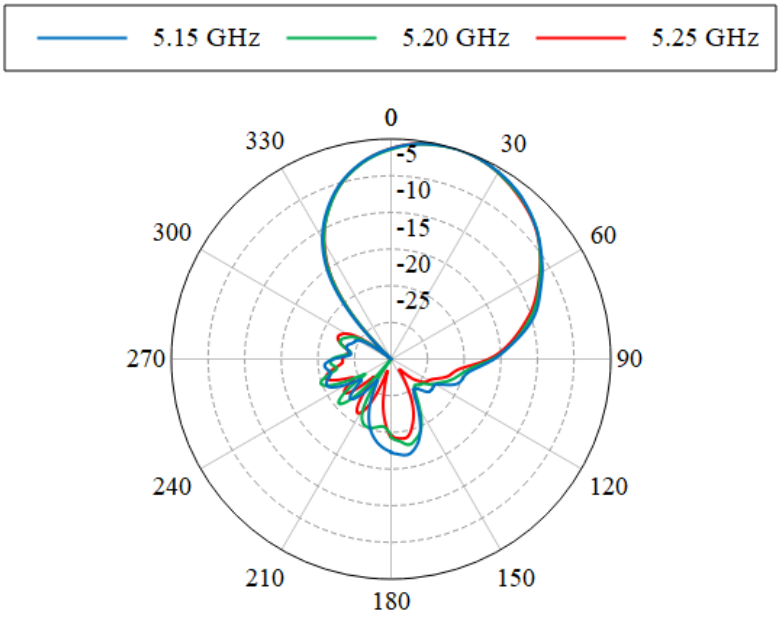

Figure 5.11. Measured radiation patterns in the *E*-plane of triple-band antenna with larger AMC ground plane in 5.2 GHz WLAN frequency band

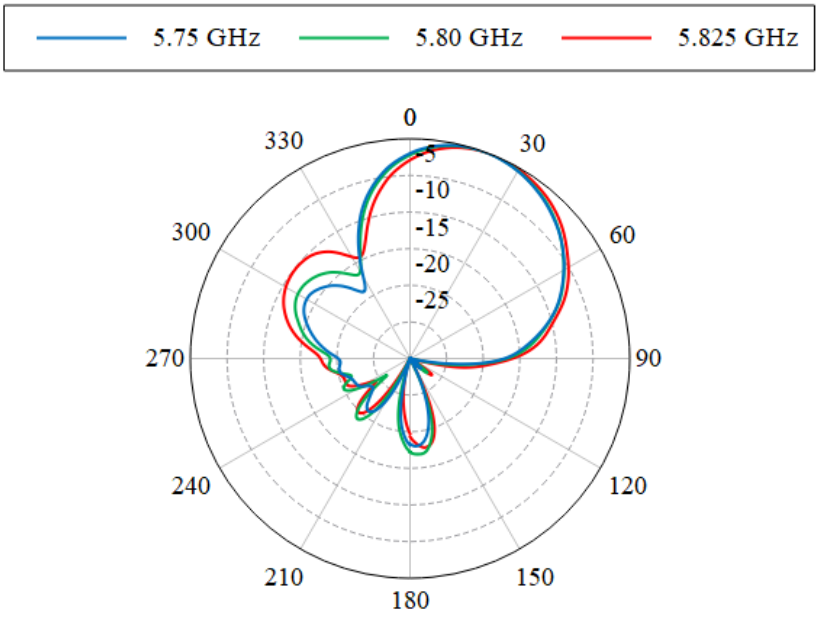

Figure 5.12. Measured radiation patterns in the *E*-plane of triple-band antenna with larger AMC ground plane in 5.75 GHz WLAN frequency band

The measured *E*-plane radiation patterns indicate that, in the respective WLAN frequency bands, the triple-band antenna has a constant radiation pattern over the three different WLAN frequency bands.

5.2.3 Gain

The gain of the antenna was also measured in the compact antenna range at the University of Pretoria. The gain of the antenna was calibrated using a standard gain horn antenna as a reference antenna. The measured *E*-plane radiation patterns illustrated that the main beam of the antenna squinted in the respective WLAN bands. To achieve accurate results, the gain of the antenna with the larger AMC ground plane was measured at boresight and then the antenna gain was peaked. The measured gain is compared to the simulated gain at boresight and at the respective peak angles.

5.2.3.1 Boresight gain

The gain of the triple-band antenna was firstly measured at boresight and compared to the simulated gain at boresight, as shown in Figure 5.13. The difference between the simulated and measured gain in each of the WLAN frequency bands are given in Table 5.2.

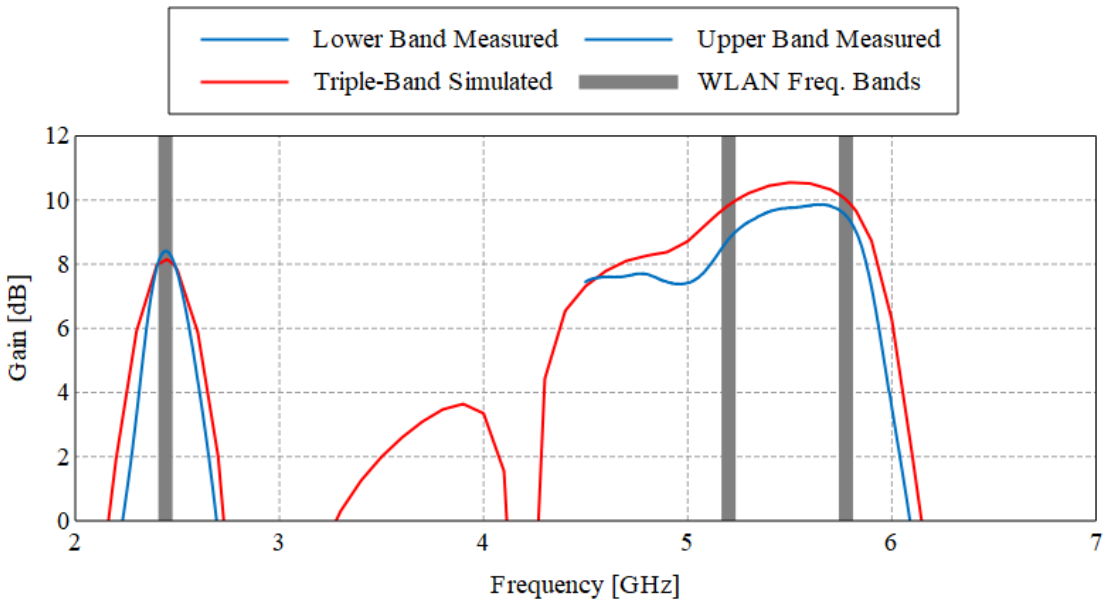

Figure 5.13. Simulated and measured gain of triple-band antenna at boresight

Table 5.2. Simulated and measured boresight gain of triple-band antenna

Frequency [GHz]	Simulated Gain [dBi]	Measured Gain [dBi]	Difference [dBi]
2.4	8.0	8.0	0.0
2.45	8.2	8.4	0.2
2.483	8.0	8.1	0.1
5.15	9.6	8.4	1.2
5.2	9.8	8.8	1.0
5.25	10.1	9.1	1.0
5.725	10.2	9.8	0.4
5.75	10.1	9.7	0.4
5.825	9.7	9.0	0.7

The average gain of the triple-band antenna at boresight across all three frequency bands was 8.8 dBi. The largest difference between the measured and simulated gain was 1.2 dBi at 5.15 GHz. The factors that could possibly influence the difference between the measured and simulated gain include small etching manufacturing tolerances. The antenna is simulated in perfect condition, where the manufactured antenna can be influenced by the setup of the antenna, such as the transmission line cable connected to the SMA connector. The antenna gain was also peaked to determine if the same difference occurs.

5.2.3.2 Peak Gain

The simulated radiation patterns of the triple-band antenna illustrated that the antenna squints in the upper 5.2 GHz and 5.8 GHz WLAN frequency bands. In the lower 2.4 GHz WLAN band the antenna was peaked at 1.8°. In the upper 5.2 GHz and 5.8 GHz WLAN frequency bands, the antenna was peaked at 16.5°. The simulated gain was also peaked at 1.8° and 16.5° for the lower and upper WLAN bands, respectively. The measured and simulated peak gain is shown in Figure 5.14. The peak gain results are summarized in Table 5.3.

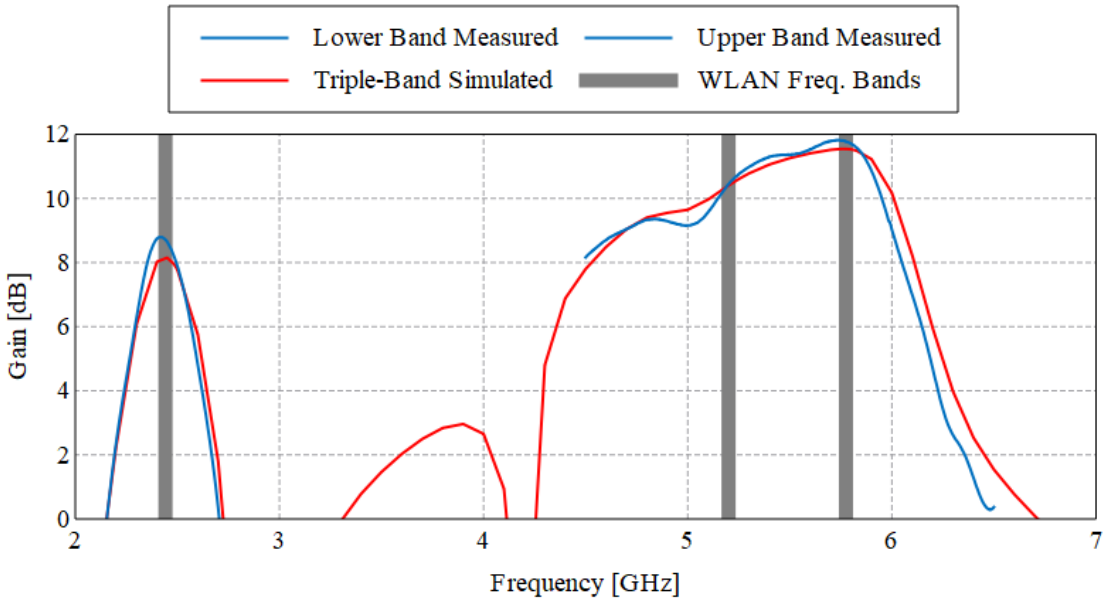

Figure 5.14. Simulated and measured peak gain of triple-band antenna with the larger ground plane

Table 5.3. Simulated and measured peak gain of triple-band antenna

Frequency [GHz]	Simulated Gain [dBi]	Measured Gain [dBi]	Difference [dBi]
2.4	8.0	8.7	0.7
2.45	8.2	8.7	0.5
2.483	8.0	8.2	0.2
5.15	10.2	10.0	0.2
5.2	10.4	10.4	0.0
5.25	10.6	10.8	0.2
5.725	11.5	11.8	0.3
5.75	11.5	11.8	0.3
5.825	11.5	11.6	0.1

The average measured gain of the triple-band antenna at the respective peaks across all three frequency bands was 10.2 dBi, which is an increase of 1.4 dBi compared to the boresight gain. The large difference between the boresight and peak gain, is due to the squinting of the main lobe of the antenna. The largest difference between the measured and simulated gain

was 0.7 dBi at 2.4 GHz. The antenna was assembled by hand and the holes were also drilled after the antenna was manufactured. The distance between the antenna and AMC reflector was not as perfect as in simulation. The triple-band antenna was simulated with the drilled holes, nylon screws and longer coaxial transmission line. The simulation results indicated that these factors did not have an influence on the gain and could not be accounted for the loss in gain.

5.3 QUAD-BAND ANTENNA

5.3.1 Reflection Coefficient

The same procedure was followed for the quad-band antenna as with the triple-band antenna. The quad-band antenna was also manufactured and assembled. The reflection coefficient of the antenna was measured with a calibrated Hewlett Packard HP8510 Vector Network Analyzer (VNA) and is shown in Figure 5.15. The results indicate that a quad-band response was achieved by the antenna, but that the measured results are not identical to the simulated results. The measured results indicate that a better -10 dB impedance bandwidth was achieved in all three resonances when compared to the simulated results. The difference in matching between the simulated and measured results could be due to small variations with the assembly of the quad-band antenna with the AMC reflector. The -10 dB impedance bandwidth obtained from the measured results were from 2.36 – 2.66 GHz (12.0%), 3.26 – 3.62 GHz (10.5%) and from 4.94 – 5.86 GHz (17.0%). The 2.4 GHz, 5.2 GHz and 5.8 GHz WLAN and 3.5 GHz WiMAX bands are covered by the quad-band antenna.

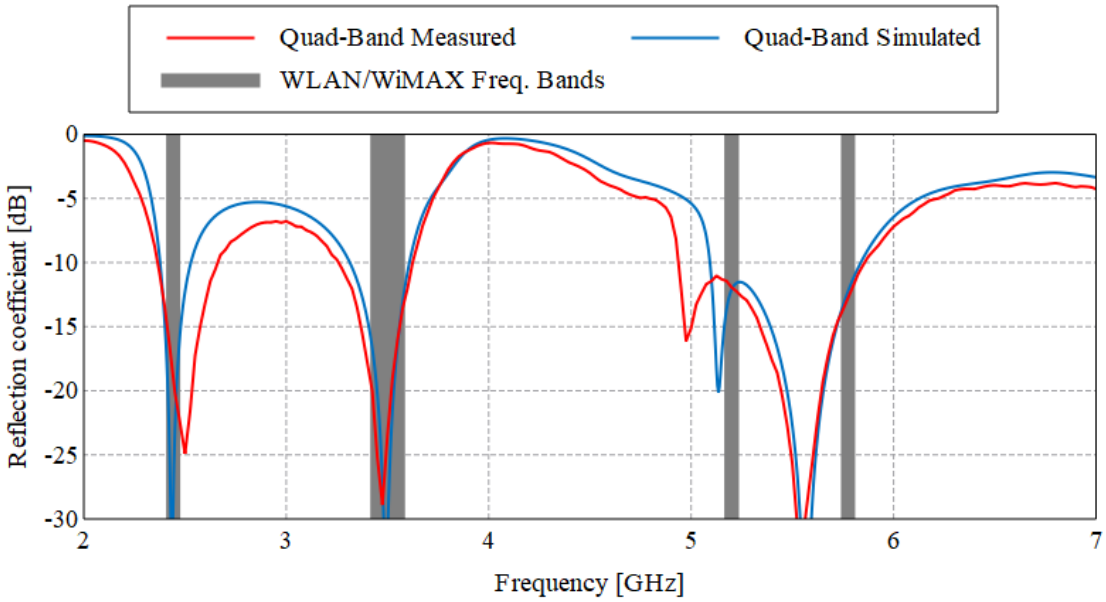

Figure 5.15. Simulated and measured reflection coefficient of quad-band antenna

5.3.2 Radiation Patterns

The radiation patterns of the quad-band antenna were also measured in the compact antenna range at the University of Pretoria. In simulation, it was found that the front-to-back ratio at 2.45 GHz was 14 dB, which was better than the triple-band antenna but could be improved. To improve the front-to-back ratio the ground plane of the AMC reflector was increased from the initial size of 53×68 mm^2 to a size of 80×80 mm^2, as was discussed in Chapter 4. The ground plane of the manufactured AMC reflector was increased. The quad-band antenna with the larger AMC ground plane for measurements is shown in Figure 5.16.

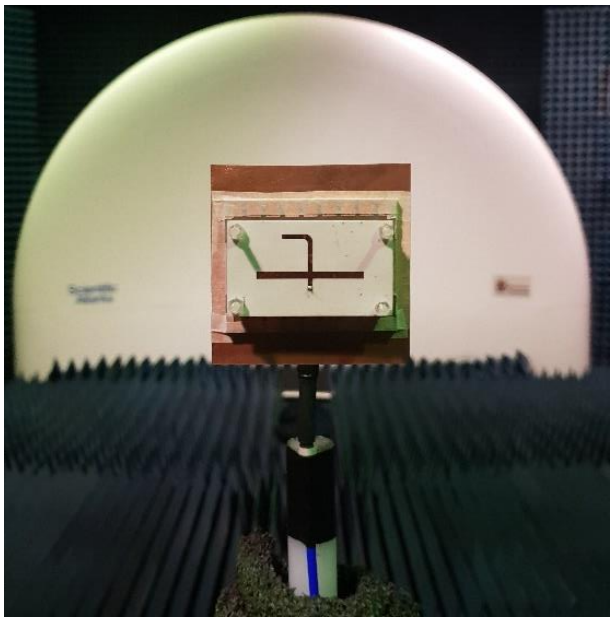

Figure 5.16. Quad-band antenna with larger AMC ground plane

The radiation patterns were measured at the center of each of the WLAN and WiMAX bands. The simulated radiation patterns in the *E*- and *H*-planes are compared to the measured results and shown in Figure 5.17 to Figure 5.24.

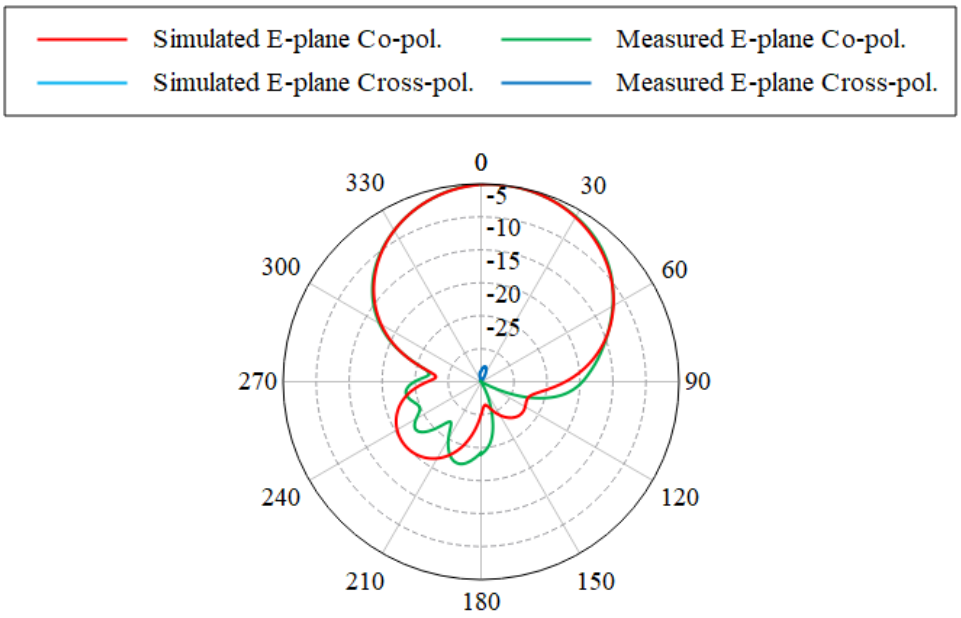

Figure 5.17. Simulated and measured radiation patterns in the *E*-plane at 2.45 GHz of quad-band antenna with the larger ground plane

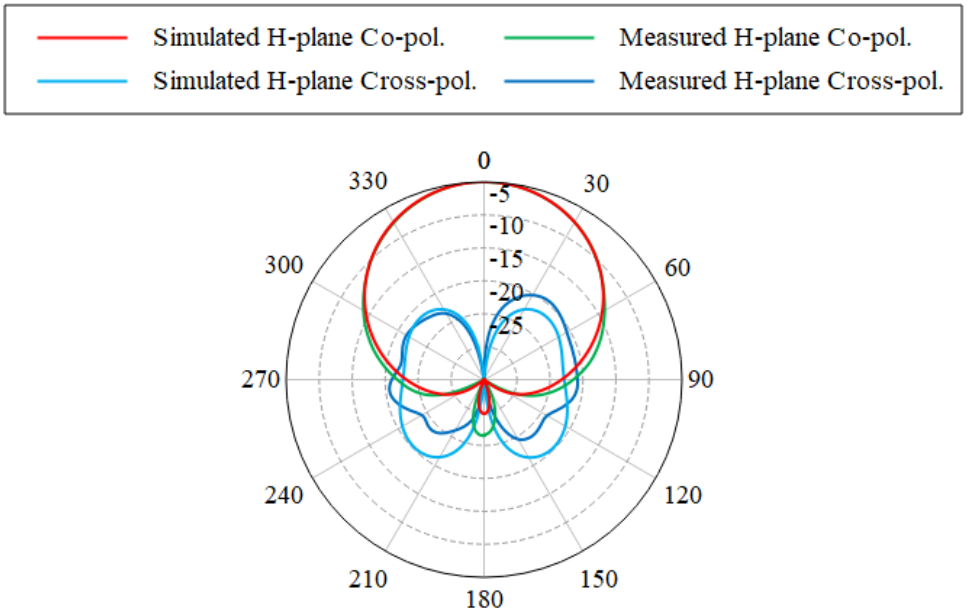

Figure 5.18. Simulated and measured radiation patterns in the *H*-plane at 2.45 GHz of quad-band antenna with the larger ground plane

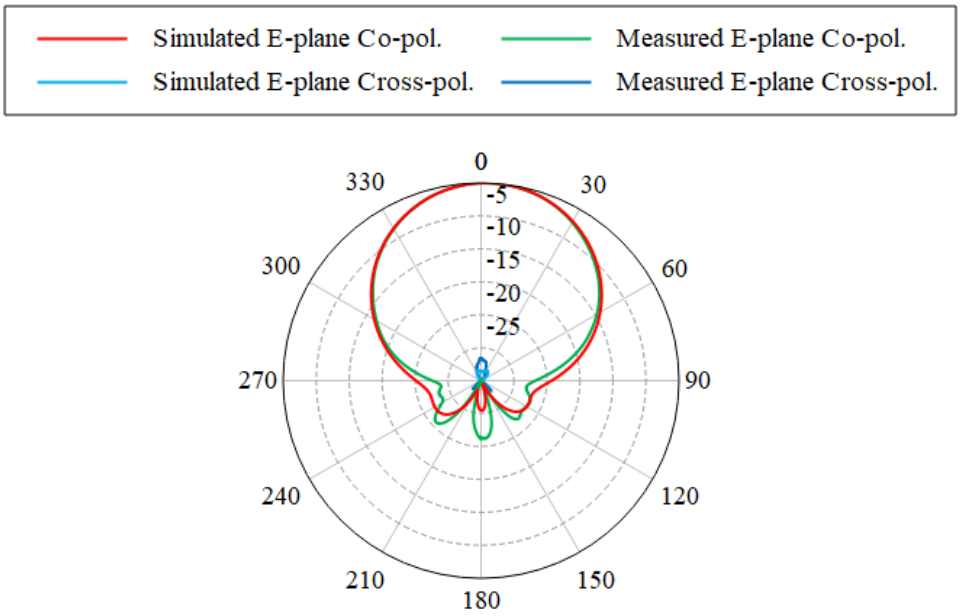

Figure 5.19. Simulated and measured radiation patterns in the *E*-plane at 3.5 GHz of quad-band antenna with the larger ground plane

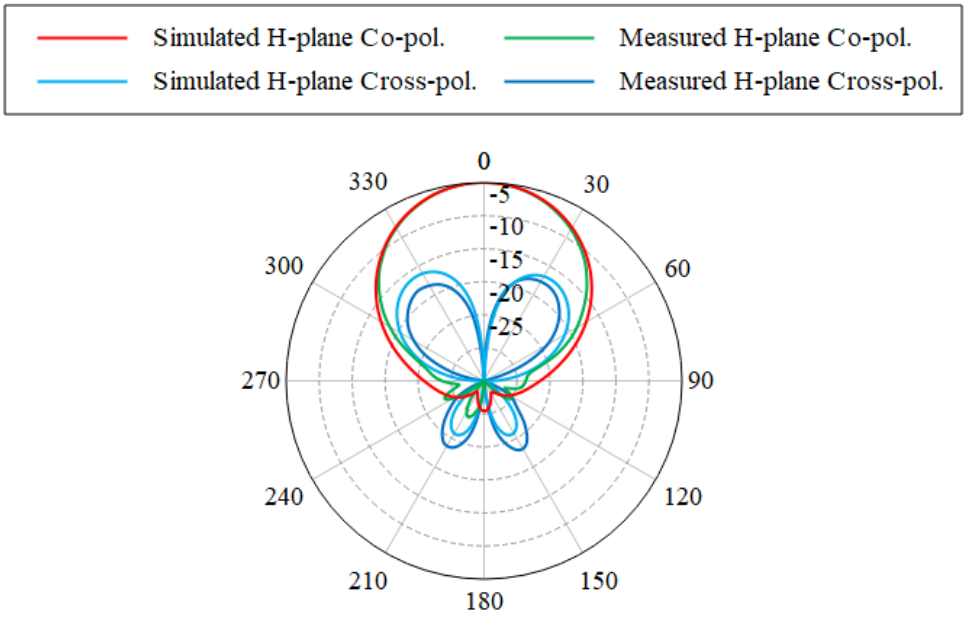

Figure 5.20. Simulated and measured radiation patterns in the *H*-plane at 3.5 GHz of quad-band antenna with the larger ground plane

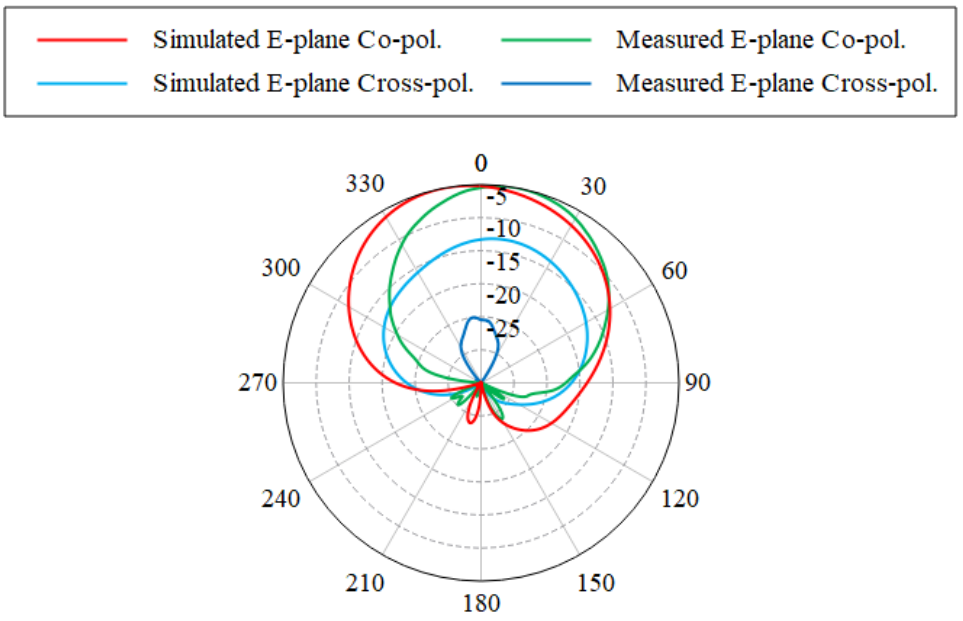

Figure 5.21. Simulated and measured radiation patterns in the *E*-plane at 5.2 GHz of quad-band antenna with the larger ground plane

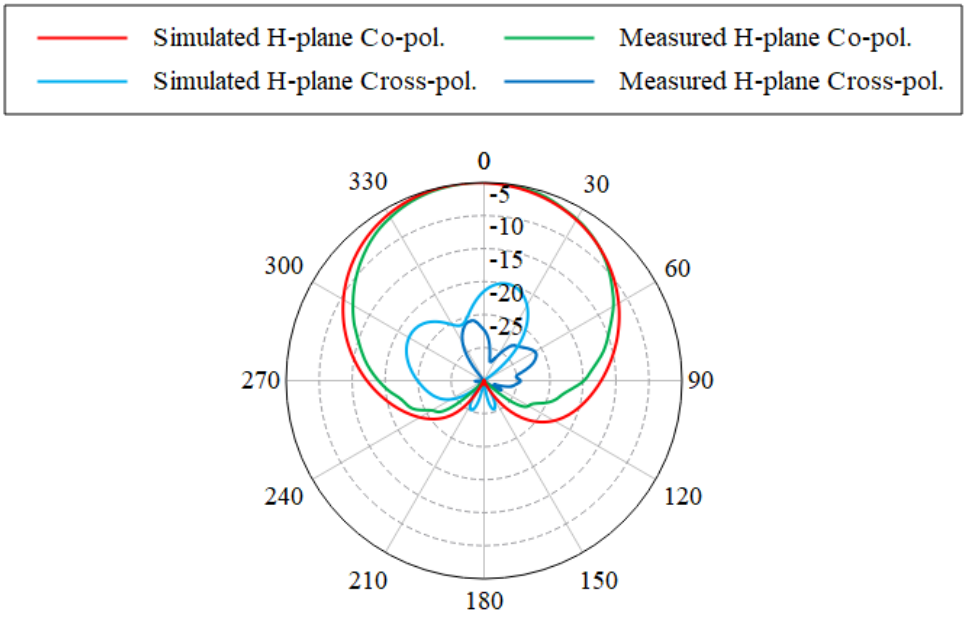

Figure 5.22. Simulated and measured radiation patterns in the *H*-plane at 5.2 GHz of quad-band antenna with the larger ground plane

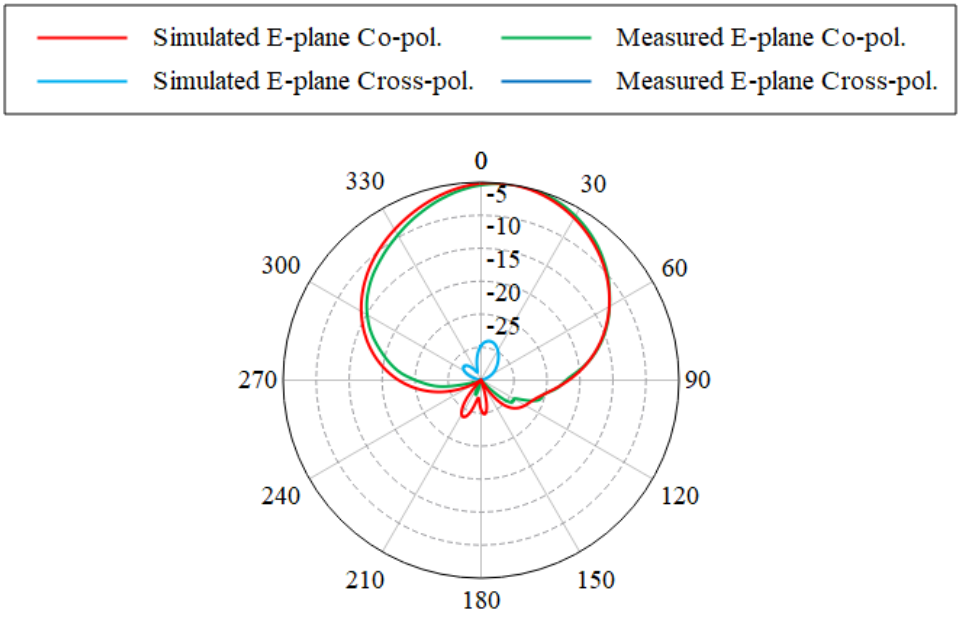

Figure 5.23. Simulated and measured radiation patterns in the *E*-plane at 5.75 GHz of quad-band antenna with the larger ground plane

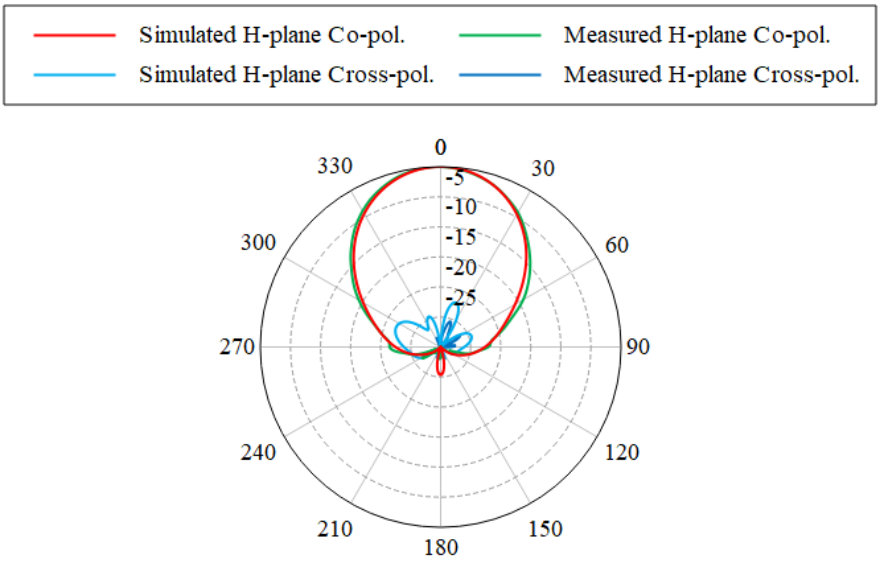

Figure 5.24. Simulated and measured radiation patterns in the *H*-plane at 5.75 GHz of quad-band antenna with the larger ground plane

The simulated and measured radiation patterns of the quad-band antenna with the larger ground plane, have good agreement. The only significant difference in results was at 5.2 GHz, where the measured *E*-plane had a much narrower main lobe than the simulated pattern and squinted. The associated parameters for the measured radiation patterns of the quad-band antenna with the larger ground plane are summarized in Table 5.4.

Table 5.4. Measured quad-band antenna radiation pattern parameters

Plane	***E*-Plane**				***H*-Plane**			
Frequency [GHz]	2.45	3.5	5.2	5.75	2.45	3.5	5.2	5.75
3-dB beam width	70.4°	61.1°	57.0°	60.3°	65.8°	55.7°	79.4°	50.9°
Main beam direction	6°	5°	11°	12°	0°	0°	0°	0°
Max side-lobe level [dB]	-17	-21	-24	-25	-22	-24	-30	-28
Front-to-back ratio [dB]	22	29	30	28	22	29	30	28
Max cross-polarization [dB]	-28	-27	-21	-32	-15	-13	-21	-25

The radiation patterns achieved by the quad-band antenna in the respective resonances were directional and have a good front-to-back ratio. The front-to-back ratio at 2.45 GHz has improved from 14 dB to 22 dB with the addition of the larger ground plane. The maximum side-lobe level is less than -17 dB for all the resonances, which indicates that most of the radiated energy from the antenna was reflected back by the AMC reflector. The quad-band antenna also experiences some squinting at 5.2 GHz and 5.75 GHz. The difference between the measured and simulated *E*-plane radiation patterns at 5.2 GHz was investigated in simulation. The various parameters that were considered in simulation was the alignment between the antenna and the AMC reflector, the effect of the nylon screws and nuts, as well as small variations in the manufacturing of the antenna. The various simulations did not have an influence on the *E*-plane radiation pattern at 5.2 GHz and could be investigated in a further study.

The *E*-plane radiation patterns were also measured at three frequencies in the respective 2.4 GHz, 5.2 GHz and 5.8 GHz WLAN bands as well as the 3.5 GHz WiMAX band. The measured *E*-plane radiation patterns, of the quad-band antenna with a larger ground plane, are shown in Figure 5.25 to Figure 5.28.

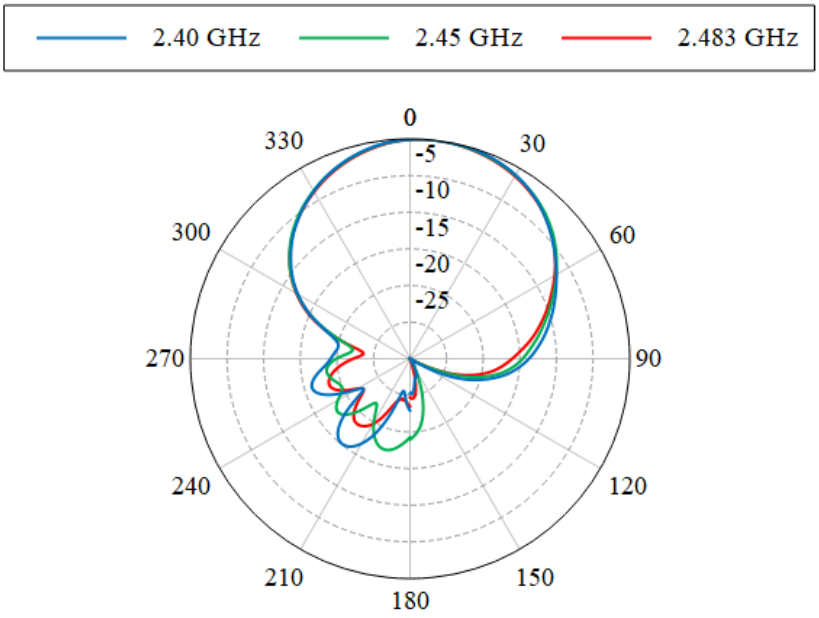

Figure 5.25. Measured radiation patterns in the *E*-plane of quad-band antenna with larger AMC ground plane in 2.4 GHz WLAN frequency band

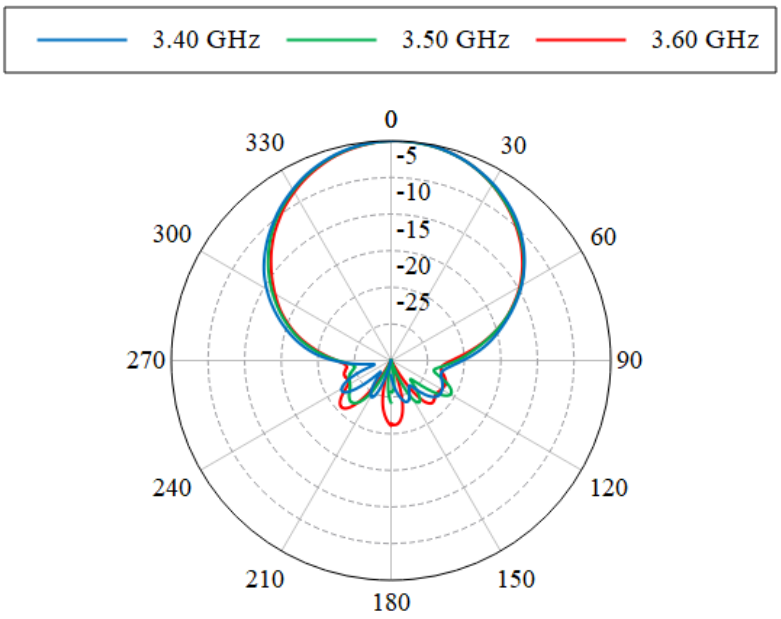

Figure 5.26. Measured radiation patterns in the *E*-plane of quad-band antenna with larger AMC ground plane in 3.5 GHz WiMAX frequency band

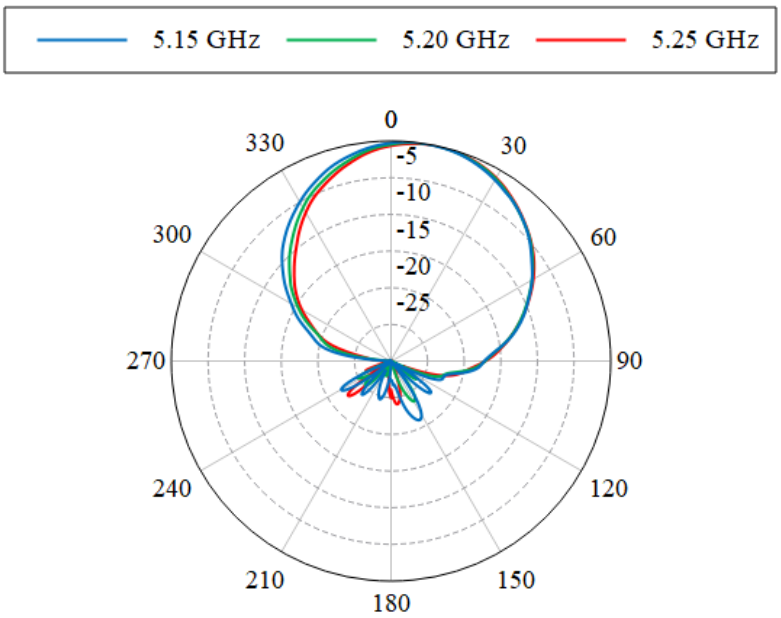

Figure 5.27. Measured radiation patterns in the *E*-plane of quad-band antenna with larger AMC ground plane in 5.2 GHz WLAN frequency band

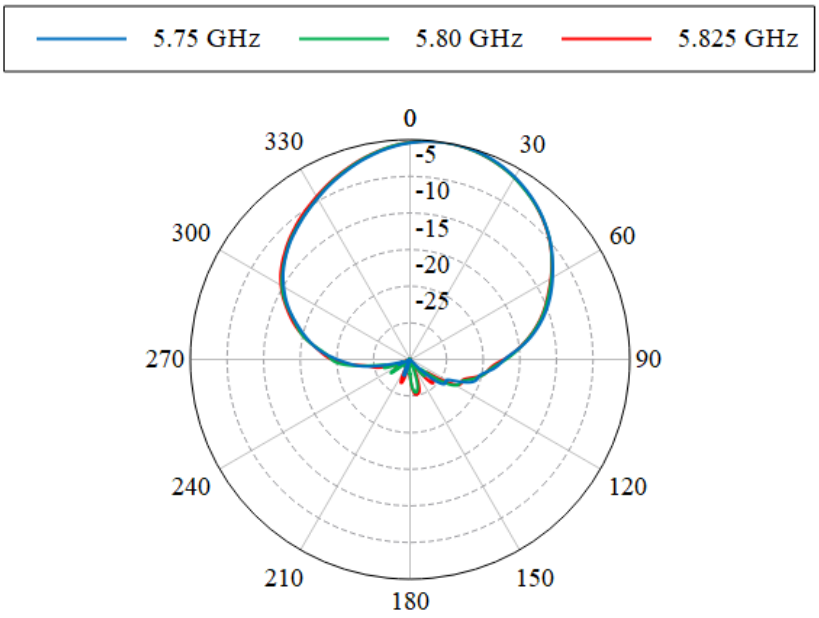

Figure 5.28. Measured radiation patterns in the *E*-plane of quad-band antenna with larger AMC ground plane in 5.75 GHz WLAN frequency band

The measured *E*-plane radiation patterns indicate that in the respective WLAN and WiMAX frequency bands, the antenna has a nearly constant radiation pattern over the different frequency bands.

5.3.3 Gain

The same procedure as with the triple-band antenna was followed. The gain of the antenna was also measured in the compact antenna range at the University of Pretoria. The gain of the antenna was calibrated using a standard gain horn antenna as a reference antenna. The measured *E*-plane radiation patterns of the quad-band antenna illustrate that the main beam of the antenna experiences some squinting at the respective 2.45 GHz, 5.2 GHz and 5.75 GHz bands. To achieve accurate results, the gain of the quad-band antenna with the larger AMC ground plane was measured at boresight and was also peaked. The measured gain is compared to the simulated gain at boresight and at the respective peak angles.

5.3.3.1 Boresight gain

The gain of the quad-band antenna was measured at boresight and compared to the simulated gain at boresight, as shown in Figure 5.29. The difference between the simulated and measured gain at three frequencies in each of the WLAN and WiMAX frequency bands are given in Table 5.5.

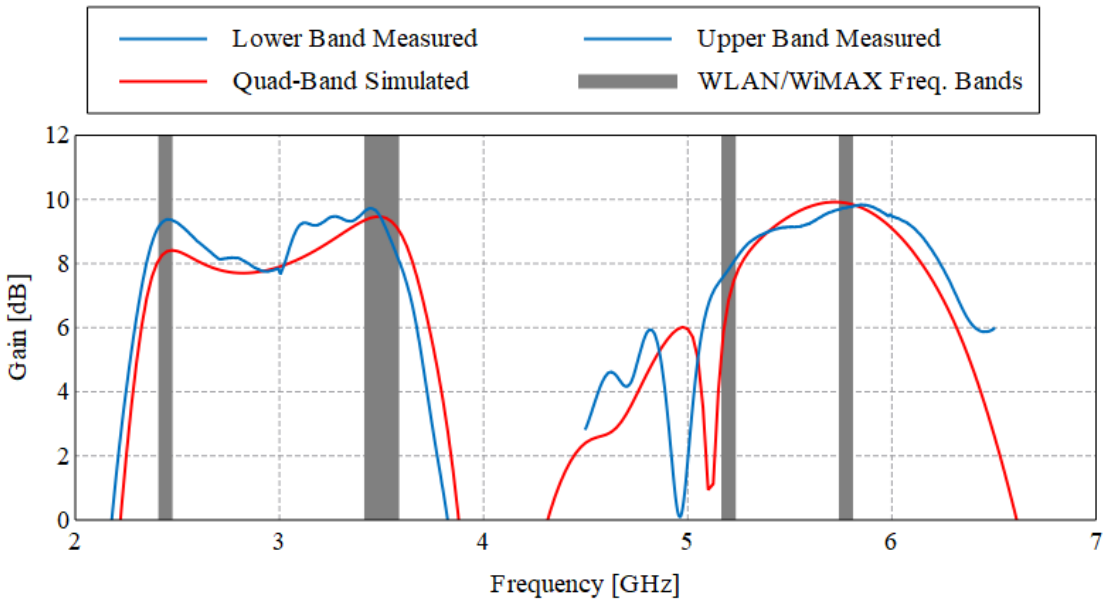

Figure 5.29. Simulated and measured boresight gain of quad-band antenna with the larger ground plane

Table 5.5. Simulated and measured boresight gain of quad-band antenna

Frequency [GHz]	Simulated Gain [dBi]	Measured Gain [dBi]	Difference [dBi]
2.4	8.0	9.1	1.1
2.45	8.4	9.4	1.0
2.483	8.4	9.3	0.9
3.4	9.3	9.5	0.2
3.5	9.5	9.4	0.1
3.6	8.8	7.8	1.0
5.15	5.1	7.1	2.0
5.2	6.8	7.8	1.0
5.25	7.8	8.3	0.5
5.725	10.1	10.0	0.1
5.75	10.2	10.1	0.1
5.825	10.2	10.1	0.1

The average measured gain of the quad-band antenna across all the WLAN and WiMAX bands of operation is 9.0 dBi. The largest difference between the simulated and measured gain is 2.0 dBi at 5.15 GHz, which is a noticeable difference between the measured and simulated gain at boresight. The antenna gain was also peaked to determine if the same difference between the simulated and measured gain occurred.

5.3.3.2 Peak Gain

The simulated radiation patterns of the quad-band antenna with the larger ground plane illustrated that the main beam squints in the upper WLAN (5.2 GHz and 5.8 GHz) frequency bands. In the 2.4 GHz band the antenna was peaked at 6.0°, in the lower 3.5 GHz WiMAX band the antenna was peaked at 0° and in the upper 5.2 GHz and 5.8 GHz WLAN bands, the antenna was peaked at 14.7°. The simulated gain was also measured at the respective angles. The simulated and measured peak gain was compared and shown in Figure 5.30. The peak gain results are summarized in Table 5.6.

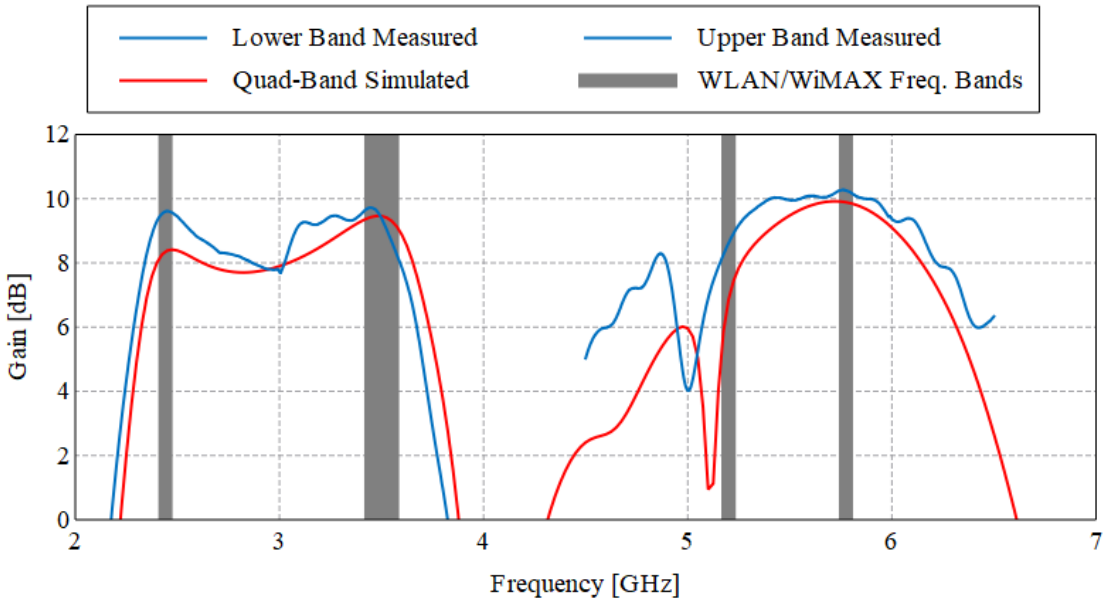

Figure 5.30. Simulated and measured peak gain of quad-band antenna with the larger ground plane

Table 5.6. Simulated and measured peak gain of quad-band antenna

Frequency [GHz]	Simulated Gain [dBi]	Measured Gain [dBi]	Difference [dBi]
2.4	8.2	9.3	1.1
2.45	8.5	9.6	1.1
2.483	8.5	9.5	1.0
3.4	9.3	9.5	0.2
3.5	9.5	9.4	0.1
3.6	8.9	7.9	1.0
5.15	4.1	7.9	3.8
5.2	7.0	8.6	1.6
5.25	7.8	9.2	1.4
5.725	10.1	10.2	0.1
5.75	10.1	10.3	0.2
5.825	9.9	10.1	0.2

The average measured peak gain of the quad-band antenna with a larger ground plane across all the WLAN and WiMAX bands of operation is 9.3 dBi. The average peak gain has increased by 0.3 dBi. The largest difference between the measured and simulated gain was 3.8 dBi at 5.15 GHz, which is a significant difference. This indicated that the size and placement of the smaller secondary slot, which is responsible for the 5.2 GHz resonance, was not the same as in simulation. The measured antenna achieved better performance than the simulated quad-band antenna. The manufactured antenna was assembled by hand and the holes were also drilled by hand. This could cause the distance between the antenna and AMC reflector to be different from the simulation.

5.4 CHAPTER SUMMARY

In summary, overall good agreement is demonstrated between the simulated and measured results for the respective triple- and quad-band antennas. The triple-band antenna was well matched and covered the respective 2.4 GHz, 5.2 GHz and 5.8 GHz WLAN bands. The antenna also achieved an average peak gain of 10.2 dBi across all three WLAN bands. The average gain was calculated by summing the measured peak gain in Table 5.3 and dividing it by 9. The triple-band antenna achieved a directional radiation pattern and a front-to-back ratio better than 24 dB across the bands of operation.

The quad-band antenna was also well matched and covered the 2.4 GHz, 5.2 GHz and 5.8 GHz WLAN bands, as well as the 3.5 GHz WiMAX band. The quad-band antenna achieved an average peak gain of 9.3 dBi across the WLAN and WiMAX bands. The antenna also achieved a directional radiation pattern with a front-to-back ratio better than 22 dB across the bands of operation.

CHAPTER 6 CONCLUSION

6.1 GENERAL CONCLUSIONS

In Chapter 1 the context of the problem was discussed along with a brief background on WLAN and WiMAX antennas. The literature study indicated that there was limited research on WLAN and WiMAX antennas for wall mounted applications, which resulted in the research gap. The research goals and objectives of the work were also formulated, as well as the contribution the work will have.

In Chapter 2 a literature study on WLAN and WiMAX antennas was performed. The literature study on WLAN and WiMAX antennas focused on omnidirectional as well as directional antennas. The literature study indicated that numerous antennas were designed with an omnidirectional pattern and that these antennas had received more attention than directional antennas. The literature study also focused on directional WLAN and WiMAX antennas. In the second half of Chapter 2, an investigation was performed on artificial magnetic conductor (AMC) surfaces with WLAN antennas. The literature study on AMC surfaces indicated that the combination of WLAN antennas with AMC surfaces achieved improved gain and low profile designs.

In Chapter 3 a strip-slot antenna was used as a starting point for the investigation of the research. The strip-slot antenna is combined with a PEC reflector to achieve a directional, high gain antenna for WLAN and WiMAX applications. The strip-slot antenna consisted of various elements, which led to a background study on slot antennas, patch antennas and the strip-slot pair structure. The design of a single-, dual- and triple-band AMC reflector was also designed to operate in the WLAN and WiMAX frequency bands of interest.

The knowledge gained from the background study in Chapter 3, was used to design the final triple- and quad-band antennas in Chapter 4. The design of the triple- and quad-band antennas was a combination of a patch antenna, a strip-slot pair, a secondary slot in the ground plane of the antenna and a single-band AMC reflector. The quad-band antenna

replaced the secondary slot element in the ground plane with a half-wavelength slot at 5.2 GHz. The triple-band antenna achieved an impedance bandwidth of less than -10 dB in the 2.4 GHz, 5.2 GHz and 5.8 GHz WLAN frequency bands. The quad-band antenna also operated in the 2.4 GHz, 5.2 GHz and 5.8 GHz WLAN bands as well as the 3.5 GHz WiMAX band. The final design of the triple- and quad-band antennas were manufactured and assembled.

In Chapter 5 the manufactured triple- and quad-band antennas were measured and compared to the simulation results. The triple-band WLAN antenna operated in the three WLAN bands from 2.4 – 2.483, 5.15 – 5.25 and 5.725 – 5.825 GHz with a reflection coefficient below -10 dB in all three WLAN bands. The antenna measured an average peak gain of 8.5 dBi, 10.4 dBi and 11.7 dBi in the 2.4 GHz, 5.2 GHz and 5.8 GHz bands, respectively. The comparison between the simulated and measured results indicated that side-lobes were present in the *E*-plane radiation pattern in the upper 5.75 GHz WLAN band, which was not present in simulation.

The quad-band WLAN and WiMAX antenna also operated in the three WLAN bands as well as the 3.5 GHz WiMAX band. The quad-band antenna has a reflection coefficient below -10 dB in the WLAN and WiMAX frequency bands with an average gain of 9.5 dBi, 9.5 dBi, 8.1 dBi and 10.2 dBi in the 2.4 GHz, 3.5 GHz, 5.2 GHz and 5.8 GHz bands, respectively. The comparison between the simulated and measured *E*-plane radiation patterns and measured gain results indicated a difference in the 5.2 GHz band, which is due to the smaller secondary slot element.

In conclusion, the design of a triple- and quad-band antenna for the 2.4 GHz, 5.2 GHz and 5.8 GHz WLAN bands, as well as the 3.5 GHz WiMAX band was achieved. Both the triple- and quad-band antennas were combined with an AMC reflector, which resulted in low profile designs, with high gain and a directional radiation pattern. The directional radiation pattern of the antennas make it suitable for wall mounted applications in the WLAN and WiMAX bands.

6.2 CONTRIBUTIONS

A new and improved high gain, directional and low profile antenna for WLAN and WiMAX applications was designed. The work took into account triple- and quad-band frequency capability, gain, overall size and total efficiency. The design of a triple- and quad-band antenna was achieved. The triple- and quad-band antennas were manufactured and compared to the simulated results.

The strip-slot antenna in [21] achieved a directional and high gain response for WLAN and WiMAX applications. This was the only directional antenna that covered both the 2.4 GHz, 5.2 GHz and 5.8 GHz WLAN bands and the 3.5 GHz WiMAX band. The antenna had an overall size of $96\times73\times14$ mm^3 ($0.768\lambda_0\times0.584\lambda_0\times0.112\lambda_0$ at 2.4 GHz) with an average gain of 9.1 dBi across the WLAN and WiMAX bands. The antenna achieved a directional radiation pattern with a front-to-back ratio better than 14 dB.

The quad-band antenna also covers the WLAN and WiMAX bands and can be compared to the strip-slot antenna. The quad-band antenna has an overall size of $80\times80\times10.01$ mm^3 ($0.64\lambda_0\times0.64\lambda_0\times0.08\lambda_0$ at 2.4 GHz), which is an overall size improvement of 34.7%. The average peak gain is 9.3 dBi, which is 2.2% better than the strip-slot antenna in [21]. The quad-band antenna also achieves a directional radiation pattern with a front-to-back ratio better than 22 dB, which is also an improvement of 57.1%. This indicates that the objectives set out were achieved.

The geometry of the antennas was an adaptation of an existing antenna geometry. The slot radiating element geometry was not intended for WLAN applications and had a very low gain and total efficiency. The gain of the slot radiating element was improved by changing the traveling wave feed to a standing wave feed. The same principle was implemented and a change in antenna geometry was also applied along with the addition of the AMC reflector.

The physical size of the triple- and quad-band antennas was $80\times80\times10.01$ mm^3 and the simulated total efficiency was more than 90% across the frequency bands of operation. The triple-band antenna was designed to function in the IEEE802.11a/b WLAN standard frequency bands and was matched with a reflection coefficient of less than -10 dB in the frequency bands. The antenna was directional and linearly-polarized with a gain of more than 8.2 dBi across all three frequency bands and an average gain of 10.2 dBi. The quad-band antenna was also designed to operate in the WLAN frequency bands, as well as the IEEE802.16d/e WiMAX standard frequency band. It was also matched with a reflection coefficient of less than -10 dB in the frequency bands. The antenna was also directional and linearly-polarized with a gain of more than 7.9 dBi across all the frequency bands and an average gain of 9.3 dBi.

The geometry of the antennas and the AMC reflector are easy to manufacture and assemble. The antenna substrate and AMC reflector can be etched, cut and drilled by a manufacturing company, while only four spacers and three soldering points are required for the assembly. The design and performance of the proposed triple- and quad-band antennas exceeded the other directional high gain WLAN and WiMAX antennas found in the literature with regards to gain and size.

REFERENCES

[1] B. Kelothu, K. R. Subhashini and G. L. Manohar, "A compact high-gain microstrip patch antenna for dual band WLAN applications," *2012 Students Conference on Engineering and Systems*, Allahabad, Uttar Pradesh, 2012, pp. 1-5.

[2] F. Rashid, M. M. Mustafiz, M. K. Ghosh and S. Hossain, "Design and performance analysis of ultra wideband Inverted-F antenna for Wi-Fi, WiMAX, WLAN and military applications," *2012 15th International Conference on Computer and Information Technology (ICCIT)*, Chittagong, 2012, pp. 610-614.

[3] F. Rahmadani and A. Munir, "Microstrip patch antenna miniaturization using artificial magnetic conductor," *2011 6th International Conference on Telecommunication Systems, Services, and Applications (TSSA)*, Bali, 2011, pp. 219-223.

[4] Yen-Liang Kuo and Kin-Lu Wong, "Printed double-T monopole antenna for 2.4/5.2 GHz dual-band WLAN operations," in *IEEE Transactions on Antennas and Propagation*, vol. 51, no. 9, pp. 2187-2192, Sept. 2003.

[5] A. Foudazi, H. R. Hassani and S. M. A. Nezhad, "A dual-band WLAN/UWB printed wide slot antenna," *2011 Loughborough Antennas & Propagation Conference*, Loughborough, 2011, pp. 1-3.

[6] A. Durka, M. Woźniak, M. Bugaj, R. Przesmycki, L. Nowosielski and M. Wnuk, "Optimization of a double — T microstrip antenna in order to obtain a largest bandwidth," *2012 19th International Conference on Microwaves, Radar & Wireless Communications*, Warsaw, 2012, pp. 251-255.

[7] J. R. Panda and R. S. Kshetrimayum, "A printed F-shaped dual-band monopole antenna for RFID and WLAN applications," *2010 International Conference on Computer and Communication Technology (ICCCT)*, Allahabad, Uttar Pradesh, 2010, pp. 789-791.

[8] Zhang and W. X. Zhang, "Comparative study on printed dual-band antennas for WLAN terminal," *2012 International Symposium on Antennas and Propagation (ISAP)*, Nagoys, 2012, pp. 1405-1408.

[9] S. Jing, Y. Yin, A. Sun, Y. Wei and Y. Yang, "Compact E-shaped monopole antenna for dual-band WLAN applications," *2011 IEEE International Conference on Microwave Technology & Computational Electromagnetics*, Beijing, 2011, pp. 305-308.

[10] M. Z. M. Nor, S. K. A. Rahim and M. I. Sabran, "Slotted square patch printed monopole antenna with dual band capabilities for WLAN application," *Asia-Pacific Microwave Conference 2011*, Melbourne, VIC, 2011, pp. 1766-1769.

[11] Ting Wu, Xiao-Wei Shi, Ping Li and Hao Bai, "Tri-band microstrip-fed monopole antenna with dual-polarization characteristics for WLAN and WiMAX applications," in *Electronics Letters*, vol. 49, no. 25, pp. 1597 -1598, 5 December 2013.

[12] L. Ge, C. Sim, H. Su, J. Lu and C. Ku, "Single-layer dual-broadband circularly polarised annular-slot antenna for WLAN applications," in *IET Microwaves, Antennas & Propagation*, vol. 12, no. 1, pp. 99-107, 10 1 2018.

[13] W. Ren, "Compact dual-band annular-ring slot antenna for WLAN applications," *IET 3rd International Conference on Wireless, Mobile and Multimedia Networks (ICWMNN 2010)*, Beijing, 2010, pp. 72-75.

[14] W. Chen, J. Yin, M. Li, F. Li and J. Yang, "Directional dual-band slotted semi-circular inverted-F antenna for WLAN applications," in *Electronics Letters*, vol. 51, no. 24, pp. 1960-1962, 19 11 2015.

[15] N. Yan, K. Ma, H. Zhang and Y. He, "Dual-band antenna with comb radiators for WLAN applications using SISL technology," in *Electronics Letters*, vol. 53, no. 13, pp. 822-824, 22 6 2017.

[16] J. Gemio, J. Parron Granados and J. Soler Castany, "Dual-Band Antenna With Fractal-Based Ground Plane for WLAN Applications," in *IEEE Antennas and Wireless Propagation Letters*, vol. 8, pp. 748-751, 2009.

[17] G. Zhang, H. Song, B. Wang and Q. Qin, "A Novel dual-band microstrip antenna for WLAN applications," *2007 International Conference on Microwave and Millimeter Wave Technology*, Builin, 2007, pp. 1-4.

[18] J. Joubert, J. W. Odendaal and J. Prinsloo, "High-gain dual-polarised planar slot array for WLAN applications," in *Electronics Letters*, vol. 46, no. 15, pp. 1048-1050, 22 July 2010.

[19] A. K. Sharma, A. Mittal and B. V. R. Reddy, "Slot embedded dual-band patch antenna for WLAN and WiMAX applications," in *Electronics Letters*, vol. 51, no. 8, pp. 608-609, 16 4 2015.

[20] S. Su and C. Lee, "Low-Cost Dual-Loop-Antenna System for Dual-WLAN-Band Access Points," in *IEEE Transactions on Antennas and Propagation*, vol. 59, no. 5, pp. 1652-1659, May 2011.

[21] M. van Rooyen, J. W. Odendaal and J. Joubert, "High-Gain Directional Antenna for WLAN and WiMAX Applications," in *IEEE Antennas and Wireless Propagation Letters*, vol. 16, pp. 286-289, 2017.

[22] H. H. Tran and I. Park, "A Dual-Wideband Circularly Polarized Antenna Using an Artificial Magnetic Conductor," in *IEEE Antennas and Wireless Propagation Letters*, vol. 15, pp. 950-953, 2016.

[23] P. J. Soh, F. N. Giman, M. F. Jamlos, H. Lago and A. A. Al-Hadi, "A C-slotted dual band textile antenna for WBAN applications," *2016 URSI Asia-Pacific Radio Science Conference (URSI AP-RASC)*, Seoul, 2016, pp. 1621-1624.

[24] V. K. Pandit and A. R. Harish, "Design of dual-band CPW-fed monopole antenna with dual-band AMC surface for WLAN," *2016 IEEE Annual India Conference (INDICON)*, Bangalore, 2016, pp. 1-4.

[25] "CST STUDIO SUITE® 2018, CST AG, Germany." [Online]. Available: www.cst.com.

[26] E. Abdo-Sanchez, J. E. Page, T. M. Martin-Guerrero, J. Esteban and C. Camacho-Penalosa, "Planar Broadband Slot Radiating Element Based on Microstrip-Slot Coupling for Series-fed Arrays," in *IEEE Transactions on Antennas and Propagation*, vol. 60, no. 12, pp. 6037-6042, Dec. 2012.

[27] J. Joubert, J. C. Vardaxoglou, W. G. Whittow and J. W. Odendaal, "CPW-Fed Cavity-Backed Slot Radiator Loaded With an AMC Reflector," in *IEEE Transactions on Antennas and Propagation*, vol. 60, no. 2, pp. 735-742, Feb. 2012.

[28] Y. F. Cao, X. Y. Zhang, and T. Mo, "Low profile Conical-Pattern Slot Antenna with Wideband Performance Using Artificial Magnetic Conductors," *IEEE Trans. Antennas Propag.*, vol. 66, no. 5, pp. 2210–2218, 2018.

[29] A. Mersani, L. Osman and I. Sfar, "Dual-band textile antenna on AMC substrate for wearable applications," *2015 IEEE 15th Mediterranean Microwave Symposium (MMS)*, Lecce, 2015, pp. 1-3.

[30] S. Yan, P. J. Soh and G. A. E. Vandenbosch, "Low profile Dual-Band Textile Antenna With Artificial Magnetic Conductor Plane," in *IEEE Transactions on Antennas and Propagation*, vol. 62, no. 12, pp. 6487-6490, Dec. 2014.

[31] N. A. Abbasi and R. J. Langley, "Multiband-integrated antenna/artificial magnetic conductor," in *IET Microwaves, Antennas & Propagation*, vol. 5, no. 6, pp. 711-717, 26 April 2011.

[32] R. Saad and K. L. Ford, "A dual band miniaturised Artificial Magnetic Conductor design methodology," *2012 Loughborough Antennas & Propagation Conference (LAPC)*, Loughborough, 2012, pp. 1-4.

[33] R. Saad and K. L. Ford, "A triple band Artificial Magnetic Conductor surface incorporating a split ring resonator antenna," *2014 Loughborough Antennas and Propagation Conference (LAPC)*, Loughborough, 2014, pp. 717-720.

[34] R. Dewan, M. K. A. Rahim, M. R. Hamid, N. A. Samsuri and B. D. Bala, "Analysis of triple band artificial magnetic conductor (AMC) band conditions to wideband antenna performance," *2014 IEEE Asia-Pacific Conference on Applied Electromagnetics (APACE)*, Johor Bahru, 2014, pp. 167-170.

[35] W. L. Stutzman and G. A. Thiele, *Antenna Theory and Design*, 3rd ed. United States of America: John Wiley & Sons, 2013.

[36] Altair, "FEKO User Manual," 2015.

[37] K. S. Yee, "Numerical Solution of Initial Boundary Value Problems Involving Maxwell's Equations in Isotropic Media," *IEEE Transactions on Antennas and Propagation*. 1966.

[38] S. Dey and R. Mittra, "A locally conformal finite-difference time-domain (FDTD) algorithm for modeling three-dimensional perfectly conducting objects," *IEEE Microw. Guid. Wave Lett.*, 1997.

[39] S. Benkler, N. Chavannes, and N. Kuster, "A new 3-D conformal PEC FDTD scheme with user-defined geometric precision and derived stability criterion," *IEEE Trans. Antennas Propag.*, 2006.

[40] C. A. Balanis, *Antenna Theory*, 2nd ed. New York, USA: Wiley, 1997.

[41] "Slotline basics | Slotline types." [Online]. Available: http://www.rfwireless-world.com/Articles/Slotline-basics-and-slotline-types.html. [Accessed: 30-May-

2018].

[42] N. K. Darimireddy, R. Ramana Reddy, and A. Mallikarjuna Prasad, “Design of triple-layer double U-slot patch antenna for wireless applications,” *J. Appl. Res. Technol.*, vol. 13, no. 5, pp. 526–534, 2015.

[43] N. Ojaroudi, M. Ojaroudi and N. Ghadimi, "Dual band-notched small monopole antenna with novel W-shaped conductor backed-plane and novel T-shaped slot for UWB applications," in *IET Microwaves, Antennas & Propagation*, vol. 7, no. 1, pp. 8-14, 11 January 2013.

[44] Z. Chen and Z. Shen, "A Compact Cavity-Backed Endfire Slot Antenna," in *IEEE Antennas and Wireless Propagation Letters*, vol. 13, pp. 281-284, 2014.

[45] C. Chulvanich, J. Nakasuwan, N. Songthanapitak, N. Anantrasirichai, and T. Wakabayashi, “Design Narrow Slot Antenna for Dual Frequency,” *PIERS Online*, vol. 3, no. 7, pp. 1024–1028, 2007.

[46] Antenna Magus (2018). *Microstrip-fed slot*. Magus Pty (Ltd).

[47] E. A. Soliman, “CPW-FED Brick-Wall Antenna with Parasitic Elements ELEMENTS,” vol. 5071, no. March, 2017.

[48] D. Sievenpiper, Lijun Zhang, R. F. J. Broas, N. G. Alexopolous and E. Yablonovitch, "High-impedance electromagnetic surfaces with a forbidden frequency band," in *IEEE Transactions on Microwave Theory and Techniques*, vol. 47, no. 11, pp. 2059-2074, Nov. 1999.